The effects of empirical mode decomposition based de-noising in improving detection of directly stimulated skeletal muscle response

Dissertation submitted in partial fulfilment for the degree of

Master of Science in Biomedical Engineering

Student: Nielen Christoff Venter (VNTNIE001)

Supervisor: Dr Lester John

Co-Supervisors: Prof. Laurie Kellaway, Dr Nicholas Sachs

February 2013

The financial assistance of the National Research Foundation (NRF) towards this research is hereby acknowledged. Opinions expressed and conclusions arrived at are those of the author, and are not necessarily to be attributed to the NRF.

Abstract

Chronaxie and rheobase are parameters used to quantify the response of excitable tissues to applied electrical potential. These parameters are beneficial to effective stimulation of these tissues. Despite their importance, reported values for skeletal muscles are inconclusive. This is particularly true for muscles that have been denervated. A potential source of error in determining the parameters is in the classification of the muscle responses. Current algorithmic methods for classifying twitches have been shown to be inferior to human observation. However, human observation is subjective, and has been shown to lead to high variability in similar fields. This aim of this dissertation was to investigate whether a de-noising strategy could improve the recognisability of twitches for algorithmic twitch classifiers. The de-noising strategy was based on empirical mode decomposition (EMD).

Sixty rat soleus muscles were directly stimulated using electrodes and a pulse generator. Of these, 30 were denervated in 3 sets of 10 for 1 week, 2 weeks and 8 weeks respectively. The remaining 30 muscles were left intact. Pulses were applied using steadily increasing pulse amplitudes at 5 constant pulse widths. The corresponding muscle twitches were digitised and recorded using a strain gauge. In addition to digital filters, the de-noising algorithm was applied to the recorded twitches. The recognisability of each twitch was quantified using an estimated signal-to-noise ratio, as well as cross correlation with a template. The effect of the de-noising algorithm on these two metrics was considered.

Muscles at differing denervation periods (including intact muscles) were considered separately. The de-noising method resulted in a significant increase ($P < 0.001$) in signal-to-noise ratios, but no significant change ($P > 0.05$) in the twitch-template correlations. This suggests that threshold-based methods of twitch detection would benefit from EMD-based de-noising. However any methods based on twitch shape (for example template matching) would not. Overall, the recognisability of the twitches was increased.

Declaration

I, Nielen Christoff Venter, hereby declare that the work on which this dissertation is based is my original work (except where acknowledgements indicate otherwise) and that neither the whole work nor any part of it has been, is being, or is to be submitted for another degree in this or any other university. I empower the university to reproduce for the purpose of research either the whole or any portion of the contents in any manner whatsoever.

The Harvard referencing style was used for citation and referencing. Each contribution to, and quotation from the work(s) of other people has been cited and referenced.

Signature: ……

Date: ……..

Acknowledgements

I owe my gratitude to my supervisors. Dr Nicholas Sachs, who initiated the project and helped out with the details of the animal handling. Dr Lester John, who took over my supervision, and helped out with the lengthy writing process, as well as provided much needed technical assistance. Finally, Prof. Lauriston Kellaway, who provided valuable advice in the last stages of the project, as well as access to important lab equipment.

Many other UCT staff members also contributed, including Charles (who built the tissue bath), the staff of the UCT animal unit and Prof. Russel (for the use of her lab).

This project wouldn't have been possible without the financial support of the NRF, as well as the University of Cape Town.

Finally, I'd like to acknowledge all my friends in Cape Town, whose support I can always count on, Ghabiba, who made the long days in the lab more fun and my family (especially my parents, without which I would not be possible).

Table of contents

List of tables

List of figures

Chapter 1: Introduction

1.1 Background

1.1.1 Electrical stimulation of skeletal muscle

Paralysis can be considered to be a malfunction of some part of the nervous system, resulting in disruption to or loss of motor and/or sensory function. Nearly 1 in 50 people suffer from some sort of paralysis (Turner et al. 2009). Of this sample, about half were paralysed as a result of damage or disease in the peripheral nervous system.

While nerves can regenerate, they do so very slowly (typically at a rate of 20µm h^{-1}). While this may allow small scale injuries to heal, some motor axons are very large. An example of this is the sciatic nerve which extends to over a metre in humans. A large injury could take a very long time, if ever, to fully heal (Davies 1987). Practically, some nerves can't regenerate regardless of healing time due to the complex terrain inside the body (Olson 2002).

Electrical stimulation can be used to rehabilitate, train and restore function in paralysed muscles. Many applications are currently being investigated, and several stimulation devices are available commercially (Peckham & Knutson 2005). These devices are known as neural prosthetics.

Skeletal muscles can be stimulated by activating the motor nerves or by directly activating the muscles themselves. Nerve stimulation requires less current and is usually preferred (J. Mortimer 1981). However, this is limited to cases where the lower motor neurons are intact. Neuron damage can result from disease (such as polio or amyotrophic lateral sclerosis), injury or other causes. If the lower motor neurons are damaged, the muscles must be stimulated directly.

1.1.2 Chronaxie and rheobase

The ease by which a particular tissue is stimulated is known as its excitability. Knowledge of excitability is highly beneficial to the design of stimulation protocols or devices. A given tissue's excitability can be characterised by its chronaxie and rheobase. These two parameters define the strength-duration curve, a plot of current magnitude and duration required to elicit response from that tissue (see Section 2.3.3).

Despite their importance, the variability in published values of these parameters is quite large for a given tissue type (Geddes 2004). This is particularly true of directly stimulated denervated skeletal muscle. The effects of denervation on excitability of skeletal muscle have been independently investigated multiple times (see Section 2.3.5). Results of these investigations are still inconclusive.

Sources of experimental error accounting for this variation have been investigated extensively (see Sections 3.2 and 3.3). Investigated sources include, but are not limited to, choice of electrodes, electrode arrangement, shape of stimulation pulse, effects of surrounding tissue and animal model used.

An additional source of error could be the method of detecting and classifying skeletal muscle responses. This is particularly difficult when muscles are stimulated directly (see Section 4.2.1).

Despite this, response detection has received relatively little attention. Current methods could be considered subjective or otherwise impractical (see Sections 4.2.2 and 4.2.3).

1.1.3 Empirical mode decomposition

Empirical mode decomposition (EMD) was developed to adaptively represent non-stationary signals. It was first proposed by N E Huang et al. (1998), and has since been improved by others. It has aided in the analysis of a variety of signals, across a broad range of specialisations. EMD based signal de-noising techniques have been shown to be effective compared to other well-known strategies (see Section 4.3.3.1).

EMD is adept at isolating physically meaningful components of a signal. This makes it particularly suitable for analysing biological signals, which often contain high levels of interference, or noise. This has made it a popular method for analysing these signals, as well as signals from many other fields (see Section 4.3.3.2).

1.2 Methodological overview

1.2.1 Objectives

This investigation aimed to address variability in tissue response classification. The variability is most pronounced in studies of healthy and denervated skeletal muscle. Therefore, these tissues were the subject of this study.

The primary objective of this investigation was to assess the effect of EMD-based de-noising on the recognisability of muscle twitches as a result of direct electrical stimulation.

1.2.2 Scope

The investigation was limited to muscles obtained from an animal model, namely the rat. Both healthy and denervated muscles were considered separately. Three periods of denervation were used: 1 week, 2 weeks and 8 weeks.

The recognisability of a muscle twitch was assessed by two separate measures. These were estimation of the signal-to-noise ratio and cross correlation with a twitch template.

1.2.3 Overview of methodology

A total of 30 rats were used for the experiments. The soleus muscles were used. All the rats were surgically denervated on one side, leaving one denervated and one healthy muscle (see Section 5.2.2). Both muscles were explanted. The muscles were directly stimulated using a pulse generator, at a variety of pulse widths and amplitudes (see Section 5.4.1).

The responses of the muscles were in the form of short contractions, or twitches. They were quantified by attaching the muscles to a strain gauge. The voltage across the strain gauge was recorded for further analysis (see Section 5.4.2).

Recorded twitches were classified using a threshold (see Section 5.6.1). EMD-based de-noising was then applied to the resulting signals (see Section 6.2). The recognisability of the twitches was measured both before and after de-noising. Recognisability was assessed using two measures. The signal-to-noise ratios of the twitches were estimated (see Section 6.3). The shapes of the twitches

were assessed by cross correlation with a template (see Section 6.4). The effect of EMD-based de-noising on the two measures was then assessed separately (see Section 6.5).

Chapter 2: Overview of electrical stimulation

2.1 Introduction

Muscles provide the force required to move the bones, and hence the body, around. They do this by contracting (or shortening). Contraction is a result of interactions between the constituent proteins of the muscle. The interactions are initiated by a signal known as an action potential. This signal transmits information throughout the body via the nervous system and other excitable tissues.

These mechanisms may be manipulated to artificially initiate contractions within muscles. With knowledge of these mechanisms, electrical stimulation has grown from a curiosity to a useful clinical tool. Many concepts are still being researched, however, and issues remain to be resolved. This chapter provides a brief review of knowledge on the subject.

2.2 Physiology of contraction

2.2.1 Muscle overview

A muscle can be broken down into several sections or compartments (see Fig. 2.1). Firstly each muscle (e.g. biceps brachii) is surrounded by a layer of connective tissue called the epimysium. Muscles are divided into fascicles. Each fascicle is separated by a layer of connective tissue called the perimysium. Fascicles are further divided into muscle fibers.

Muscle fibers are separated by a layer of connective tissue called the endomysium, and surrounded by the sarcolemma. Muscle fibers are even further divided into myofibrils, which are cylindrical bundles of contractile proteins. Myofibrils are only about 1-2 μm in diameter. Surrounding the myofibrils is the sarcoplasm. The sarcoplasm of the muscle fiber is comparable to cytoplasm of other cells.

Physiologically the smallest unit of contraction is the sarcomere. The sarcomere is the repeating subunit of the myofibril (see Fig. 2.2). The sarcomeres are separated on their lateral boundaries by perpendicular protein plates called Z discs. Thin protein filaments extend from the Z discs and lie parallel to (and partially overlapping) the thick filaments. The thin protein filaments are called actin filaments. The thick protein filaments are called myosin filaments. The thick filaments are held together by M line proteins.

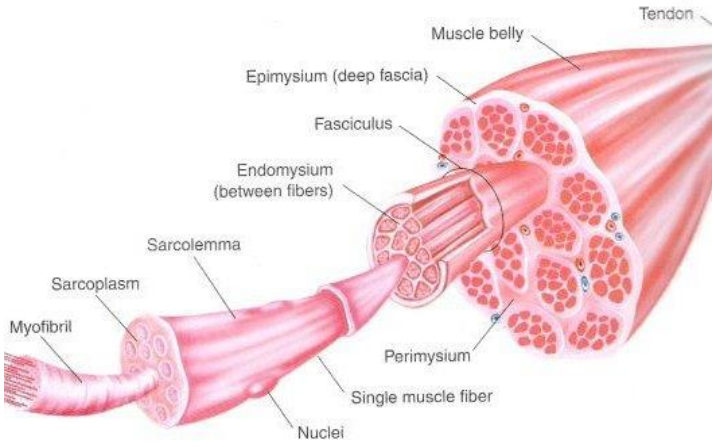

Figure 2.1: **Components of a skeletal muscle. Muscles are divided into fascicles, which are further divided into muscle fibers. Muscle fibers are divided into myofibrils.** (Baechle & Earle 2008)

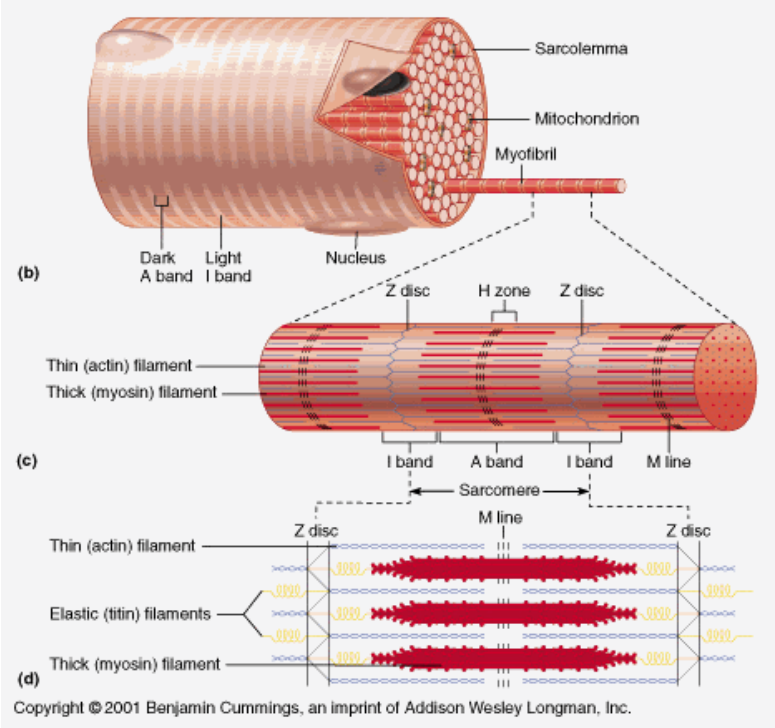

Figure 2.2: **Components of a muscle fiber showing the contractile proteins within the myofibril.** (Marieb 2001)

2.2.2 Mechanism of contraction

The muscle contracts when the thin and thick filaments attach and pull on each other. This brings the Z discs closer and increases the overlap between the filaments. The muscle relaxes by doing the opposite. Titin, an elastic protein coil, keeps the thick filaments anchored in the case of relaxation.

Attachment of the thick filaments to the thin filaments is regulated by two proteins, one called tropomyosin and the other called troponin. Tropomyosin is coiled around the thin filaments and

blocks the attachment sites for the thick filaments thus inhibiting contraction. Troponin is also attached to the thin filament and controls the position of the tropomyosin.

This control is regulated by the sarcoplasmic calcium levels (Sulakhe et al. 1973). When the calcium levels rise, the troponin moves the tropomyosin away from its blocking position. This allows the thick filaments to bind with the thin filaments and cause contraction.

2.2.3 Circuit model of excitable tissue

A potential difference exists across the membrane of an excitable cell at rest. The potential is due to the ion distribution inside and outside the cell, particularly sodium (Na^+), potassium (K^+) ions and chloride (Cl^-). The resting transmembrane potential of nervous cells is typically about -70 mV (the inside of the cell is negative relative to the outside). The resting transmembrane potential of skeletal muscle cells is typically about -90 mV. This non-zero resting state is therefore referred to as polarised.

A circuit model is constructed of the cell membrane, to describe the electrical activity in the cell (See Fig. 2.3). While skeletal muscle membrane and its properties are continuous, the circuit is divided into nodes to help describe action potential propagation (see Section 2.2.5). Each node is modelled as a leaky capacitor with capacitance C_m and resistance R_m. A voltage source is included to represent the ion distributions at rest. Resistors R_e and R_i are included to account for the resistance in the physiological medium between nodes.

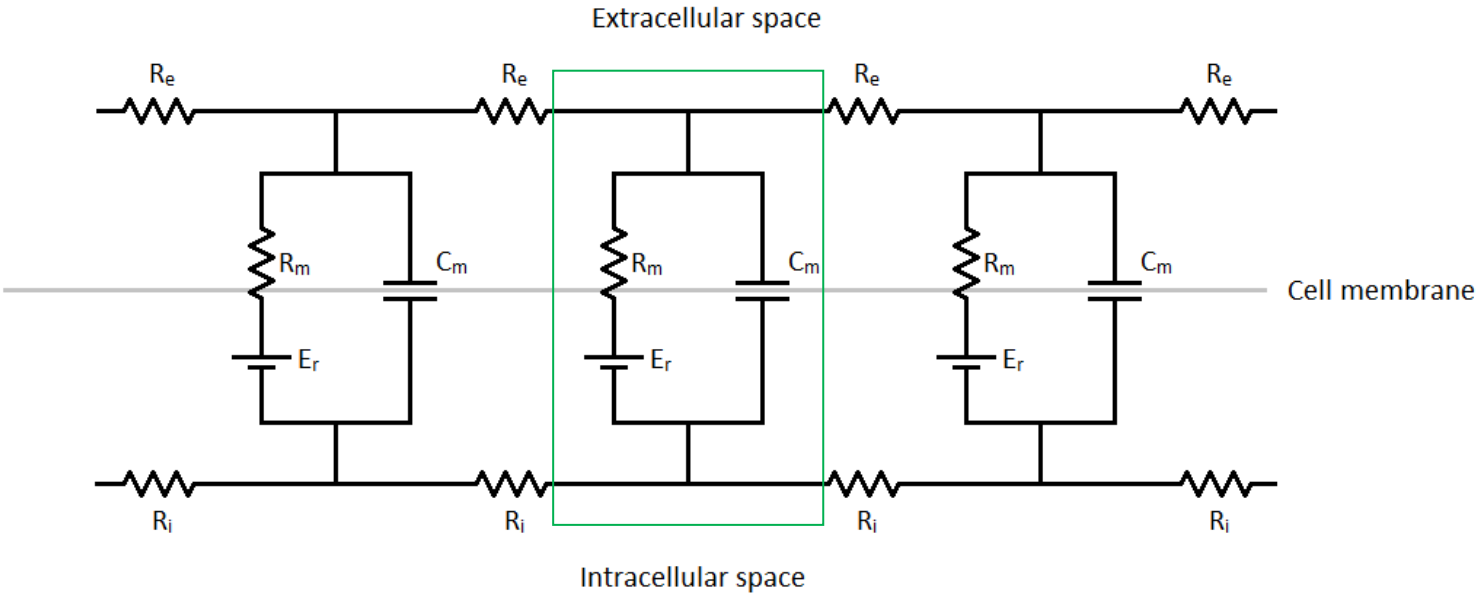

Figure 2.3: **Circuit model of an excitable cell membrane, with one node highlighted in green. R_e = extracellular resistance between nodes, R_i = intracellular resistance between nodes, C_m = membrane capacitance, R_m = membrane resistance and E_r = ion distribution potential.** (Durand 2006)

Since there are multiple charge carriers the current in a node is composed of contributions from each separate ion flow:

$$I_m = I_{Na+} + I_{K+} + I_{Cl-} + I_{Leak} \quad (1)$$

where I_m is the total current through one node, I_{Na+}, I_{K+} and I_{Cl-} are currents due to the movements of sodium, potassium and chloride ions respectively (see Fig. 2.4). Finally, I_{Leak} represents leakage current. Similarly each ion type has a separate resting potential and resistance. Resistances are commonly represented in their inverse form as conductances (Hodgkin & Huxley 1952).

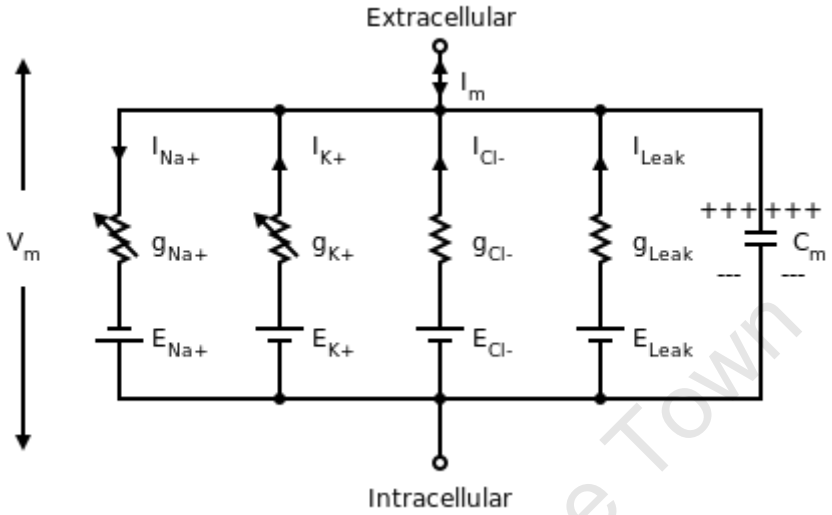

Figure 2.4: **Circuit model of a node within an excitable cell membrane. V_m = Voltage across the node, C_m = membrane capacitance, I_m = total current through the node. Except for the capacitive branch, each branch represents one ion channel, from left to right: sodium, potassium, chloride and a channel for leakage. In each ion channel, I = current, g = conductance and E = ion distribution potential.** (Durand 2006)

The conductance of the both the sodium and potassium channels are functions of the membrane voltage. The channels are therefore referred to as 'voltage-gated'. At rest the conductance values are zero and no ions can flow. If the conductance values rise, the gates are said to 'open'. This allows ions to cross the membrane.

2.2.4 Action potentials

The release of calcium into the sarcoplasm, and hence contraction, is caused by an action potential. Action potentials are defined as the rapid rising and subsequent falling of the membrane potential of an excitable cell (see Fig. 2.5). This is also known as the depolarisation and repolarisation of that cell. In the case of skeletal muscle, the cell is the muscle fiber, and the cell membrane is the sarcolemma.

An action potential is initiated when the cell membrane potential increases to a certain depolarisation threshold. This threshold is typically about -55 mV. When the threshold is reached, voltage gated sodium channels open. Sodium ions then flow into the cell. This movement of positive ions further depolarises the membrane.

The transmembrane voltage continues to increase until it becomes positive, normally reaching about 30 mV. When the transmembrane voltage becomes positive voltage gated potassium channels open. These channels allow potassium ions (positive) to flow out of the cell. The movement of potassium ions repolarises the cell membrane and returns it to its original resting potential.

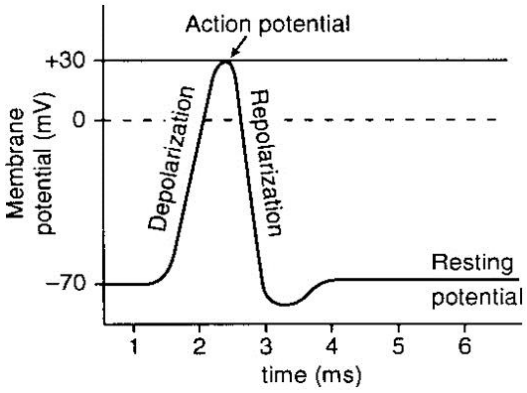

Figure 2.5: **Membrane potential of a nervous cell plotted against time during excitation, also known as an action potential.** (Kent 2006)

2.2.5 Action potential propagation

If the transmembrane voltage rises above the threshold, an action potential will be initiated in that cell. The depolarisation of a cell membrane causes the adjacent membrane to depolarise as well. This is how action potentials propagate throughout all excitable tissue (see Fig. 2.6).

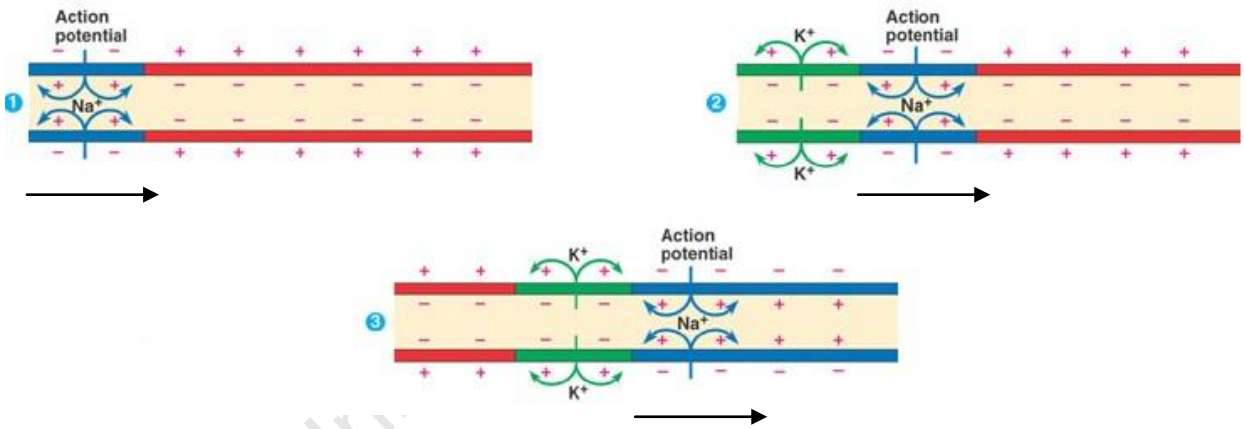

Figure 2.6: **Action potential propagation at three different nodes. 1) The action potential is at the furthest left node; 2) The action potential has moved one node to the right, the furthest left node is repolarising; 3) The action potential has moved one node to the right, the previous node is repolarising.** (ehumanbiofield 2012)

Action potentials propagate through an axon until they reach that axon's terminal branch synapses. In the case of a motor nerve, these synapses can be connected to another nerve, or a skeletal muscle. An axon of a motor nerve is typically connected to a group of muscle fibers, known as a motor unit. The interface between the axon and the fiber is known as a neuromuscular junction.

When an action potential reaches a neuromuscular junction, a neurotransmitter called acetylcholine is released into the muscle. Acetylcholine stimulates the muscle fibers to create an action potential of their own by opening the fiber sodium channels. This action potential propagates along the sarcolemma, from the neuromuscular junction outwards and throughout the muscle in the same manner as the neuronal action potential.

2.2.6 Artificial initiation of action potentials

Cell membranes can be artificially depolarised by an applied source of electrical potential. This potential is provided via electrodes placed in the extracellular space near the tissue to be excited. Ideally, electrodes would be placed inside the target cells to localise stimulation. Practically, the technology doesn't exist to interface individually with large numbers of single axons or muscle fibers in this way.

Sufficient depolarisation will initiate an action potential. Hyperpolarisation can prevent action potentials from propagating. Sub-threshold stimulation has no lasting effect on membrane potential (see Fig. 2.7).

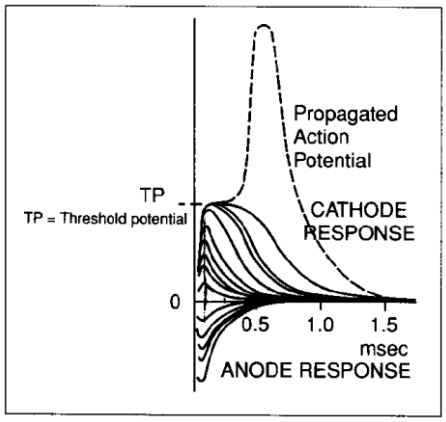

Figure 2.7: **Illustration of the effects of applied potentials. Only applied potentials above the threshold initiate an action potential. Note that the vertical axis has the resting membrane potential as reference.** (Geddes 1994)

Skeletal muscles can be stimulated indirectly, by depolarising the supplying nerve cells. Alternatively they can be directly stimulated by depolarising the muscle fibers themselves.

2.2.7 Twitch vs. tetanic force

Muscles respond to an action potential with a contraction, immediately followed by relaxation. This is known as a twitch. The peak force of this twitch is proportional to the number of fibers responding to the action potential.

If a second action potential passes through the muscle before it has completely relaxed, the force output will be increased above the previous peak value. This is known as twitch summation. If sufficient twitches are summed, the output force will stabilise. This is known as a tetanic contraction (see Fig. 2.8).

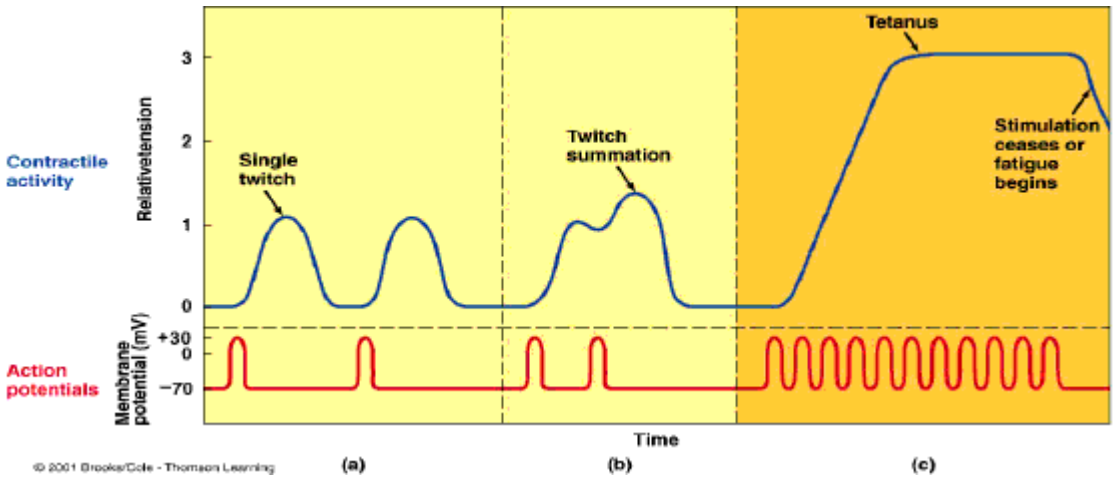

Figure 2.8: **Force output of a muscle in relation to applied action potentials, with a) Twitch type contractions; b) Twitch summation; c) Tetanic type contraction.** (Sherwood 2001)

2.3 Review of chronaxie and rheobase

2.3.1 A brief history

The exact origin of electrophysiology is unclear. Connections between electricity and functioning of the human body had been studied at least as early as 1740. Some researchers of the time had even reported that electricity could initiate muscular contractions. The link was disputed by many prominent physiologists however, and the theory of electrical excitation was not very popular at that time (Kipnis 1987).

Whether deserving or not, Luigi Galvani is generally credited with pioneering the field. He discovered that a frog's leg in a nerve muscle preparation would twitch if connected to a metal arc. The metal arc was usually made up of two different metals. He famously first became aware of the phenomenon in 1786 when he decided to hang a number of frogs corpses from the iron railing of his balcony using copper hooks. While it's not clear why he decided to do this, the frogs "gave him a lively display of step-dancing". This kicked off the study of not only electrophysiology but of some of the most important modern concepts of electricity itself (Gillespie 1932).

Early experiments were limited by both workers' knowledge of electricity and the devices by which to accurately use it. Researchers most commonly used a combination of a static electricity generator and the Leyden jar (the first capacitor) to apply electrical pulses to numerous living tissues. Difficulty arose in creating stimuli with known parameters using this apparatus and results were more qualitative than quantitative (Geddes 1994).

One of the first accepted laws of excitation was developed in 1849 (Du Bois-Reymond 1849). It had been observed that the duration of the applied current had no effect on the magnitude required for stimulation. Also observed was that an applied current magnitude, which would normally cause excitation if switched on instantly, would not cause contraction if raised to that magnitude gradually. He proposed that excitation was primarily a function of the rate of increasing current. This implied excitation occurred only at the initiation of a direct current.

Du Bois Reymond's law was first challenged 15 years later (Fick 1863). It was observed that current duration did have a previously unnoticed effect. The effect became apparent when the duration was decreased to below a certain value; the smallest current magnitude required to cause excitation increased. This put the focus on stimulating currents of short duration, and hence the relationship between duration and current magnitude. These short currents are referred to as pulses.

2.3.2 The strength-duration curve: a quantitative description of excitability

One of the most prominent researchers to take note of Galvani's work was Alessandro Volta. Galvani had proposed that electricity was created inside an animal. Contraction occurred when it was allowed to pass from nerve to muscle. Volta saw an animal more as a kind of electrical measuring device, with the electricity being generated by the contact of the dissimilar metals. In 1800 he duplicated the effect by layering discs of copper and zinc, separating each pair from the next by saline-moistened cardboard. This arrangement, known as the Voltaic pile, was the first electrochemical cell (Mauro 1969).

Voltage levels could be set by electrochemical cells connected in series. Finer control came with the introduction of the rheocord (the first potentiometer) by Wheatstone in 1843. Despite these discoveries, it was only in 1881 that d'Arsonval suggested these voltages could be used to charge capacitors to known levels, hence creating quantitative stimulators (Geddes 1994).

This arrangement was used by Hoorweg to conduct the first quantitative study of electrical excitability, using the capacitor discharges as stimulating pulses (Hoorweg 1892). He plotted the minimum capacitor voltage required to produce excitation for a number of pulse durations. He also plotted the delivered charge and energy of each pulse against the pulse duration. This type of plot is now known as a strength-duration curve (see Fig. 2.9).

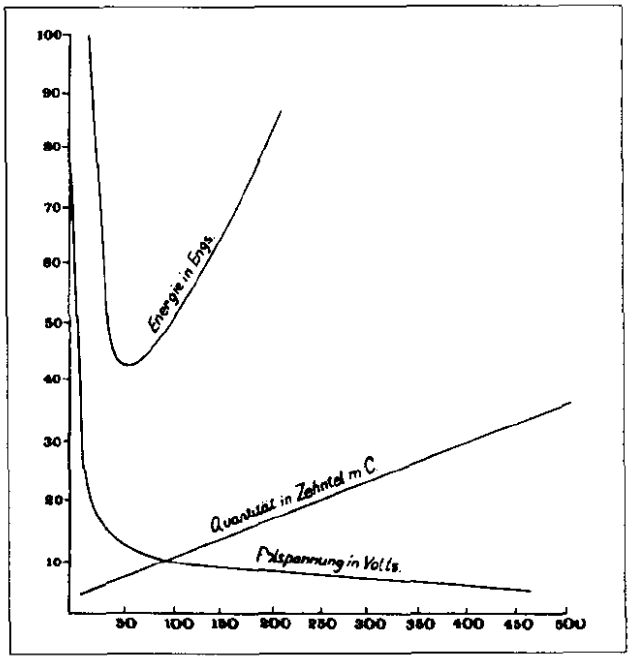

Figure 2.9: **A print of Hoorweg's original strength-duration curve. "Polspannung in Volts" refers to pulse amplitude (in volts). "Energie in Engs" refers to energy. "Quantität in Zehntel mC" refers to total charge transferred.** (Geddes 1994)

2.3.3 An empirical model of exciting stimuli

To keep track of the new developments in stimulating technology the Commission International du Parc-aux-Prince charged a man named George Weiss to produce a report on the devices in use. The report was intended to classify and compare the various devices so that the experimental results would be more meaningful. Specifically to be addressed was a means to accurately quantify the currents of short duration (Irnich 2002).

Weiss realised that it still wasn't clear by what mechanism or electrical property excitation was actually occurring. He launched an investigation into the matter and conducted an excitation study of his own. His apparatus was an ingenious combination of capacitor discharges controlled by pencils, string and an air rifle. He applied constant current pulses to frog, toad and turtle muscles. He proposed a new fundamental law of stimulation in 1901, which was the first general expression for the requirements of a stimulus:

$$Q = a + bt \tag{2}$$

Where Q was the charge delivered by a minimally exciting pulse, t was the pulse duration and a and b were constants and had to be determined experimentally for each tissue and stimulating apparatus combination. He also showed that there was a particular t that provided a minimum of delivered energy (Weiss 1901).

A similar, but better known, stimulus expression was developed by a researcher named Louis Lapicque. The expression first appeared in a thesis on the subject written by Lapicque's wife and supervised by him (Geddes 1994). She used capacitor discharges to stimulate frog, crab and sea slug muscles. The expression she obtained was:

$$V = \frac{k}{C} + bR \tag{3}$$

Where V was the voltage on the capacitor, C was the capacitance, R was the resistance of the circuit and b and k were constants.

When arranged using Ohm's law the expression for pulse current I becomes:

$$I = \frac{k}{RC} + b \tag{4}$$

The time constant RC of the stimulator was considered to be the duration of the stimulus, making this expression nearly identical to the expression obtained by Weiss. Lapicque's most well-known contribution, however, was the introduction of two new terms defining these curves and giving meaning to the constants in them (Irnich 2010).

The first term, rheobase, is the minimum current magnitude required to cause excitation if applied for an infinite duration. In other words, it is the horizontal asymptote of the strength-duration curve (see Fig. 2.10). The second term, chronaxie, is the minimum pulse duration required to cause excitation for a current magnitude of twice the rheobase (Lapicque 1909).

The law of stimulation in terms of these characteristics is expressed as:

$$I = r\left(1 + \frac{c}{t}\right) \tag{5}$$

Where r is the rheobase current and c is the chronaxie time, both being dependant on the tissue and experimental conditions.

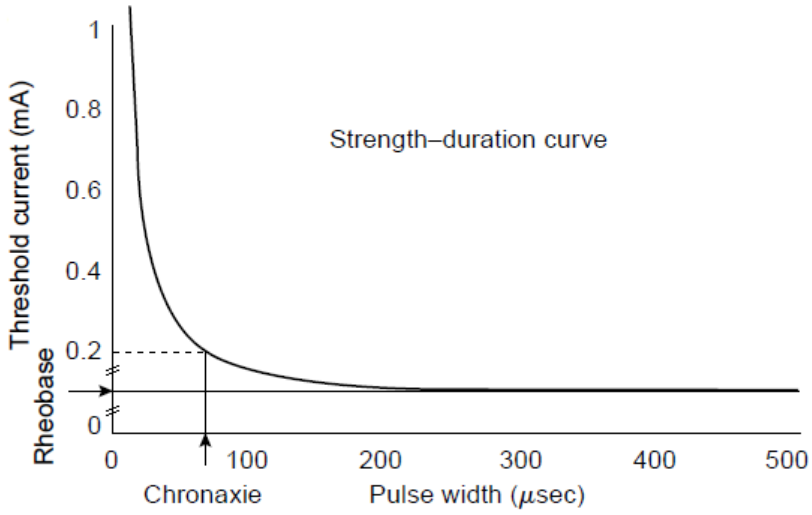

Figure 2.10: A strength-duration curve with rheobase and chronaxie values indicated. (Durand 2006)

2.3.4 Chronaxie today

The chronaxie and rheobase values are still used today. These parameters allow for quantitative comparisons of excitability. Comparisons include different tissues or changes in experimental conditions. They are also important in the design of clinical stimulators, whether for rehabilitation or restoration of function. Both values are required to accurately characterise the strength-duration curve of a particular tissue, hence also for effective stimulation of that tissue.

Lapicque didn't consider the rheobase of much importance. He also mentioned that its calculation was inevitably imprecise as the value was approached asymptotically. However, inaccuracies in rheobase determination will, by definition, lead to inaccuracies in chronaxie determination.

Rheobase also has its role in the design of stimulating devices. To excite a certain tissue, the device must be able to produce current pulses of magnitude at least equal to the rheobase of that tissue. Conversely, if stimulation of certain tissue needs to be avoided, the current of the stimulating pulses should not exceed the rheobase of that tissue. The latter could be for safety considerations, comfort of the patient (e.g. avoidance of sensory nerves) or precise control, in the case of functional stimulation (Irnich 2010).

Chronaxie is generally considered to be the true measure of excitability. It represents the strength-duration curve in the same way the time constant (RC) represents a capacitor-resistor circuit. In addition, while Lapicque gave no reason for choosing his definition of chronaxie, it was later shown to be the pulse width corresponding to the stimulus of least energy (Geddes & Bourland 1985).

The strength-duration curve also identifies the total charge delivered at each pulse width. This plays an important role in the case of battery operated implantable stimulators, where charge output might need to be minimised (Geddes 2004). Finally the curve completely describes the minimal current needed to elicit a response at any chosen pulse width. Minimising stimulating pulses is beneficial to any receiving patient as excess current has been shown to cause tissue damage (see Section 3.2.2.3).

As expected, the importance of the chronaxie has led to many studies attempting to determine and record it for various tissues. Despite this, the variability of the recorded values for each tissue is relatively large (Geddes 2004). An example of this is the chronaxie values for human denervated skeletal muscle at body temperature. The values range from 9.5 to 30 ms, a ratio of 3.16 (Ritchie 1944). Another example is mammalian ventricles at body temperature. These values range from 0.5 ms to 4.1 ms, a ratio of 8.2 (Geddes 1999). Earlier studies resulted in even more variability, with some values being recording with orders of magnitude difference (Watts 1924).

2.3.5 Healthy vs. denervated muscle

The variation in chronaxie determination is particularly noticeable in a range of studies comparing directly stimulated healthy and denervated muscle. This is to track how excitability of a skeletal muscle changes after denervation.

The first study comparing these two tissues in terms of their chronaxie and rheobase values was done by Watts (1924). He found a slight increase in rheobase, with no change in chronaxie. A similar study by De Smedt (1950) reported that rheobase decreased, but chronaxie increased; a seemingly contradictory result. Soon after Nicholls (1956) confirmed the reported decrease in rheobase, however he couldn't account for the increased chronaxie.

More recently a study was done by Ashley et al. (2005) who found no permanent change in rheobase and a 3-fold increase in chronaxie. The change in chronaxie was observed soon (1 to 2 weeks) after denervation and remained stable throughout the rest of the denervation period (24 weeks). A similar study by Adami et al. (2007) reported a 5-fold increase in chronaxie after 2 days, a 100- to 200-fold increase after a month and found some muscles completely unresponsive after 6 months.

It is generally accepted that more current is required to stimulate denervated muscle (A. Eberstein & S. Eberstein 1996; Salmons et al. 2005). However, quantitative results regarding the chronaxie and rheobase values are not conclusive.

2.4 Summary and conclusions

The basic unit of contraction is a muscle twitch, from which all other types of contraction are produced. A single twitch is the end result of the propagation of a single action potential, first through the motor nerve and then through the muscle fibers themselves. The action potential is an all-or-nothing event, initiated when the potential difference across the cell membrane exceeds, or is depolarised beyond, a certain threshold.

Muscle contraction can be artificially initiated by the correct application of an external source of potential. Such a source can be used to depolarise a section of the nerve-muscle complex, and hence cause an action potential to be propagated. This is known as electrical stimulation. Muscles can be indirectly stimulated, via depolarisation of the supplying nerve cells. They can also be directly stimulated, by depolarising the muscle fibers themselves.

Whether an applied current pulse is effective in stimulating a particular muscle or nerve is a function of the magnitude and duration of that pulse. The minimum current magnitude, for a given duration, required to cause such stimulation is plotted on a strength-duration curve. This curve can be completely described by two values; the chronaxie and the rheobase. These values vary between different muscles and nerves, and can therefore be considered to characterise the sensitivity of a tissue to electrical stimulation. This sensitivity is known as excitability.

Knowledge of the excitability of a muscle is critical to effective stimulation of that muscle. However, excitability is not always easy to determine. This is particularly true for directly stimulated skeletal muscles, and more so when the muscles are denervated. This indicates that extra measures may be required to improve accuracy of chronaxie and rheobase determination for both healthy and denervated skeletal muscle.

Chapter 3: Experimental considerations

3.1 Introduction

Many factors influence the measured excitability of experimentally stimulated muscles. As knowledge of muscle stimulation increases, known factors and their effects are documented. This chapter reviews these factors.

The chapter is broken into two main categories: factors relating to the muscle itself and factors relating to how the muscle is stimulated.

3.2 Muscle acquisition

3.2.1 Introduction

Muscles are complex biological structures, no two are quite alike. Excitability of a muscle can vary as a function of the specific muscle, the animal species and external factors such as temperature. Careful choice of muscle, as well as maintenance of the conditions under which it's stimulated, can help reduce variability in excitability experiments.

3.2.2 Muscle characteristics

3.2.2.1 Muscle chosen

Ideally individual muscle fibers should be tested in studies of their excitability. However there is a high risk of damage to the tissue especially during dissociation of long fibers (Bekoff & Betz 1977). For this reason, whole muscles are almost always used.

Muscles from the limbs are commonly chosen. These muscles are relatively long and their fibers are generally parallel. This allows for better control of electrode placement relative to the muscle. Their simple structure also makes monitoring of response easier. Often these muscles are denervated unilaterally: one limb is denervated while the other is unaffected. This allows for a direct comparison, reducing variability between subjects.

Typical examples of chosen muscles are extensor digitorum longus (Nicholls 1956), tibialis anterior (Ashley et al. 2005) and sartorius (Lucas 1907c; Watts 1924).

3.2.2.2 Animal model

Excitable tissues from a wide variety of animals have been used in experiments inducing electrical stimulation. The list includes lizards, turtles, geese, canaries, dogs, lobsters, goats, pigs, chickens within eggs and many others (Von Humboldt & Holl 2009).

By far the most common animal used in early studies of excitation was the frog. However, it has been shown that frog muscle could not be directly compared to that of humans (Conrad et al. 1936). Frog muscle is largely resistive, and has almost none of the capacitive element of human muscle (see Section 2.2.3). Recent studies have favoured using small mammals as test subjects, for example rats (Jung et al. 2009) or rabbits (Ashley et al. 2005).

3.2.3 Denervation of muscle

3.2.3.1 Procedure

Denervation of skeletal muscles is achieved by disruption of the nerve supplying it. The most effective way of achieving this is complete division of the nerve, also known as neurotmesis. Under normal circumstances, recovery practically never occurs (Seddon 1942).

While rare, it is possible for nerves to regenerate and reinnervate muscles. This is especially true if the nerve is surgically severed and there are no obstructions caused by damage to the surrounding tissue. To prevent this nerves are typically sectioned, with at least 1 cm of nerve removed. The nerve stumps are then ligated to prevent growth.

3.2.3.2 Denervation effects

The most noticeable effect of denervation is reduction in the size of the muscle, also known as atrophy. This includes a significant reduction in mass and cross sectional area. The reduction varies depending on the muscle (Midrio 2006). In rats, the mass has been shown to decrease by 82% and cross sectional area by 97% over a period of about 24-40 weeks. The most dramatic decrease in mass (a decrease of about 50%) occurs over the first 2 weeks (Pellegrino 1963). This is due to both reduction in fiber size, and reduction in number of fibers within the muscle (Gutmann & Zelena 1962).

In the case of electrical stimulation, atrophy has been suggested to lead to increased shunting of the current; with smaller muscles, proportionally more current flows through the extracellular fluid and other surrounding tissue (Nicholls 1956). This is especially true when external electrodes are used.

The force generating capabilities of denervated muscles are significantly reduced (Midrio 2006). The most commonly reported effect is a slowing of the contraction speed. This effect is not always permanent; in the rat the contraction time partially recovers after about 3 weeks, regardless of activity. Peak tetanic and twitch force are also noticeably reduced. Twitch force decreases proportionally to the rate of atrophy, and is considered a result of loss in contractile machinery (Finol et al. 1981).

Tetanic force decreases exponentially soon after denervation, particularly in the soleus muscle of the rat (Al-Amood & Lewis 1989). The maximum tetanic force of rat muscle has been shown to decrease by 98% in about 8 weeks (Carlson et al. 1996). The drop in tetanic force is attributed to the drop in twitch force and the reduction in maximum twitch frequency, due to the slower contraction speed (Kotsias & Muchnik 1987).

Most of the physiological changes in the muscle occur 30-40 hours after denervation (Thesleff 1974). The resting membrane potential increases by about 15 mV (to about -60 mV). There is also a complete degeneration of the neuromuscular junctions, which has been shown to take between 30 and 70 hours (Gutmann & Zelena 1962).

The rate of polarisation and depolarisation is decreased, leading to prolonged action potential duration. This can be explained by a doubling of the transmembrane resistance with no change in the transmembrane capacitance, therefore increasing the time constant. This has been suggested to account for the change in contraction time (Lewis 1972).

An important factor to consider is the length of time between section of the nerve and testing of the muscle, or the denervation period. Denervation periods in other studies range from 15 (Nicholls 1956) to 365 days (Adami et al. 2007). In almost all cases the minimum period is 21 days (3 weeks). Longer periods improve the likelihood of including all of the possible effects due to denervation.

3.2.4 External factors

3.2.4.1 Tissue bath

Muscles are typically stored in a tissue bath. The bath is usually made of a non-conductive and non-reactive material, e.g. glass. It is usually filled with Ringer's solution (Lapicque 1931b). This solution imitates the physiological conditions inside the body. It was originally proposed to maintain contractility in the heart but has since become a standard physiological solution for a variety of studies (Miller 2004). The standard composition is described by Ringer as a mixture of 100 c.c. saline, 5 c.c. sodium bicarbonate, 5 c.c. calcium chloride and 1 c.c. potassium chloride (Ringer 1883).

3.2.4.2 Temperature

Temperature can be controlled *in vitro*, and is often kept at approximately blood temperature via monitoring of the bathing fluid. The temperature of *In vivo* experiments, however, must be estimated.

One key difference between healthy and denervated muscle is the blood flow, particularly during exercise. While the temperature of a healthy muscle may drop due to external conditions, it is immediately raised following the great influx of blood during even the slightest activity. Although denervated muscle has a higher resting blood flow, there is no increase during activity. Therefore, unless special precautions are taken, it is unlikely denervated muscles will be at the same temperature as their healthy counterparts (Doupe 1943).

The effects of temperature on excitability were first observed by (Gotch & Macdonald 1896). They showed that a decrease in temperature resulted in an increase in excitability of muscle. While this was true regardless of pulse duration in muscle, the effect was different in nerves. When stimulating nervous tissue, a decrease in temperature increased excitability to pulses of long duration, but decreased excitability to pulses of short duration. This was later confirmed by (Lucas & Mines 1907), with the changes shown to be continuous.

3.3 Muscle stimulation

3.3.1 Introduction

The manner of charge delivery affects the muscle response. Charge delivery occurs at the electrode-tissue interface. Factors affecting charge delivery include, but are not limited to, electrode material, electrode arrangement and stimulation pulse shape. Consideration of these factors allows for effective stimulation. It also limits permanent changes, or damage, to the muscle and electrodes.

3.3.2 Electrode-tissue interface

3.3.2.1 Mechanism of charge transfer

The electrodes and the physiological medium use different charge carriers. In the metal electrodes and surrounding circuitry, charge is carried by electrons. In the physiological medium, an electrolyte,

the charge is carried by ions. When stimulating muscle or nerve, the physiological medium is the extracellular fluid. In this case, the charge is typically carried by sodium (Na^+), potassium (K^+) and chloride (Cl^-) ions.

When the electrodes and the physiological medium come into contact, an interface is formed between them. There are two ways charge can be transferred across the interface. One is a non-Faradaic reaction, which means no electrons are transferred. This results in redistribution of charged chemical species within the physiological medium. The other is through a Faradaic reaction, where electrons are transferred. This results in reduction and oxidation of the chemical species within the medium.

3.3.2.2 A circuit model of the electrode interface

In the case of non-Faradaic charge transfer, the interface can be modelled as a simple capacitor. In the case of Faradaic reactions the interface is modelled as Faradaic impedance. The two mechanisms are mutually exclusive and are modelled as parallel components. The total current flow is therefore the sum of the current through each branch:

$$i_{total} = i_C + i_F \tag{6}$$

where i_C is the capacitive current and i_F is the Faradaic current.

If the electrochemical potentials of two phases are unequal when they are brought into contact, electron transfer will take place until equilibrium is achieved. At this equilibrium each phase has a certain electrical potential in the bulk of that phase. This potential is known as the inner potential ϕ. The difference between the inner electrical potentials of the phases is known as the electrode interfacial potential $\Delta\phi$.

The full circuit model of the electrode interface is shown in Fig. 3.1:

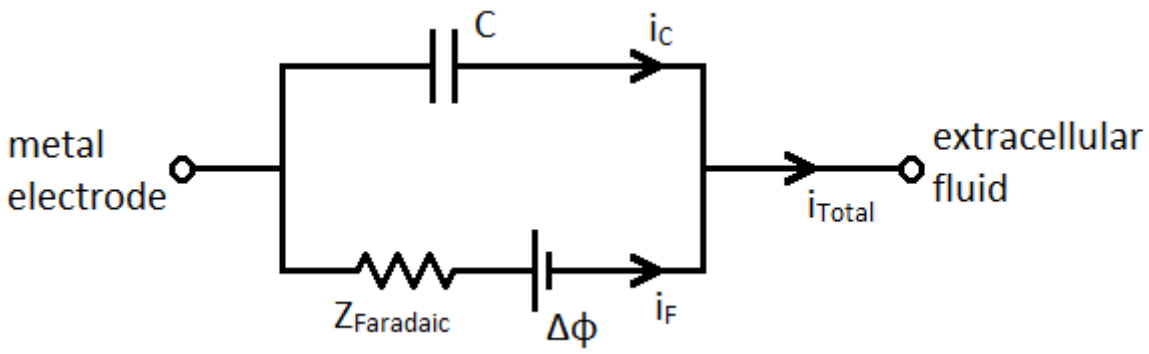

Figure 3.1: **Circuit model of the electrode-tissue interface, where i_C = non-Faradaic current, C = capacitance in the non-Faradaic branch, i_F = Faradaic current, $Z_{Faradaic}$ = Faradaic impedance, $\Delta\phi$ = electrode interfacial potential and i_{Total} = total current.** (Merrill et al. 2005)

If the potential of an electrode is shifted from its equilibrium value, the electrode is said to be polarised. Polarisation is measured by the difference between the electrode's potential and its equilibrium potential. This is measure is known as overpotential. Faradaic current increases exponentially with overpotential (Bard & L. R. Faulkner 1980).

If the overpotential is relatively small, current flows primarily through the capacitive branch of the interface circuit. As more charge is delivered across the interface, more charge is stored by the capacitor, which increases the overpotential and hence increases the proportion of Faradaic current relative to capacitive current.

3.3.2.3 Tissue and electrode damage

Non-Faradaic charge redistribution as a result of an applied voltage across the electrode can be completely reversed if the applied voltage is also reversed. The charge stored on the capacitor can be fully recovered in this way.

Faradaic charge transfer as a result of an applied voltage causes reduction (the addition of electrons) at the cathode, and oxidation (the removal of electrons) at the anode. As a result, chemical products are formed in the solution. The total mass of the products formed is directly proportional to the charge delivered by Faradaic reactions.

If these products diffuse away from the electrode, the charge cannot be recovered by reversing the applied voltage. Therefore there is a net change in the chemical environment. This is known as an irreversible Faradaic reaction.

Changes to the chemical environment of the physiological medium can potentially be harmful to the tissue or damaging to the electrodes. Electrical stimulation devices should therefore always be designed to avoid irreversible Faradaic reactions. This can be achieved by reducing the total charge transferred and by reducing the proportion of total charge transferred by Faradaic reaction (i.e. reducing the current in the Faradaic branch of the electrode circuit model).

3.3.3 Electrodes

3.3.3.1 Electrode material

Capacitance C can be defined according to the formula:

$$C = A\left(\frac{C}{A}\right) \tag{7}$$

where A is the cross sectional area of the capacitor. Capacitance per area $\left(\frac{C}{A}\right)$ is a property of the electrode used, referred to as intrinsic capacitance. A high capacitance means that relatively more charge can be stored for a given change in potential across that capacitor:

$$C \equiv \frac{dQ}{dV} \tag{8}$$

where q is stored charge and V is potential difference. Therefore a stimulating electrode with a large area and high intrinsic capacitance can transfer more charge through non-Faradaic redistribution at a given overpotential.

Besides providing relatively high intrinsic capacitance, electrode materials should also be biocompatible. This means they should not result in adverse effects or excessive immune response when in contact with the tissue.

Platinum (Chouard et al. 1995; Majji et al. 1999) and stainless steel (Babb & Kupfer 1984) are examples of non-toxic materials and are both commonly used as stimulating electrodes. Platinum has better intrinsic capacitance, but is relatively soft. Stainless steel is stronger and therefore more commonly used for intramuscular stimulation (Merrill et al. 2005). Teflon, which has also been shown to be biocompatible (S. S. Stensaas & L. J. Stensaas 1978), can be used as a coating to reduce corrosion. Many early studies used silver electrodes which have now been shown to be toxic and result in necrosis, even without applied current (Fisher et al. 1961).

3.3.3.2 Electrode arrangement

At least two electrodes are required to complete the circuit for charge conduction. One electrode is the stimulating electrode while the other acts as a reference.

When electrodes are submerged in Ringer's solution they are known as fluid electrodes (Lucas 1907a). Submersion has been found to be necessary for direct stimulation of the muscle (Lapicque 1931b).

If the reference electrode is relatively far from the intended stimulation site, the configuration is known as monopolar. If the reference electrode is relatively near the configuration is known as bipolar. Bipolar configurations require more current to achieve stimulation when fluid electrodes are used, although the difference is small (Follett & Mann 1986). Bipolar stimulation provides more localised current and hence better control over the stimulation site (Durand 2006).

Muscle fibers in an electric field are excited proportionally to the component of the field in the direction of the muscle (Rushton 1927). Therefore, electrodes in a bipolar configuration will be most effective if the line connecting the two conducting ends is parallel to the muscle fiber.

3.3.4 Stimulation pulse

3.3.4.1 Constant-current vs. constant-voltage pulses

Chronaxie and rheobase are defined as parameters of a strength-duration curve determined using constant-current pulses (Lapicque 1909). Despite this, both constant-current and constant-voltage pulses have been used to determine these parameters (Ranck 1975). The impedance of the electrode-tissue interface has been shown to vary with stimulation voltage and frequency (Bard & L. R. Faulkner 1980), however, and results from the two types of pulses are not directly comparable.

If constant-voltage pulses are used, chronaxie and rheobase must be estimated. The estimations can be made to within 6% of the corresponding constant-current values, if the load impedance is assumed to increase linearly with pulse width (Holsheimer et al. 2000).

The electrode discharge during constant-voltage pulsing is rapid compared to constant-current pulsing. Unrecoverable charge accumulation is therefore lower during interpulse intervals when using constant-voltage stimulation (Merrill et al. 2005).

3.3.4.2 Monophasic vs. biphasic pulsing

The traditional square constant-current pulse that is used to define the strength-duration curve is known as a monophasic pulse. The pulse is defined by its magnitude and pulse width. Stimulation is more effectively achieved with a cathodic pulse, although the same effect can be achieved with anodic pulses at higher current (Durand 2006).

If the capacitive branch of the electrode is not given sufficient time to discharge between monophasic pulses, charge can accumulate and subsequent pulses will have greater overpotentials. This can be prevented by discharging the electrode directly after the stimulating pulse with an equal but opposite pulse. This is known as biphasic stimulation (see Fig. 3.2).

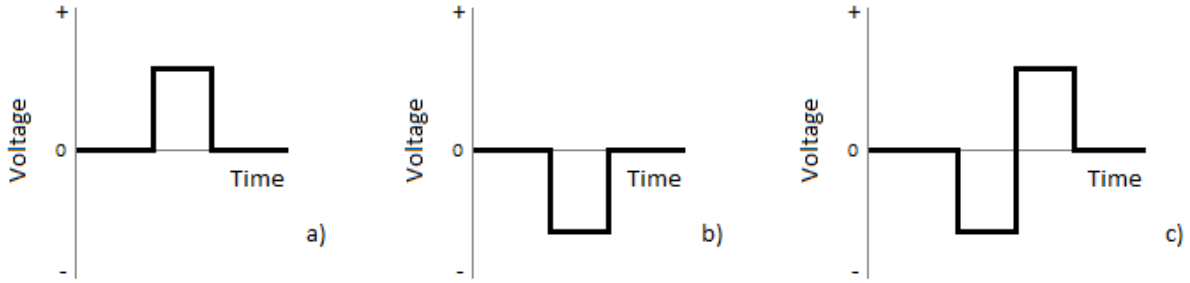

Figure 3.2: **Different current pulses at the stimulating electrode: a) anodic pulse; b) cathodic pulse; c) biphasic pulse, (cathodic followed by anodic).**

Loss of excitability and tissue damage as a result of monophasic stimulation was demonstrated by Lilly et al (Lilly et al. 1952). When using biphasic stimulation, no such effects were reported (Lilly et al. 1955). The greater damaging effect of monophasic compared to biphasic pulsing has since been confirmed in multiple studies (J. T. Mortimer et al. 1970; Pudenz, Bullara, Dru, et al. 1975; Pudenz, Bullara, Jacques, et al. 1975).

3.3.5 Excitable substances within the nerve muscle complex

Lucas was the first to observe different excitabilities within the nerve muscle complex (Lucas 1907b). He made this discovery before the term chronaxie was invented. Instead, he used the pulse width that corresponded to the least delivered energy as a measure of excitability. This was later shown to be equivalent to chronaxie (see Section 2.3.4).

Lucas found three distinct excitabilities. He attributed them to different substances within the muscle itself (Lucas 1907c). He named the substances α, β and γ. The α substance was found to be the least excitable, having the largest chronaxie. It was suggested to be the muscle itself. The γ substance was more excitable and was suggested to be the nerve innervating the muscle, including intramuscular nerve twigs.

The β substance was the most excitable of the three, and was suggested to belong to the link between nerve and muscle. This substance is now known as the neuromuscular junction, or motor end plate. Most mammalian muscles are focally innervated, meaning they have single neuromuscular junctions near their centres (Engel 2008).

Lucas's results were initially opposed, and the different excitabilities were attributed to experimental error (Lapicque 1931a). However, their presence was later confirmed (Rushton 1930). Rushton also showed that they likely corresponded to the muscle fibers (Rushton 1932a) and motor nerves (Rushton 1932b).

3.4 Summary and conclusions

Excitabilities of muscles vary between different animal species, different subjects of the same species and even different muscles within a particular subject. If denervated, excitability of a given muscle also varies with time.

An appropriate animal model needs to be chosen, preferably mammalian. This increases comparability of results to those of human muscles. A specific muscle also needs to be chosen. The muscle should be relatively large and composed of uniform fibers. Ideally such a muscle should have a symmetrical counterpart within the body, to allow unilateral denervation.

If muscles are removed from the body, they should be stored (and stimulated) in Ringer's solution. This solution maintains muscle integrity and function by mimicking bodily fluids normally surrounding muscles within the body. Muscles should also be stimulated at a known temperature. Ideally this temperature should be close to normal body temperature (i.e. 36.5^{o} C). This further replicates the muscles' typical environment within the body.

Tissue and electrode damage are both proportional to the overpotential of the electrode. Minimising overpotential is therefore important when considering the experimental design. Overpotential increases with the total charge stored capacitively by the electrode. This can be reduced by minimising the stimulating current. The electrode should also be discharged between current pulses to reduce excess charge accumulation. Electrodes can also be chosen such that they have a high capacitance, thus reducing the potential for a given stored charge. This includes choosing electrodes that have a large cross-sectional area and high intrinsic capacitance (a function of the electrode material).

Excitability of a muscle can vary depending on where the charge is injected. This is likely due to different tissues within the muscle itself. Care should be taken to ensure that muscle fibers are being stimulated and not intramuscular nerves or neuromuscular junctions. These junctions are typically located in the centre of mammalian skeletal muscle, and can be avoided by careful placement of the electrodes.

Both the nerves and neuromuscular junctions are more excitable (i.e. they require less current to excite), and proximity is not enough to guarantee muscle fiber stimulation. Therefore, current should also be localised. This can be achieved with a bipolar configuration, particularly if oriented in the direction of the fibers. The electrodes should also ideally have a small cross-sectional area, contradicting the larger area required for high capacitance.

Despite knowledge of these sources of experimental variation explaining many previous inconclusive results, the exact values of chronaxie and rheobase are still not clear. This suggests that other sources of variation exist.

Chapter 4: Muscle response

4.1 Introduction

The way in which the muscle response is discerned is a potential source of variation in any excitability experiment. Different methods of detection have been used and are reviewed in this chapter.

Signal processing techniques have been used in many fields to isolate and enhance information in digital signals. Different signal processing techniques are reviewed. Particular attention is given to empirical mode decomposition (EMD), which is proposed as a method of reducing variability in twitch detection.

4.2 Twitch detection

4.2.1 Initial response

A muscle is composed of multiple individually excitable fibers. Contraction force of the muscle is increased by stimulating (recruiting) more fibers. The initial response of the muscle can be defined as the moment when the first discrete unit of recruitment is stimulated.

When a muscle is stimulated via its motor nerve, the smallest unit that can be recruited is the motor unit. The number of muscle fibers in a motor unit can vary depending on the muscle (English et al. 1993). The soleus muscle of the rat, for example, has between 84 and 161 fibers in a unit (Chamberlain & Lewis 1989). The largest motor units are preferentially stimulated by external currents (McNeal 1976). Therefore, minimal response to stimulation of a motor nerve can be discerned relatively easily (Powers et al. 1978).

When muscle fiber is stimulated directly, the smallest unit is the individual muscle fiber. Therefore, accurately determining the first response is more difficult. Difficulty in detection of twitches is exacerbated by denervation atrophy, due to the reduction in produced force and contraction speed (see Section 3.1.2.2).

4.2.2 Method of detection

The strength-duration curve describes the minimum current parameters required for initiating a response. Ideally, the response should be identified by observation of the generated action potential as it propagates through the tissue of interest. In the case of muscle stimulation this would involve recording the action potential within a single fiber. In an intact muscle, however, this is nearly impossible.

Most studies detect stimulation indirectly by observing (Jung et al. 2009) or palpating the muscle (Ashley et al. 2005; Adami et al. 2007). These methods rely on judgement from the researchers and are thus subjective, with potential to introduce bias. They are also inevitably imprecise, particularly if the contraction being detected is small (Doupe 1943).

4.2.3 Other methods

To quantify the muscle response, some studies have recorded the force output over time, using mechanical (Doupe 1943) or electrical (Jung et al. 2009) transducers. In these cases a threshold was applied to the output. Any force in excess of the threshold was classified as a muscular contraction (or twitch). The threshold value, however, was either not described or was chosen subjectively.

Jung et al. (2009) compared detection by their threshold with detection by visual observation. The results were highly correlated. The most noteworthy difference was the relative simplicity of the latter. This may explain why the threshold technique was abandoned.

Alternatively, instead of a minimum response, strength-duration curves have been described in terms of a so-called bulk response. Minimum current duration and strength required to elicit a certain percentage of the maximum response are plotted. This technique was first used to compare excitability of human nerves (Powers et al. 1978) and later for directly stimulated muscles (Dennis & Dow 2007).

To determine the maximum response a supra-maximal current pulse is required. This is a current pulse for which a significant increase in amplitude results in no change in response magnitude. Excess current can lead to tissue and electrode damage (see Section 3.2.2.3), which could be considered unacceptable for human patients. This is particularly true for long term stimulators, where stimulation parameters might need to be recalculated regularly.

4.2.4 Spike sorting

Detecting the response of a muscle using a force transducer output is similar to detecting action potentials using extracellular electrodes. This is the first step in a process known as spike sorting. Spike sorting differentiates and classifies these action potential spikes from the background noise and each other.

Manual spike sorting, or spike sorting by inspection, has been shown to lead to a high number of misclassifications (Wood et al. 2004). Spike sorting is therefore almost always done algorithmically, after the signal from the electrodes has been digitised.

The first step in spike sorting is to de-noise the signal (see Section 4.3). Spikes are then typically classified by comparison to a threshold (Lewicki 1998). This threshold is commonly based on the variation in the noise (see Section 5.6.1). Noise variation can be estimated, or calculated from a known noise-only signal (see Section 5.5.3).

An example of such a threshold is given by:

$$\lambda_{std} = \bar{x} + d\left(\frac{1}{N-1}\sum_{n=1}^{N}(x(n)-\bar{x})^2\right)^{\frac{1}{2}} \quad (9)$$

where d is a constant, $x(n)$ is the value of the noise-only signal at a sample n, N is the total number of samples and $\bar{x}$ is the mean of the signal. This threshold represents the mean plus a multiple (d) of the standard deviation of the signal. This threshold was first proposed by Di Fabio (1987) and is commonly used in studies of EMG events, with d typically set to 2.

Spike sorting methods also include spike feature and shape analysis. Examples include comparison of manually chosen features (such as spike height and width), principal component analysis (see Section 4.3.3.1) and template matching. Template matching has been reported to provide the highest classification accuracy of these techniques (Wheeler & Heetderks 1982). Template matching essentially compares each spike to a pre-determined spike template. This template can be obtained from a database, or derived from the test data (see Section 6.4.1).

4.3 Signal de-noising

4.3.1 Definition of noise

Measured data is divided into useful signal and noise. Noise is an unwanted by-product of other activities and distorts the useful signal. Measured data can thus be represented as:

$$S(t) = x(t) + n(t) \tag{10}$$

where $x(t)$ is the desired signal and $n(t)$ is noise.

Noise that is concentrated in a particular frequency band is known as coloured noise. Noise that is spread relatively equally over the frequency spectrum (i.e. its power spectral density is flat) is known as white noise. White noise is prevalent in all electrical signals (Agarwal & Tsoukalas 2007).

Common types of noise include low frequency signal "drift", narrow spikes known as "salt and pepper" noise, mains line interference (at 50 Hz in South Africa) and thermal noise, the primary source of white noise (Tomasi 2001).

4.3.2 Noise removal strategies

Ideally sources of noise should be isolated and minimised before being measured. For example the power supply should be shielded or kept a significant distance away from the data acquisition system to prevent main line interference (Dennis & Kosnik 2002).

Once the signal is digitally recorded, filters can be used to remove noise outside of the signal frequency range without significantly altering the signal. The unaltered frequency range is known as the passband. This is the most common way of removing noise when spike sorting.

To remove noise within the passband, the signal is first decomposed into components such as linear functions. Each component is assessed for relative signal or noise content. This is typically done by comparison to a threshold. Components are then preserved, altered or set to zero based on their perceived relevant content. Finally the signal is reconstructed from the altered components (Rosas-Orea et al. 2005).

4.3.3 Decomposition

4.3.3.1 Brief overview of decomposition methods

Decomposition is a type of mathematical transformation that breaks a signal into two or more additive components. These components are so-called basis functions, specific to the type of decomposition used. Basis functions are essentially simpler signals, which usually highlight particular properties of the original signal, and hence aid in interpretation.

There are many decomposition methods, each with different basis functions. Possibly the most prominent (particularly in electrical engineering) is the Fourier transform, also known as the Fourier spectral analysis. The Fourier transform decomposes a signal into a linear combination of sine and cosine functions. These functions represent the constituent frequencies of the signal, or its frequency spectrum. Therefore, the transform can be thought of as a conversion from the time domain to the frequency domain.

The Fourier transform requires signals that are linear. Therefore, natural phenomena have to be approximated by linear systems to be fully transformed. The transform also requires stationary signals if the transform is to have significant physical meaning. This is due to the loss of time information, or loss of locality, on conversion to the frequency domain (Titchmarsh 1948).

The short term Fourier transform, also known as the spectrogram, was introduced to address the loss of locality (Haykin 1995). This method separates the signal into sections using a window function. The Fourier transform is then applied to each section. This method is popular due to its simplicity and ease of use, particularly in identification of phonetic sounds (Flanagan 1972). However, the method's effectiveness is limited by the choice of window width. Narrow windows improve time resolution but decrease frequency resolution. There is no one window size that is guaranteed to reveal all the useful information in a signal.

The wavelet transform overcomes the problem of conflicting resolutions (Graps 1995). The term wavelet refers to the finite, oscillatory window function used. The technique is similar to the short term Fourier transform, except the window width is not fixed; the wavelet is compressed and dilated throughout the transformation. The result is a variable resolution for each frequency band. This allows for non-stationary analysis and has made the transform very popular (Astaf'eva 1996).

Many different wavelet functions have been proposed (Daubechies 1992), all with their own advantages and disadvantages. However, only one wavelet function is used per transformation. The transformation is therefore not adaptive to the data. Since the transform is Fourier based, its effectiveness is also limited in nonlinear signals.

Another Fourier based method is the Wigner-Ville distribution, described in detail by Claasen and Mecklenbräuker (Claasen & Mecklenbräuker, 1980a, 1980b, 1980c). It is defined as the Fourier transform of the central covariance of the signal. While it was originally introduced to study quantum mechanics, it has since been applied to many other fields. Despite its uses, the method results in severe artefacts, known as cross terms.

The evolutionary spectrum was proposed as an expansion to the Fourier analysis (Priestley 1965). This is done by using a family of orthogonal basis functions instead of sinusoids. These functions have to be defined, but no systematic way of doing so has been offered. This limits the method to very specific applications, for example studies of earthquake data (S. C. Liu 1970).

Principal component analysis (PCA), a non-Fourier based method, seeks to convert a set of possibly correlated observed variables into uncorrelated variables (Wold et al. 1987). The components are separated by their variance, and are therefore adaptive to the data. PCA is also known as singular value decomposition or empirical orthogonal function analysis. The adaptive property of PCA has made it very popular, particularly in oceanography (Monahan 2001) and meteorology (Ogallo 1989).

Since the components are derived by their variance, they don't necessarily represent frequency information of the original signal. They are also not guaranteed to be linear or stationary, making further analysis difficult.

4.3.3.2 Empirical mode decomposition

Empirical mode decomposition (EMD) was developed specifically for analysing nonlinear and non-stationary signals (N. E. Huang et al. 1998). This describes the majority of signals, particularly those occurring from natural phenomenon.

EMD decomposes any signal into a finite number of so-called intrinsic mode functions (IMFs). The decomposition has been shown to be complete and orthogonal, a requirement for all signal expansion methods. It is also local, allowing events to be identified by the time of their occurrences. Finally it is adaptive to the data, making it suitable for general use. These properties were demonstrated by Huang and confirmed by (Zhang 2006). Despite these studies, the mathematical theory is incomplete and EMD is essentially described by an algorithm.

EMD has become a popular method of analysing and de-noising signals in a wide variety of areas. Examples include watermarking (Bi et al. 2007), audio processing (Molla & Hirose 2007), oceanography (N. E. Huang et al. 1999), finance (N. E. Huang et al. 2003), fault diagnosis (Zhong & Yan 2002), image processing (Qin & Shi 2002) and many others (Kopsinis & McLaughlin 2009). EMD is particularly well suited to analysing biological signals, finding extensive use in electrocardiography (ECG) (Karagiannis & Constantinou 2008; Karagiannis & Constantinou 2009; Weng et al. 2006) and electroencephalography (EEG) (Y. Li et al. 2009).

4.3.3.3 Description of EMD algorithm

While improvements have been made (Kaleem et al. 2011; Rilling et al. 2003), the base algorithm is still the same as originally proposed by Huang. The decomposition is described by the following equation:

$$S(t) = \sum_{1}^{L} h^{(i)}(t) + d(t) \tag{11}$$

where $h^{(i)}(t)$ is the i[th] IMF, $d(t)$ is the remainder and L is the total number of IMFS.

IMFs are first estimated, and then refined using an iterative process called sifting. The estimate $h_n^{(i)}$ is given by the residual of S(t) at that stage of the decomposition:

$$h_n^{(i)}(t) = \begin{cases} S(t), & i = 1 \\ S(t) - \sum_{j=1}^{i-1} h^{(j)}(t), & i \geq 2 \end{cases} \tag{12}$$

The sifting process is described by the following steps. First the local maxima and minima of $h_n^{(i)}$ are found. Next all the local maxima are interpolated to form an upper envelope. Similarly a lower envelope is formed using the local minima. The mean of these two envelopes is then calculated. A refined estimate $h_{n+1}^{(i)}$ of the IMF is obtained by subtracting this mean from the previous estimate $h_n^{(i)}$. This process is repeated until a stopping criterion has been fulfilled. The final and most refined estimate then becomes the IMF.

IMFs are subtracted from the signal until the remainder is a non-zero-mean, slowly varying function with few extrema.

4.3.3.4 Properties of IMFs

IMFs are intended to represent the instantaneous frequency of a signal. The concept of instantaneous frequency is controversial, as frequency is typically defined by an oscillation period. It is formally defined as the derivative of the instantaneous phase of the signal. The concept is useful for describing nonlinear signals whose frequencies change rapidly within periods of oscillation. An example of this is human speech, with complex combinations of tones and friction type sounds (N. E. Huang 2011).

An IMF is a function that satisfies two conditions. First the number of zero crossing must be equal to the number of extrema, or differ at most by one. This results in a signal that oscillates from positive to negative extrema. Therefore, all the maxima must be positive and all the minima must be negative. Second, the mean of the upper and lower envelopes must be equal to zero at any point.

IMFS typically resemble narrow-band frequency-modulated (FM) and amplitude-modulated (AM) sinusoids. They can be considered to represent modes of oscillation of the signal. IMFs often, but not always, reveal physical processes within the signal. The remainder reveals overall trends in the data.

4.3.4 IMF selection

Traditional EMD based de-noising strategies consider IMFs as a whole. Signal content of IMFs can be predicted due to assumptions of IMF properties, assessed by inspection or thresholded based on a bulk property of the IMF. If an IMF is considered to be noise-dominated, all the samples of that IMF are set to zero.

White noise behaves predictably when EMD is applied to a signal. It is distributed primarily in the lower order IMFs. This is especially true of the first IMF, which is often assumed to contain no signal. In many cases the first IMF is not included in the reconstruction, based on this assumption. Conversely, higher order IMFs are often assumed to be relatively noise-free. This assumption allows for optional thresholding of these IMFs.

IMFs can also be selected based on their total energy. The method involves creating a version of the signal containing only the noise from the original signal. The noise-only signal is then decomposed. The rationale of the method is that signal-dominated IMFs would have more energy than the corresponding IMFs of the noise-only signal.

Creating a noise-only signal is simple in artificial test waveforms, but practically impossible in real waveforms. An alternative is to estimate the noise-only IMF energies. This is based on a model of white noise energy distribution in IMFs, with the first IMF as a reference. Only IMFs with significantly higher energy than the estimated noise-only IMFs are selected (Flandrin et al. 2004).

Alternatively, IMFs can be selected based on the assumption that noise is zero mean, while the signal of interest is not. This method is used in identifying ECG signals. If a particular combination of IMFs is found to have close to zero mean, they are considered to be noise-dominated (Weng et al. 2006).

4.3.5 IMF Thresholding

4.3.5.1 Interval thresholding

Most IMFs contain a mix of signal and noise. Each IMF sample can therefore also be assessed for relevant signal content. This is done by comparison to a threshold.

Usually, when signals are thresholded each sample is considered. In the case of thresholding IMFs, some modifications have to be made due to their shape. As IMFs oscillate between positive and negative extrema they will fall below any threshold. This is true regardless of signal content of the IMF. This means that a threshold applied to individual components can remove relevant content as well as causing discontinuities.

To prevent this, the IMF is separated into intervals. Intervals span between zero crossings. The extrema contained in the interval is considered as representative of the signal content of that interval (Kopsinis & Mclaughlin 2008a).

4.3.5.2 Hard and soft thresholding

Hard thresholding sets all the samples of a signal below a given threshold to zero:

$$\check{y}(t) = \begin{cases} y(t), & |y(t)| > \lambda \\ 0, & |y(t)| \leq \lambda \end{cases} \tag{13}$$

where $\check{y}(t)$ is the thresholded value, $y(t)$ is the original signal value and λ is the threshold.

In the case of interval thresholding, single samples are replaced with intervals:

$$\check{h}^{(i)}\left(\boldsymbol{z}_j^{(i)}\right) = \begin{cases} h^{(i)}\left(\boldsymbol{z}_j^{(i)}\right), & |h^{(i)}\left(r_j^{(i)}\right)| > \lambda_i \\ 0, & |h^{(i)}\left(r_j^{(i)}\right)| \leq \lambda_i \end{cases} \tag{14}$$

where $\check{h}^{(i)}(t)$ is the thresholded i[th] IMF, $\boldsymbol{z}_j^{(i)}$ is the interval $[z_j^{(i)}\ z_{j+1}^{(i)}]$ containing t and $r_j^{(i)}$ is the extrema in that interval. The values $z_j^{(i)}$ and $z_{j+1}^{(i)}$ represent sample numbers of adjacent zero crossings.

Hard thresholding results in sharp discontinuities if any signal values are significantly above the threshold value. An alternative is soft thresholding, where all samples are reduced by the threshold value (Donoho 1995):

$$\check{y}(t) = \begin{cases} sign(y(t))(|y(t)| - \lambda), & |y(t)| > \lambda \\ 0, & |y(t)| \leq \lambda \end{cases} \tag{15}$$

Soft thresholding on intervals can be described mathematically by (Kopsinis & Mclaughlin 2008a):

$$\check{h}^{(i)}\left(\boldsymbol{z}_j^{(i)}\right) = \begin{cases} h^{(i)}\left(\boldsymbol{z}_j^{(i)}\right)\dfrac{\left|h^{(i)}\left(r_j^{(i)}\right)\right| - \lambda_i}{\left|h^{(i)}\left(r_j^{(i)}\right)\right|}, & |h^{(i)}\left(r_j^{(i)}\right)| > \lambda_i \\ 0, & |h^{(i)}\left(r_j^{(i)}\right)| \leq \lambda_i \end{cases} \tag{16}$$

Soft thresholding typically provides smoother results, but can unnecessarily reduce signal components significantly above the threshold value. This could be considered as a distortion of the

useful signal. This effect can be reduced by a modification known as the smoothly clipped absolute deviation (SCAD) penalty (Antoniadis & Fan 2001):

$$\check{y}(t) = \begin{cases} y(t), & |y(t)| > \alpha\lambda \\ \dfrac{(\alpha-1)y(t) - \alpha\lambda sign(y(t))}{\alpha - 2}, & 2\lambda < |y(t)| \leq \alpha\lambda \\ sign\big(y(t)\big)\max\big(0, (|y(t)| - \lambda)\big), & |y(t)| \leq 2\lambda \end{cases} \tag{17}$$

where α is a constant, and is typically set to 3.7 (Fan & R. Li 2001). The SCAD threshold when modified to alter intervals can be described by:

$$\check{h}^{(i)}\left(\boldsymbol{z}_j^{(i)}\right) = \begin{cases} h^{(i)}\left(\boldsymbol{z}_j^{(i)}\right), & \left|h^{(i)}\left(r_j^{(i)}\right)\right| > \alpha\lambda_i \\ h^{(i)}\left(\boldsymbol{z}_j^{(i)}\right)\dfrac{(\alpha-1)\left|h^{(i)}\left(r_j^{(i)}\right)\right| - \alpha\lambda_i}{\alpha - 2}, & 2\lambda_i < \left|h^{(i)}\left(r_j^{(i)}\right)\right| \leq \alpha\lambda_i \\ h^{(i)}\left(\boldsymbol{z}_j^{(i)}\right)\dfrac{\max(0, \left|h^{(i)}\left(r_j^{(i)}\right)\right| - \lambda_i)}{\left|h^{(i)}\left(r_j^{(i)}\right)\right|}, & |h^{(i)}\left(r_j^{(i)}\right)| \leq 2\lambda_i \end{cases} \tag{18}$$

The soft threshold with SCAD can be considered as a compromise between traditional hard and soft thresholding. It has also been shown to result in higher signal-to-noise-ratios than these two strategies when thresholding IMFs for the purpose of de-noising a signal (Kopsinis & Mclaughlin 2008b).

4.3.5.3 Universal threshold

The universal threshold (also known as VisuShrink) is a popular data-derived threshold (Donoho & Johnstone 1994). It is given by:

$$\lambda = c\left(\sigma\sqrt{2\log(n)}\right) \tag{19}$$

where σ is the standard deviation of the noise and n is the number of samples in the signal. The constant c allows multiples of the threshold to be used. It is set according to the de-noising method.

The standard deviation of the noise is estimated by:

$$\sigma \cong \frac{MAD}{0.6745} \tag{20}$$

where MAD is the median of the absolute values of the components of the decomposed signal.

4.3.6 Reconstruction

4.3.6.1 Overview

The signal is reconstructed by summing the altered IMFs. Reconstruction is given by:

$$\check{S}(t) = \sum_{i=M_1}^{M_2} \check{h}^{(i)}(t) + \sum_{i=M_2+1}^{L} h^{(i)}(t) + d(t) \tag{21}$$

where M_1 allows for exclusion of lower order IMFs, and M_2 allows for optional thresholding of higher orders. The remainder is not always included in the final summation.

4.3.6.2 Iterative interval thresholding

To improve the final de-noised signal a method called iterative interval thresholding (IIT) is applied. Iterative interval thresholding creates multiple versions of the original noisy signal. Each version is de-noised separately. All the de-noised versions are then averaged for the final de-noised signal.

De-noised versions are created in three steps. First the signal is decomposed using EMD. The samples of the first IMF are randomly altered. The signal is then reconstructed by summing the other IMFs with the altered first IMF (Kopsinis & Mclaughlin 2008a). This is based on the assumption that the first IMF contains purely noise.

4.4 Conclusions

Current methods of discerning and classifying muscle twitches are not ideal. The methods could be considered subjective, inaccurate or impractical for use outside of academia. This is primarily because the initial twitches are relatively small in magnitude.

The force output of the muscle can be digitised and amplified using an electrical force transducer. Subjectivity can be reduced if the twitches are detected according to a repeatable criteria based on this quantified force output. Any electrical signal, however, is distorted by background noise. The challenge then becomes isolating the useful signal (i.e. the twitch, if it exists) from this noise. Similar problems exist in various fields, for example identifying a heartbeat from an ECG signal.

Various signal processing techniques have been developed to address these types of problems. A good candidate is a de-noising technique based on EMD. EMD is effective at decomposing nonlinear and non-stationary signals, which describes the force output of muscles (and most real signals). EMD is also adaptive to data, making it relatively easy to use in any similar future studies. The de-noising technique, known as iterative interval thresholding, has been shown to be effective at removing noise in a variety of signals.

This de-noising technique has the potential to increase the accuracy of twitch classification. If this is the case it would improve chronaxie and rheobase determination in skeletal muscles, and hence the effectiveness of electrical stimulation of those muscles. The effect of the technique on twitch recognisability and classification is therefore the subject of this study.

Summary of literature review

Conclusions of literature review

Chronaxie and rheobase characterise the response of excitable tissues to electrical stimulation. Therefore, knowledge of these parameters is highly beneficial to the design of such stimulation protocols or devices. Despite many studies, exact values for chronaxie and rheobase are inconclusive. This is particularly true of directly stimulated skeletal muscle, especially if denervated.

A potential area of improvement is in the detection of the muscle response when stimulated. Ideally the response should be quantified to reduce subjectivity. This can be done by converting the force output of the muscle to an electrical signal using a transducer. In this case the problem becomes identifying the muscle response amongst electrical noise in the detection system.

The problem of separating signal from noise (known as signal de-noising) exists in multiple fields and is well studied. EMD-based de-noising techniques have been shown to be effective in a broad range of studies. One such method is known as iterative interval thresholding. This method, therefore, has potential to improve the detection of muscle responses, and hence provide for an objective of chronaxie and rheobase.

Overview of methodology

The aim of this thesis is to investigate the effects of EMD-based de-noising on the recognisability of skeletal muscle twitches in response to electrical stimulation.

Suitable skeletal muscles were selected and isolated. This includes both healthy and denervated muscles. The muscles were attached to a force transducer such that the majority of any force generated by contraction was converted to an electrical signal. The muscles were then electrically stimulated by external electrodes, using a pulse generator. The force transducer output signals were recorded for further analysis.

Muscle twitches were identified within the recorded signals. The recognisability of these twitches was then quantified by two separate measures. The first was an estimate of the signal-to-noise ratios. The second assessed the shape of the twitches by cross correlating them with a template.

Muscle twitch signals were de-noised using the EMD-based iterative interval thresholding technique. The effect of the de-noising on the recognisability of the muscle twitches was then assessed.

The de-noising technique was considered to have improved the signal if the recognisability of the muscle twitches was increased. Groups were compared using a non-parametric, repeated measures statistical hypothesis test, known as the Wilcoxon signed-rank test.

Chapter 5: Twitch acquisition

5.1 Introduction

This chapter describes the muscles used for the experiment. It also describes the care of the animals, surgical procedures (for both denervation and explantation) and storage procedures for the muscles once removed.

The chosen muscles could then be electrically stimulated, with the force output recorded. This involved creating a stimulation apparatus and protocol, as well as converting the force output to an electrical, and eventually digital, signal.

The digitised force output was divided into useful sections, based on the stimulation pulses. Sections could either potentially contain muscle twitches, or were known to be noise-only. Potential twitch sections were classified as either containing a twitch or not based on a threshold.

5.2 Muscle used

5.2.1 Rats as an animal model

Rats were used as an animal model. Ethics approval was obtained for the entire experiment from the University of Cape Town, Health Science Research Ethics Committee (see Appendix A).

The rat muscles were denervated by means of a surgical procedure, stored for a fixed time and the rats were finally euthanised so that the relevant muscles could be explanted and used for further experimentation.

35 rats were used in total. 5 were used in a pilot study and for a practice group for all the procedures. The remaining 30 were split into 3 groups of 10 each. 1 group was short term. Rats in this group were denervated and stored for 1 week prior to explantation of the muscles. 1 group was medium term, stored for 2 weeks. The final group was long term, stored for 8 weeks. In each case, the denervated muscles were allowed to atrophy naturally for the entire period.

Of the limb muscles (see Section 3.2.2.1), the soleus muscle was chosen for the denervation procedure as both the muscle and the corresponding motor nerve (the sciatic nerve) are relatively accessible.

5.2.2 Denervation procedure

All the rats were denervated by sectioning the right sciatic nerve as it leaves the right sciatic notch. This resulted in complete denervation of the soleus muscle of the right leg. The left leg remained innervated so that the healthy and atrophied muscles could be directly compared. It was assumed that the rat was symmetrical in terms of muscle physiology.

Each rat was initially injected with Meloxicam (an analgesic) one hour before the procedure. They were then anaesthetised using a mixture of 4% Halothane and 96% Carbogen (95% oxygen, 5% carbon dioxide). They were placed in a container while the mixture flowed in. The container had no other outlet. Once they were no longer responding to any kind of movement or touch they were

taken out of the container and placed on a heating pad. Anaesthesia was maintained using a mixture of 1.5% Halothane and 98.5% Carbogen supplied through a face mask.

The heating pad was maintained at 36.5°C (body temperature) to prevent hypothermia. Each rat was positioned on its left side. The right leg was raised into the air and secured. Betadine was applied to the posterior thigh of the right leg. The area was then shaved, first using scissors and then a size 23 scalpel blade.

An incision was made sagittally along the posterior right thigh, through the skin. The muscles were parted using blunt scissors until the sciatic nerve was located. Blunt scissors helped avoid unnecessary damage to the surrounding structures. Two sutures were tied around the nerve, one as proximal as possible and one as distal as possible. A section of nerve between the sutures was then removed. Lentrax (an antibiotic) was injected into the wound using a 21 gauge needle. The wound was sealed using sutures. Betadine was applied over the sutures.

A shot of Lentrax was given intramuscularly to the left leg. Each rat was marked on the ears. The anaesthetic was then removed, allowing it to regain consciousness. For two days following the procedure, Meloxicam was injected to reduce pain.

The success of the denervation procedure was assessed by observing the rats once they were conscious and moving around. The loss of the use of the soleus muscle (and other muscles enervated by the sciatic nerve) led to a distinct change in the way they moved: their right legs dragged them behind as they walked.

5.2.3 Housing of rats

Rats were initially isolated in cages following the denervation procedure. This was to prevent other rats (both normal and recovered) panicking as a result of observing any injury or blood. Once the rat had sufficiently recovered it was moved into a group cage. It was considered recovered when the wound had healed enough to prevent bleeding and the rat was in no visible pain. The group cages eventually contained 4 rats at a time as they are social animals and are distressed by isolation.

The rats were monitored daily for any signs of distress. This included lack of grooming, abnormal behaviour or self-mutilation. They were also weighed every three days to check for any sudden decrease of weight. A loss of 20% was considered an indication of distress. If any of the rats were found to be in distress they would be euthanized.

5.2.4 Explantation procedure

The rat was euthanized by means of decapitation. An incision was made encircling the ankle joint of each leg and the skin was removed up to just proximal to the knee joint. The soleus muscles were isolated and removed at the tendons. The muscles were stored in containers of Krebs-Ringer solution which were placed in ice packs prior to testing.

5.3 Experimental apparatus

5.3.1 Tissue bath

A Perspex tissue bath was constructed that acted as a container for the muscle during stimulation. The bath was filled with Ringer's solution (as described in Section 3.2.4.1). Carbogen was bubbled through the solution in the bath to provide the muscle with natural metabolic needs.

The bath also had pipes running through it that could channel hot water from a thermal regulator. Temperature in the bath was maintained at 36.5 °C. The bath therefore simulated the conditions that muscles experience in the body.

Inside the bath was a fixed hook that one side of the explanted muscles could be secured to. Muscles were tied using sutures.

5.3.2 Stimulating electrodes and pulse generator

Two needle EMG electrodes were used. They were arranged in a bi-polar configuration. They were made of surgical grade stainless steel and coated in Teflon. They were 0.45 mm in diameter (26 gauge) and 50 mm in length.

The electrode ends were separated 2 mm apart. A thin plastic bristle was attached which extended 1 mm past them downwards. The bristle acted as an insulated spacer between the electrodes and the muscle. This allowed the electrodes to be lowered to the same known height above the muscle for each test.

The Pulsar 6bp stimulator was used. It was connected to the electrodes via a 1 kΩ series resistor. The stimulator has 5 variable settings: pulse duration (also known as pulse width), train interval, pulse delay, cycle time and train pulses (see Fig. 5.1). Both constant-current and constant-voltage outputs are available.

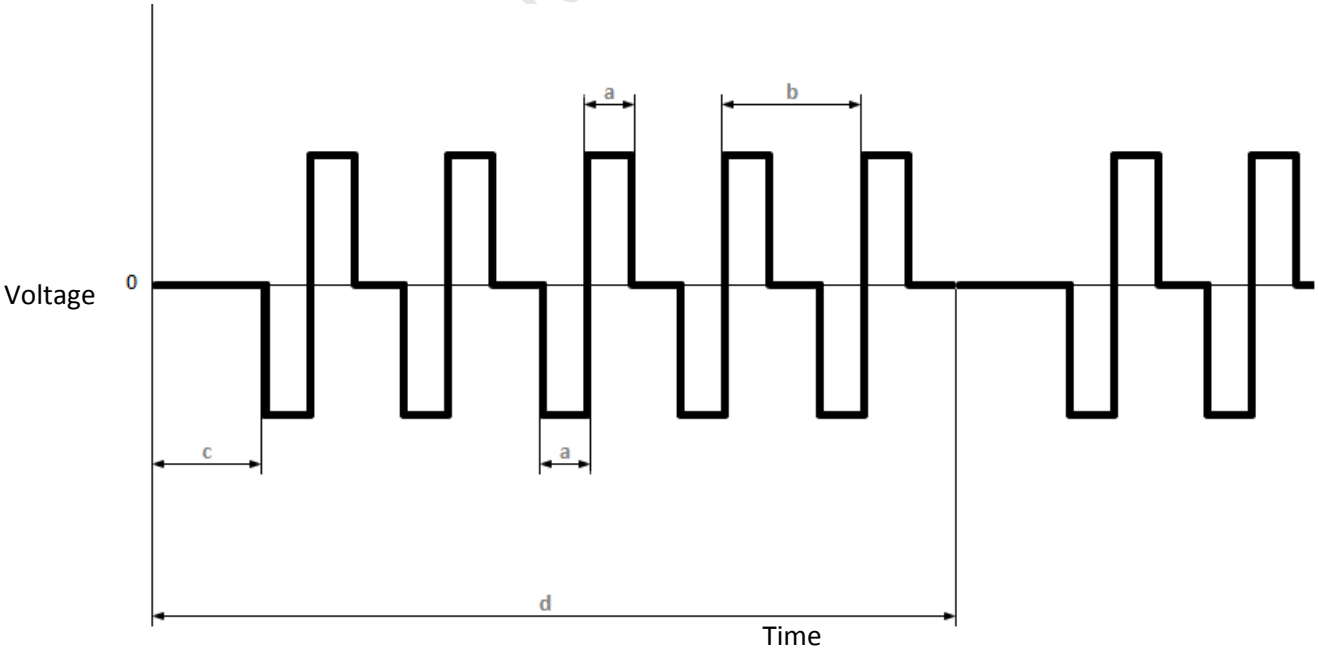

Figure 5.1: **Pulsar output voltage with 5 biphasic pulses, indicating: a) Pulse width; b) Pulse interval; c) Train latency; d) Cycle time.**

5.3.3 Recording apparatus

An existing force transducer was used. The transducer was comprised of strain gauges connected in a Wheatstone bridge configuration and converted any applied force to a recordable voltage. It was lowered into the bath, where one side of the muscles could be secured (see Fig 5.2). This voltage was amplified and fed into the Powerlab biological amplifier, which was connected to a PC. LabView 7 software was installed on the PC and was used to record the data.

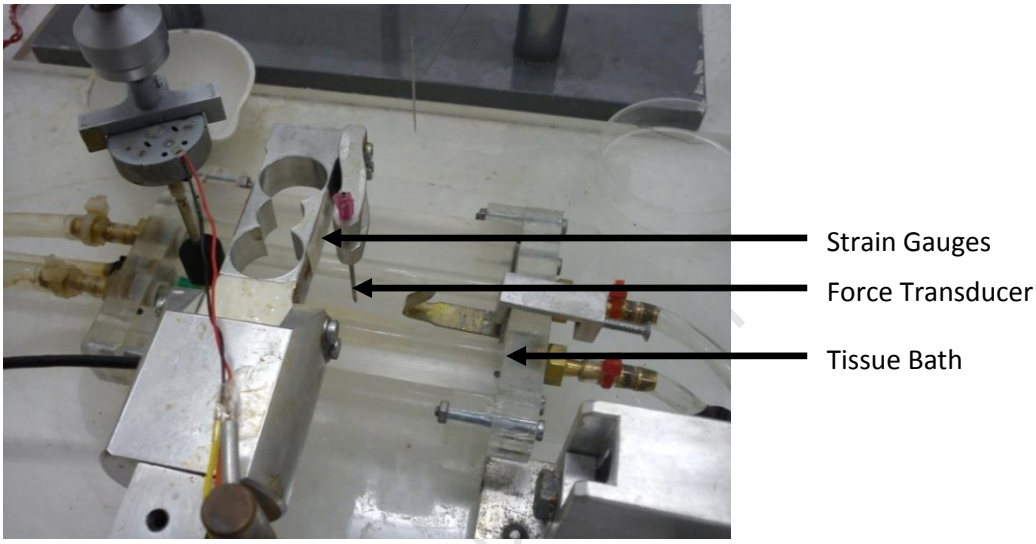

Figure 5.2: Tissue bath and force transducer apparatus.

5.4 Stimulation protocol

5.4.1 Electrical stimulation

The electrodes were positioned about ¼ of the length of the entire muscle away from the tendon. The anode was placed further from the middle of the muscles and closer to the nearest attachments than the cathode. The line between them was parallel to the muscle fibers (see Fig. 5.3). The tips of the electrodes were submerged in the tissue bath solution. In order to standardise the electrode placement, a micro-positioning tool was used.

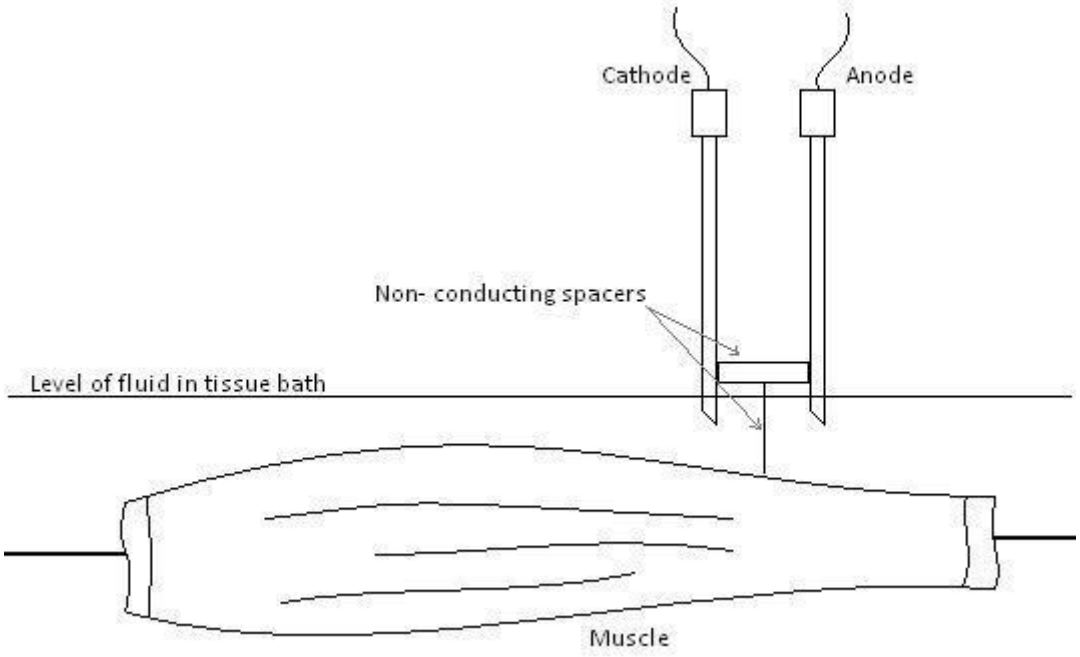

Figure 5.3: **Experimental setup showing the muscle, cathode, anode, the spacer controlling distance between electrodes, a non-conductive spacer controlling distance between muscle and electrodes and the level of fluid in tissue bath.**

The pulse interval was set to 300 ms, train latency to 3 s, cycle time to 4.5 s and number of train pulses was set to 5. Biphasic, constant voltage pulses were used (see Section 3.3.4.2). Each muscle was stimulated using a total of 5 pulse widths. These pulse widths were 0.5, 1, 2, 5 and 10 ms.

The pulse magnitude started at 0 V and was increased in steps of 1 V until it reached 50 V or the muscle reached its maximum level of contraction. The magnitude was incremented for each pulse train, i.e. every 5 pulses. This sequence was repeated for each pulse width.

The muscle was fixed at both ends and hence contractions resulting from stimulation were isometric.

5.4.2 Recording force output

The outputs of the force transducer and amplifier were recorded using the LabView 7 software package. The outputs were recorded at 2000 samples per second. The voltage across the 1 kΩ resistor (see Section 5.3.2) was also recorded and displayed. This allowed a direct relationship between the input stimulation pulses and the output of the force transducer to be established (see Fig. 5.4).

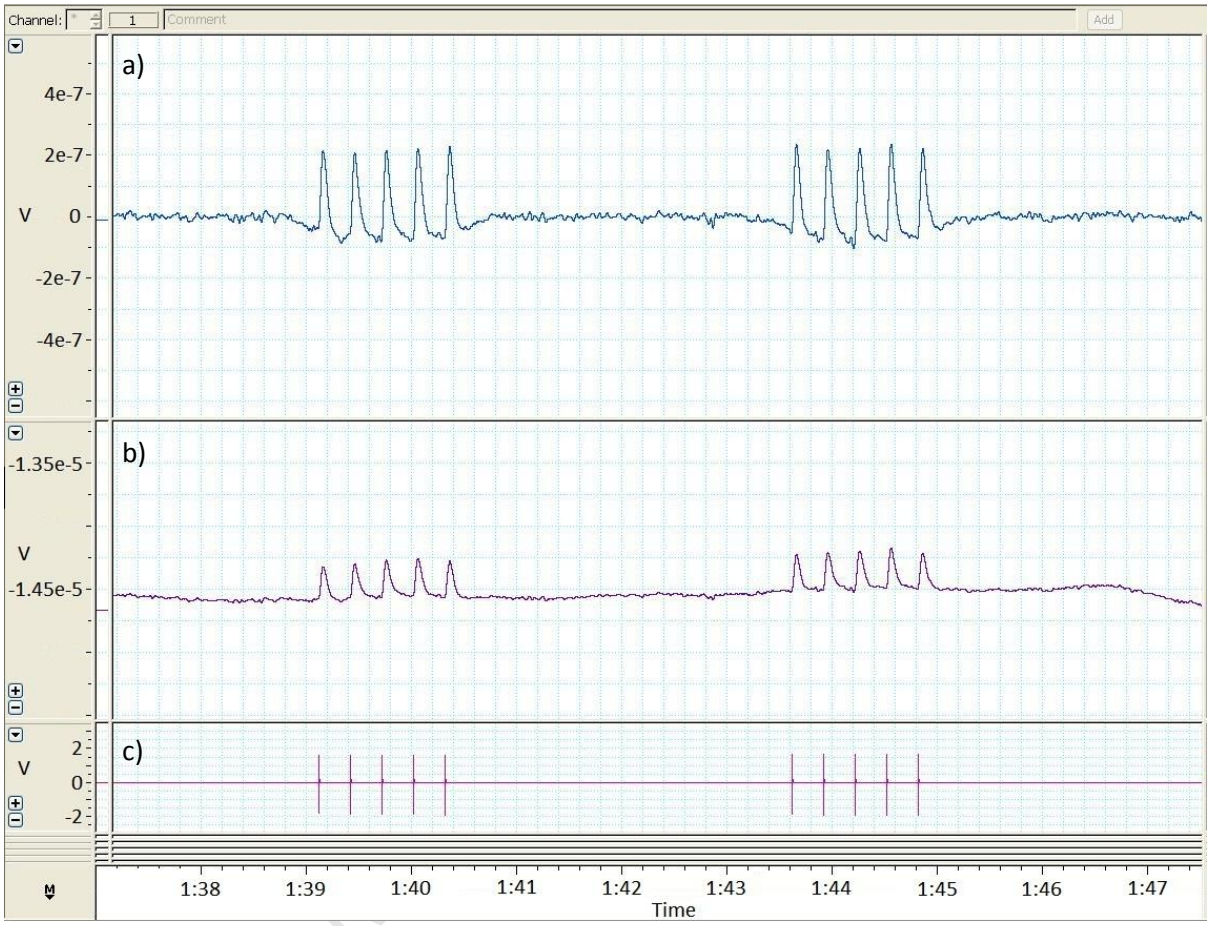

Figure 5.4: **Outputs of the force transducer and pulse generator in LabView 7 during muscle twitches: a) The force transducer output, band-pass filtered between 0.1 Hz and 25 Hz, is plotted in blue; b) The force transducer output, low-pass filtered at 25 Hz, is plotted in purple; c) The voltage across the 1 kΩ resistor (i.e. the pulse generator output) is plotted in pink.**

The signal was low pass filtered at 25 Hz to remove excess high frequency noise, including the mains artefact. It was then high pass filtered at 0.1 Hz to remove signal drift (see Fig 5.5). Finite impulse response (FIR) filters built into LabView 7 were used.

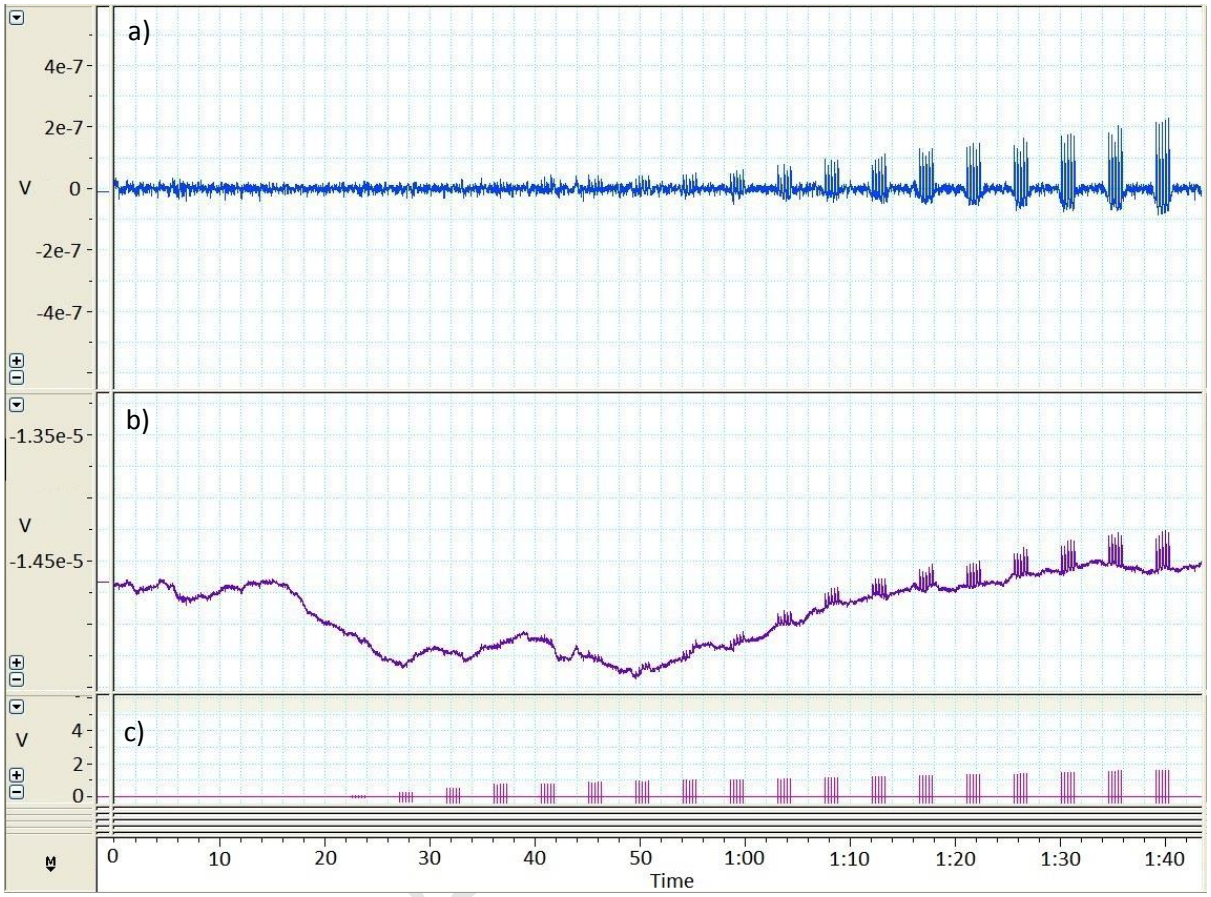

Figure 5.5: **Output of the force transducer and pulse generator in LabView 7 during a wide range of muscle responses: a) The force transducer output, band-pass filtered between 0.1 Hz and 25 Hz, is plotted in blue; b) The force transducer output, low-pass filtered at 25 Hz, is plotted in purple; c) The voltage across the 1 kΩ resistor is plotted in pink.**

The band-pass filtered force transducer output signal and the stimulation pulse signal were exported to Matlab for further analysis (see Fig. 5.6).

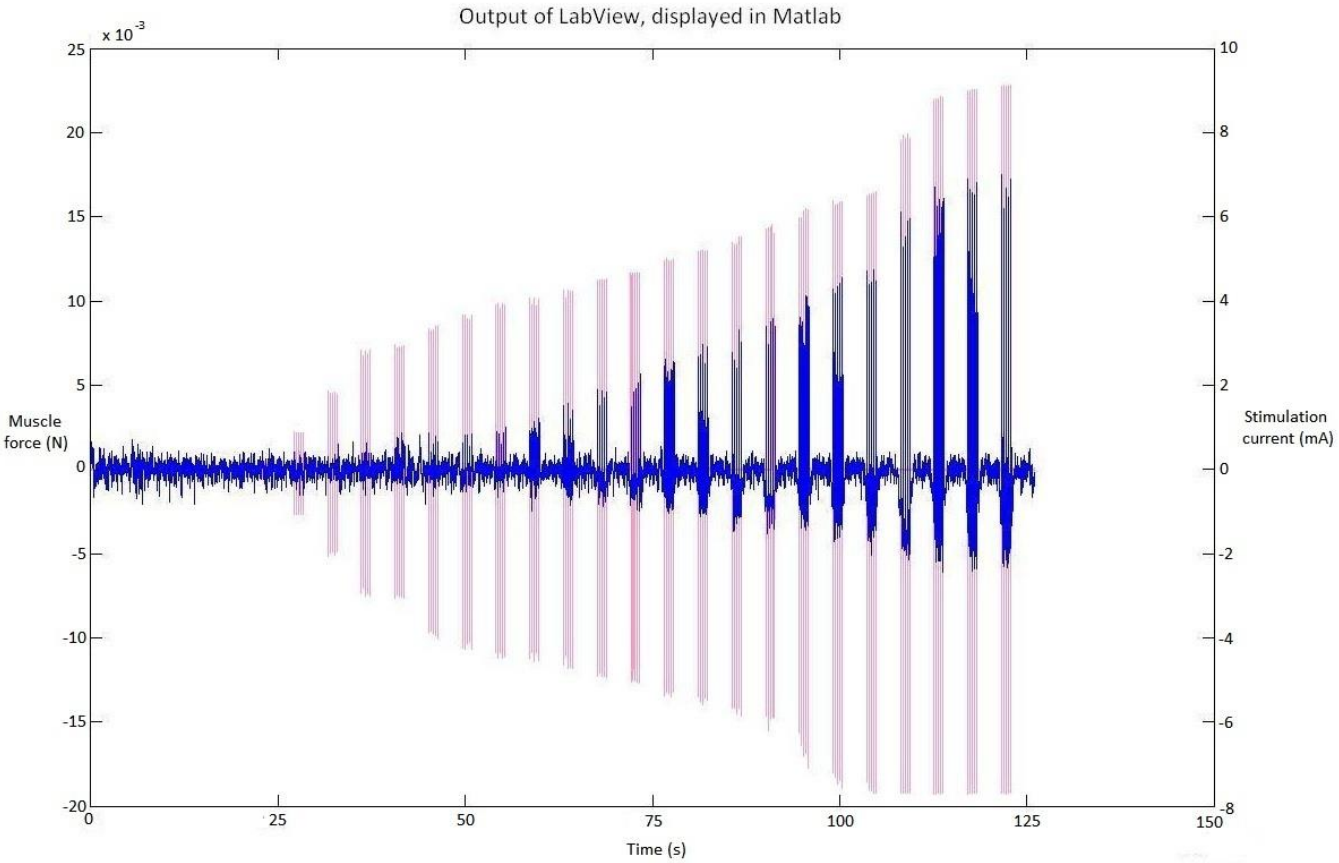

Figure 5.6: **The force transducer output (band-pass filtered at 0.1 – 25 Hz), displayed in Matlab. The force transducer output is plotted in blue and voltage across the 1 kΩ resistor is plotted in pink.**

5.5 Signal sectioning

5.5.1 Potential twitch sections

Sections of the output force signals were selected for further analysis. Each section corresponded to a stimulation pulse train. These sections are referred to as potential twitch sections. The recognisability of particular potential twitch sections could then be quantified and used to assess the effects of the de-noising.

Sections were automatically identified according to the input pulse times (see Fig. 5.7). This ensured that twitches, if they existed, would always occur near known landmark times. Sections begin 2.75 s before the first pulse of the train, and extend 2.5 s after the last pulse of that train. The total length of a section is 6.75 s.

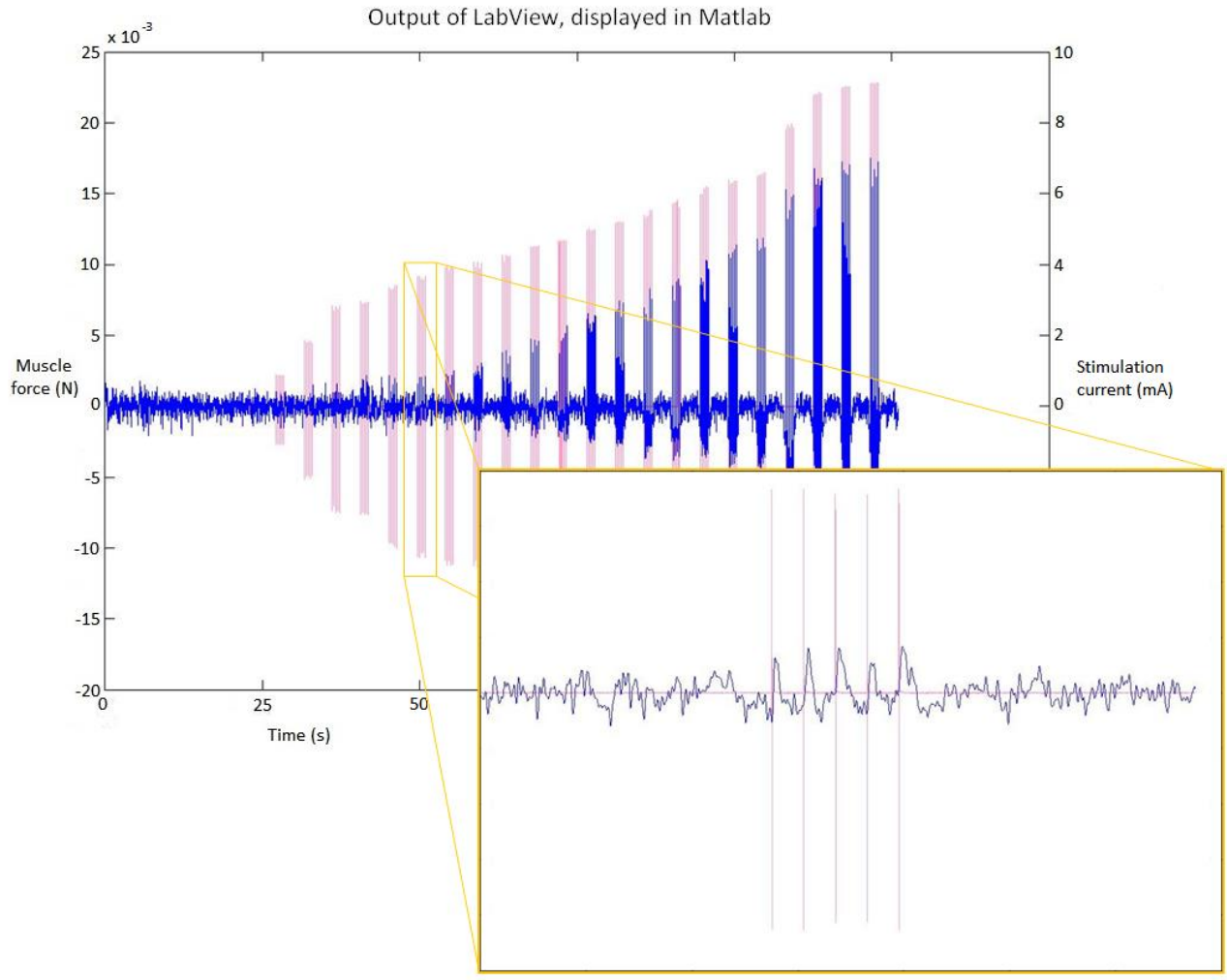

Figure 5.7: **Example of a potential twitch section. The section is enlarged and highlighted in yellow. The output of the force transducer is plotted in blue and the voltage across the 1 kΩ resistor is plotted in pink.**

5.5.2 Apparent twitches

When stimulation pulses were sufficiently large (in both amplitude and pulse width), the muscle response became apparent and easy to identify (see Fig. 5.8). These sections were used to identify the expected shape and timing of the muscle response.

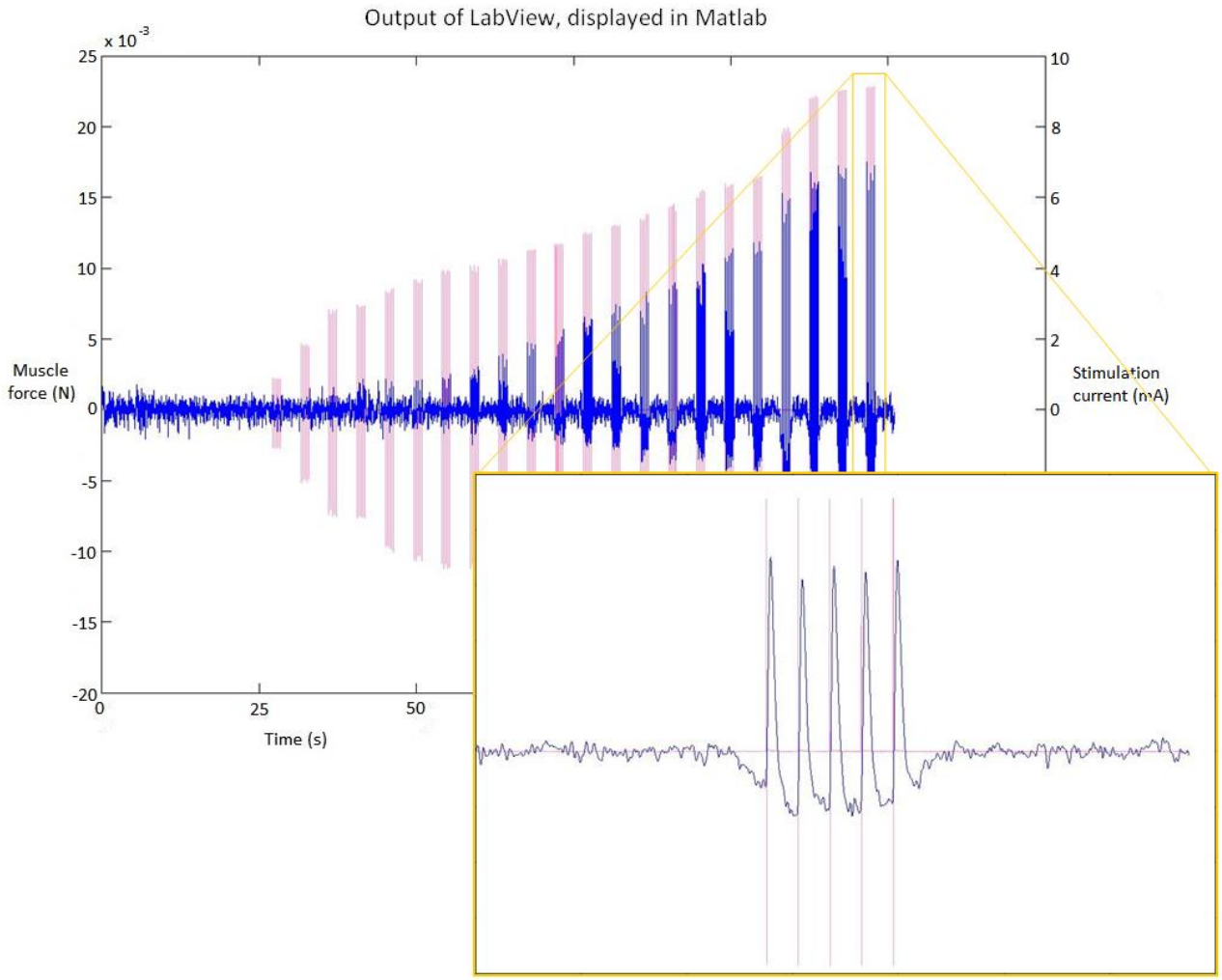

Figure 5.8: **Example of an apparent twitch section. The section is enlarged and highlighted in yellow. The output of the force transducer is plotted in blue and the voltage across the 1 kΩ resistor is plotted in pink.**

Twitches were observed to be almost completely contained in the 0.3 s following the corresponding stimulating pulse.

5.5.3 Noise-only signal

A known noise-only signal was created to act as a basis of comparison for all methods (see Fig. 5.9). The output of the force transducer was recorded for at least 20 s before the stimulation pulses started.

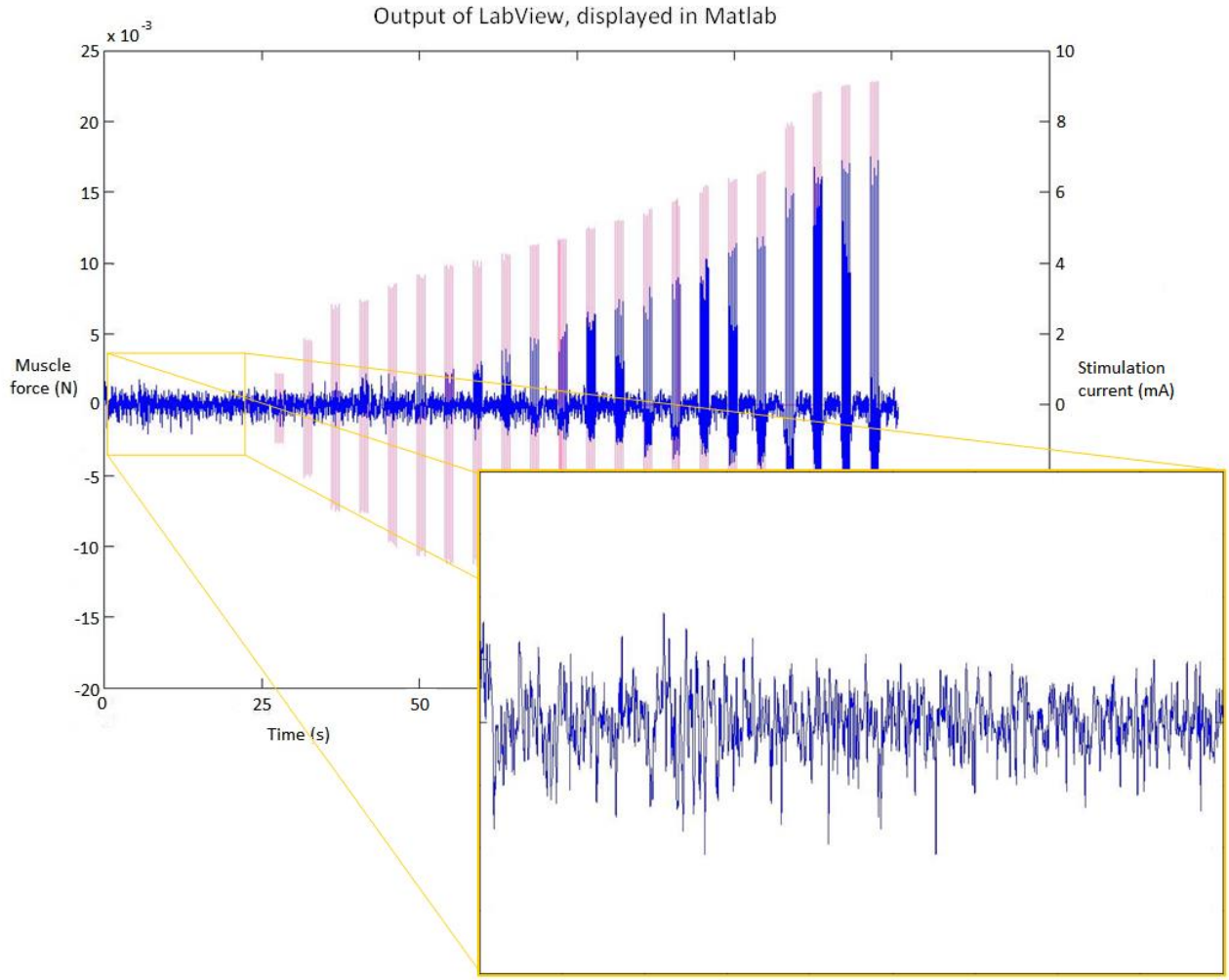

Figure 5.9: **Example of a noise-only section. The section is enlarged and highlighted in yellow. The output of the force transducer is plotted in blue and the voltage across the 1 kΩ resistor is plotted in pink.**

Subsections of the same length as potential twitch sections (i.e. 6.75 s) were selected at random from the noise-only signal. This allowed direct comparison to potential twitch sections. Similar sections of 0.3 s were selected for comparison to individual twitches (see Section 6.5.1).

5.6 Twitch classification

5.6.1 Classification threshold

Twitches were classified using a threshold applied to the produced output force. This is a commonly used method (for example (Doupe 1943; Vitro et al. 2007)), likely due to its simplicity and ease of implementation. The threshold was computed based on the noise-only signal (see Fig. 5.10).

The threshold was calculated using equation (9), with d set to 2.

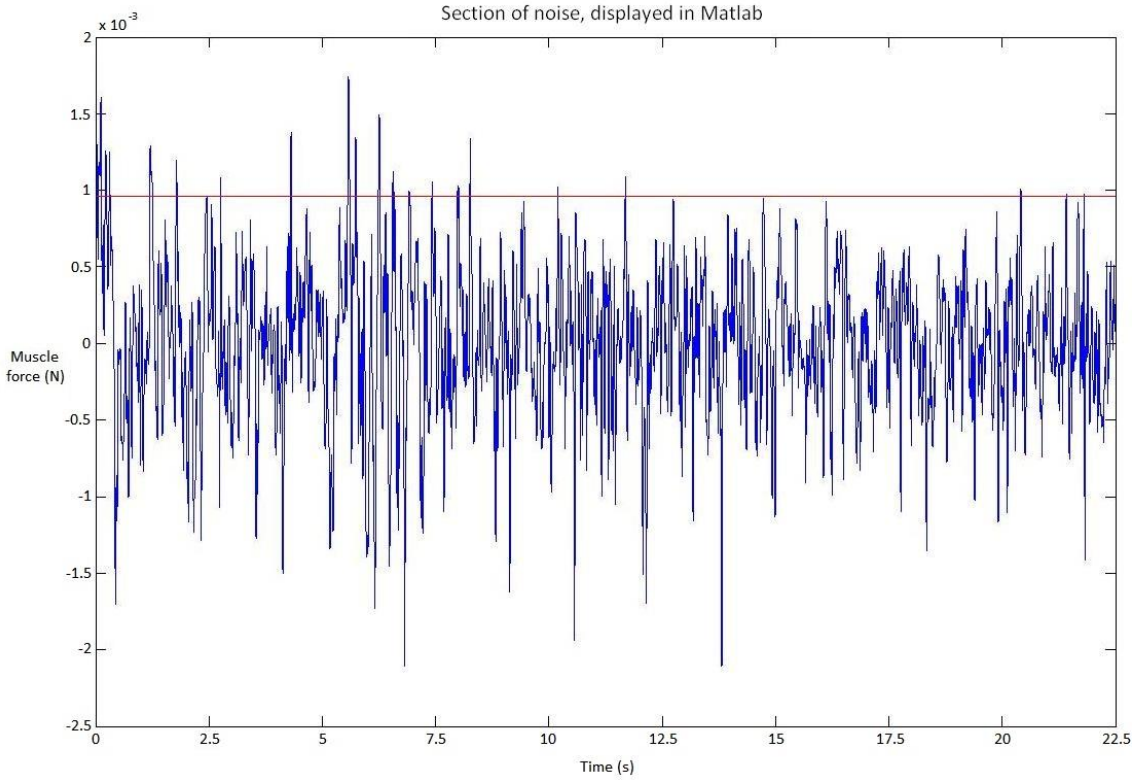

Figure 5.10: Threshold calculated according to equation (9), with d equal to 2. The threshold is plotted in red and the noise-only signal (see Section 5.5.3) is plotted in blue.

A section was classified as containing a twitch only if the signal was greater than the threshold in the regions near all 5 stimulation pulses (see Fig. 5.11). These regions were defined as the 600 samples following each pulse (see Section 5.5.2). Considering all 5 regions reduced the number of sections being falsely classified as containing twitches due to spikes in the noise.

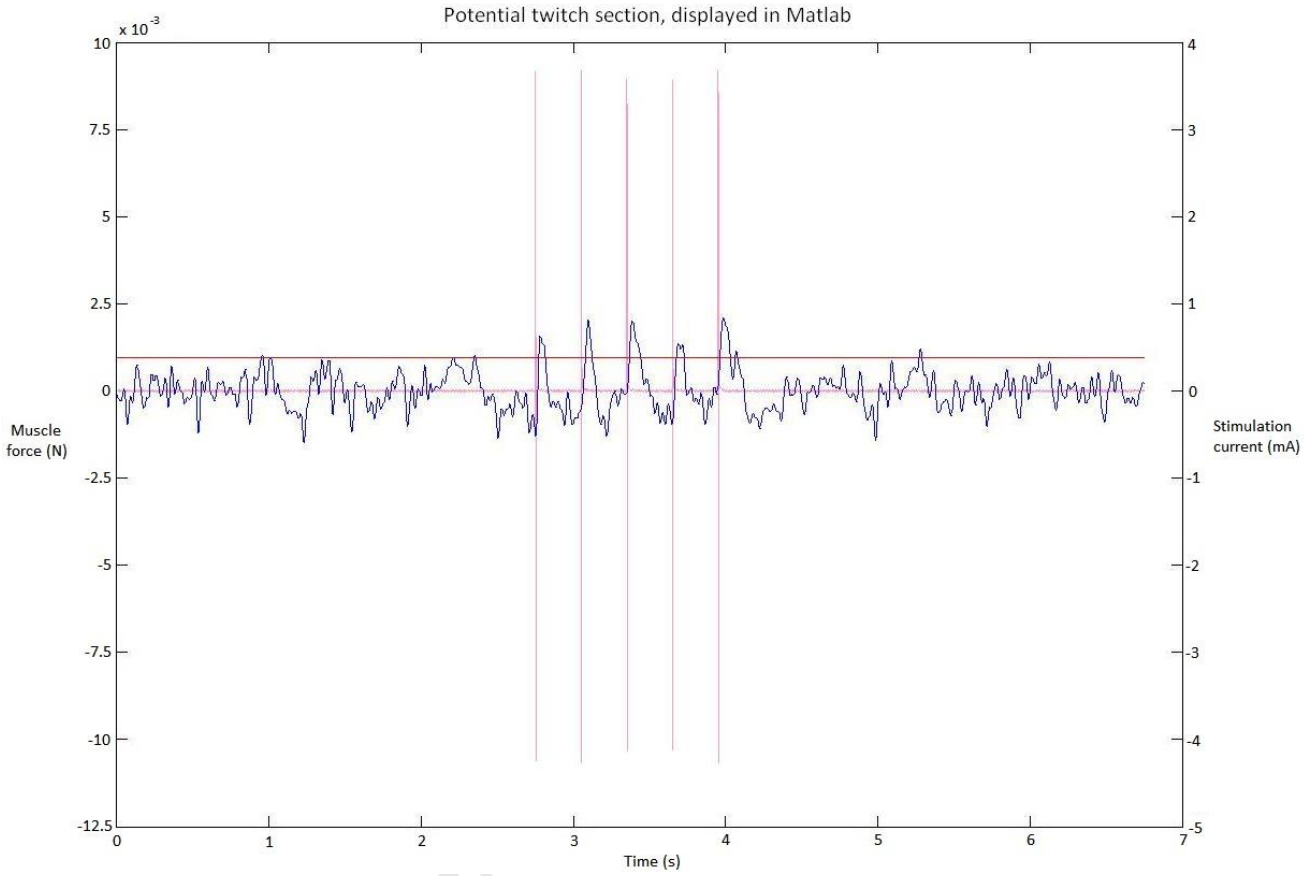

Figure 5.11: Potential twitch section with applied threshold. The threshold is plotted in red, the force output is plotted in blue and the voltage across the 1 kΩ resistor is plotted in pink. The force output was compared to the threshold in the 600 samples following each stimulation pulse. In this case the force output exceeded the threshold in all five regions. This section was classified as containing a twitch.

5.6.2 Signal to be analysed

This study is concerned with the recognisability of twitches at the lowest pulse amplitude for a given pulse width. These are referred to as the first twitches, and are contained in the first twitch section. Only the first twitch section (as classified by the threshold described in Section 5.6.1) was considered for further analysis (see Fig. 5.12). The signal portion before this section was also included.

If no twitch was detected, the signal was discarded (see Section 7.4.1).

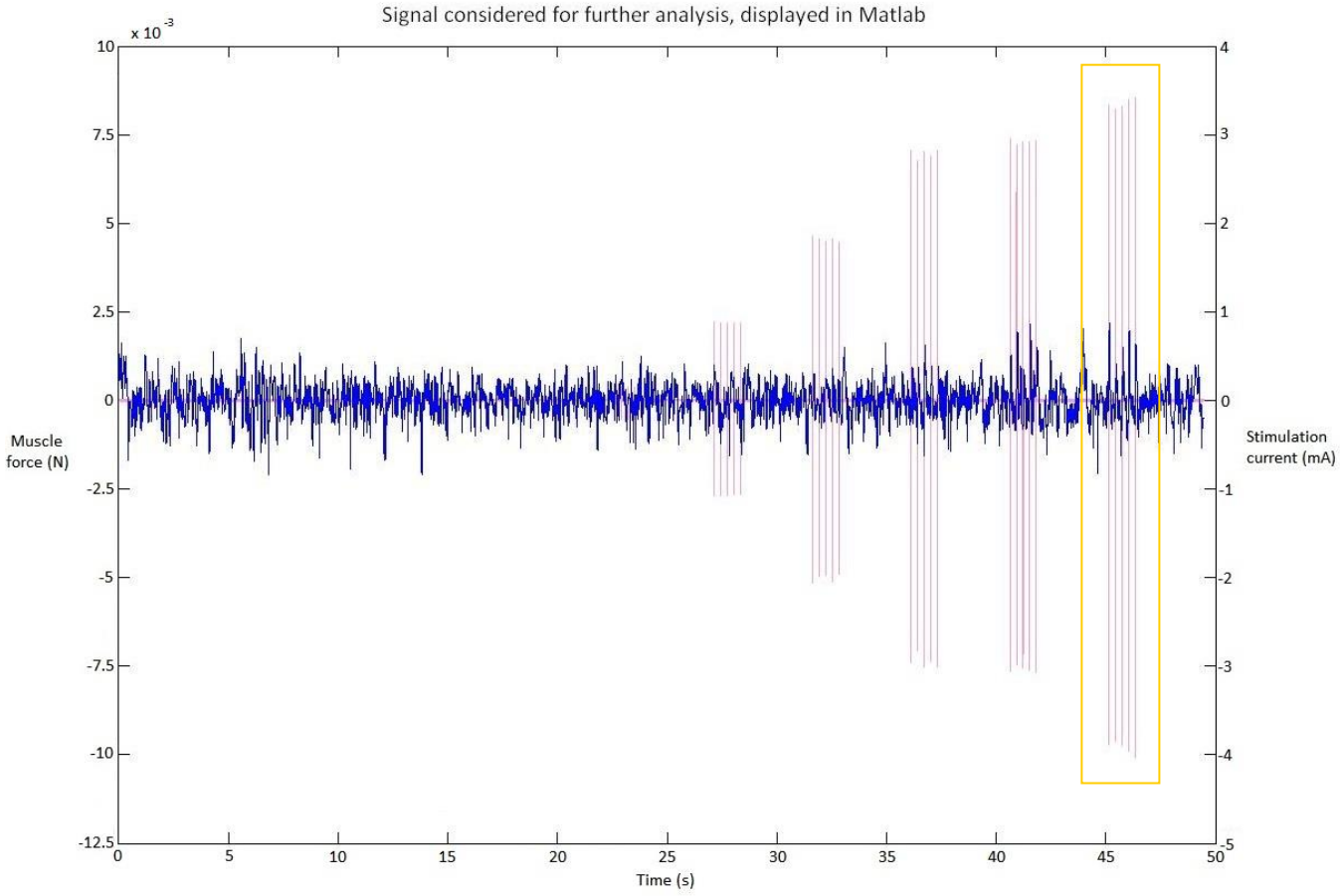

Figure 5.12: **Signal section extracted for further analysis. The force transducer output is plotted in blue and the stimulation pulses are plotted in pink. The twitch section corresponding to the lowest stimulation voltage (classified as per Section 5.6.1) is highlighted with a yellow box.**

Chapter 6: Twitch recognisability

6.1 Introduction

The selected muscle response was analysed, with the goal of quantifying the recognisability of the muscle twitches. The recognisability was assessed by two separate measures. The signal-to-noise-ratio was estimated, to assess the effectiveness of the noise removal. The shape of the twitches was also considered, by cross correlating the twitches with a template.

An EMD-based de-noising method (discussed in Section 4.3) was applied to the muscle response. The recognisability of the twitches before and after de-noising was compared.

6.2 EMD de-noising

The signal was decomposed using the standard EMD algorithm (see Section 4.3.3.3 and Fig. 6.1). Extrema were interpolated using a cubic spline (Reinsch 1967). Each IMF was sifted 8 times.

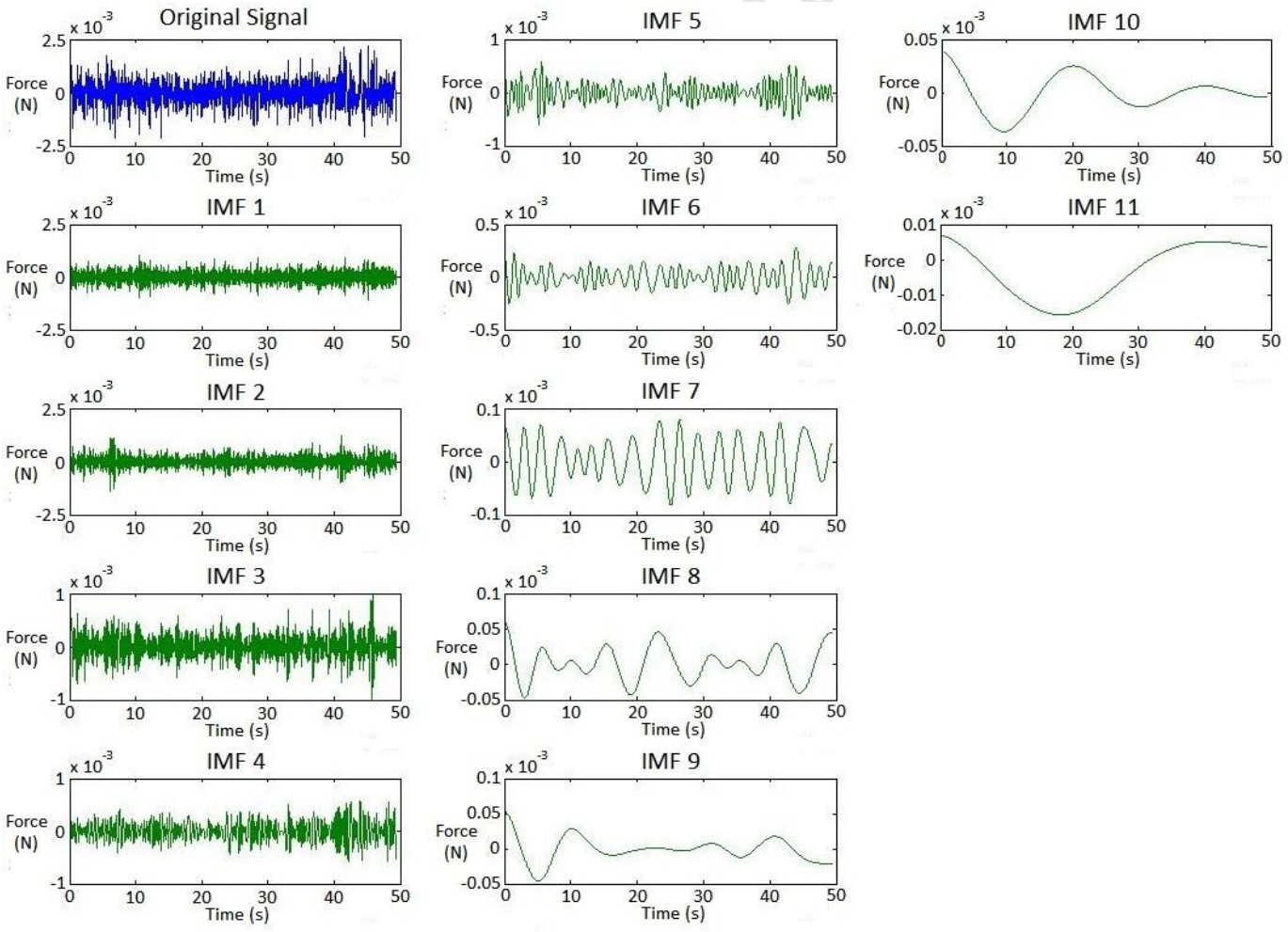

Figure 6.1: **The original signal, plotted in blue (top left), and its associated IMFs, plotted in green.**

The universal threshold was used, as per equation (19) with *c* set to 0.4 (see Fig. 6.2). Intervals between zero-crossings were considered, as opposed to individual samples (see Section 4.3.5.1). The soft SCAD thresholding strategy was used (see Section 4.3.5.2).

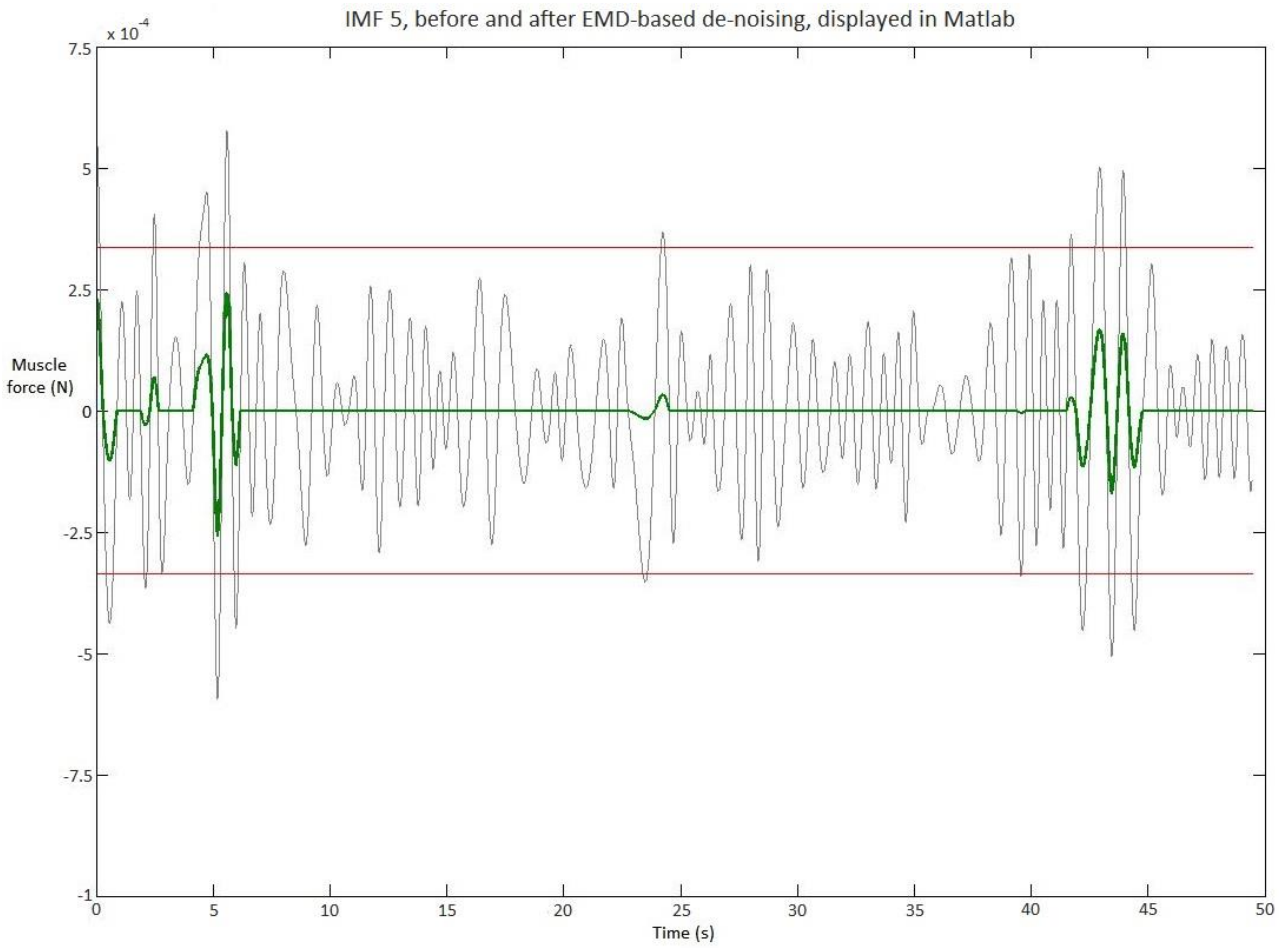

Figure 6.2: **Soft SCAD thresholding (threshold value given by the universal threshold multiplied by 0.4). Thresholded 5th IMF is plotted in green, threshold is plotted in red and unaffected 5th IMF is plotted in grey for direct comparison.**

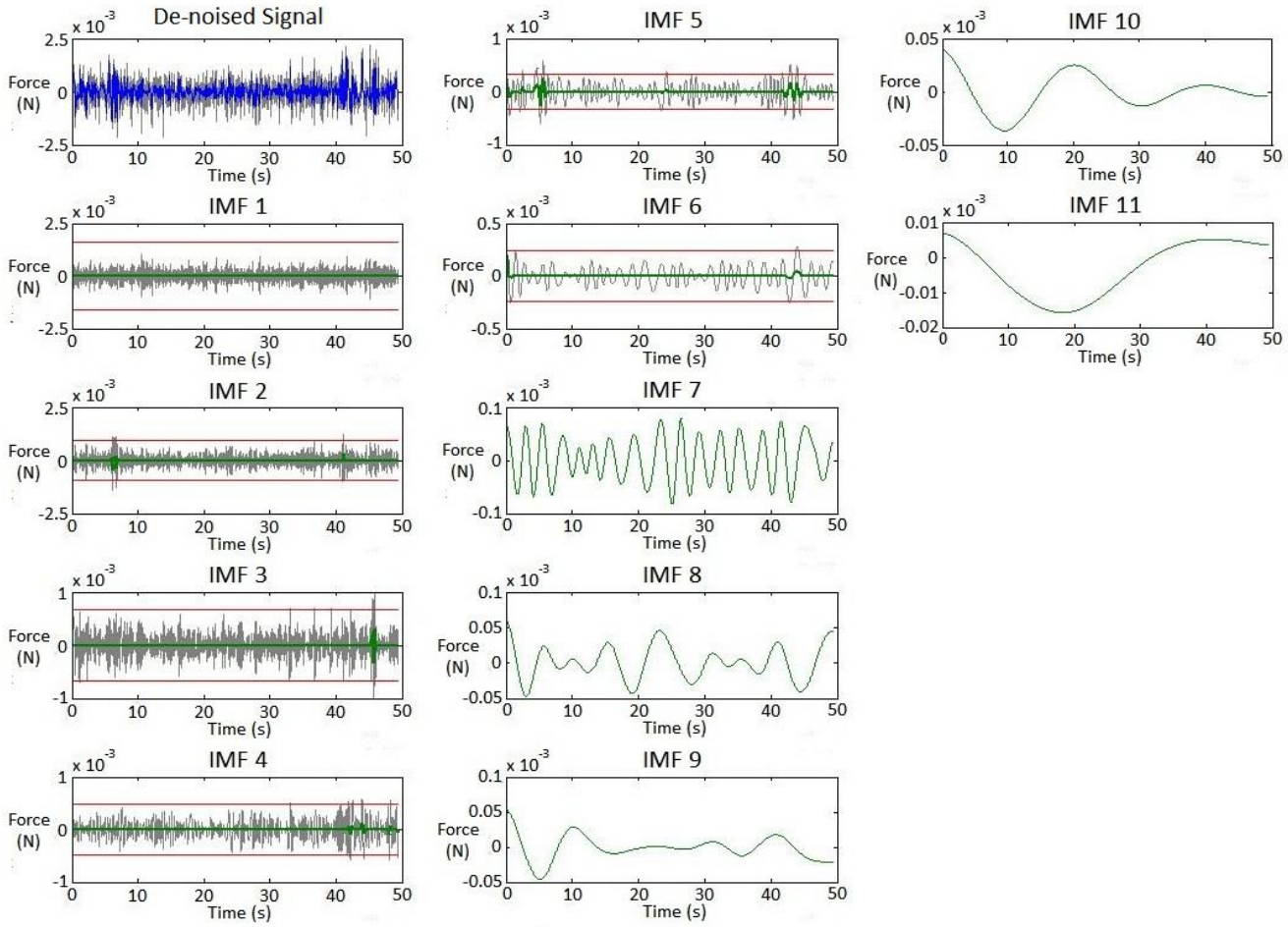

Figure 6.3: **The de-noised signal, plotted in blue (top left) and its associated (thresholded) IMFs, plotted in green. Where applicable, the original signal is plotted in grey for direct comparison. Note that only the first 6 IMFs were thresholded, and the remaining 5 are unaffected. All IMFs are summed to reconstruct the de-noised signal.**

Signals were reconstructed as per equation (21). M_1 was set to 2 in each case, i.e. all IMFs, except the first, were included in the final reconstructions. M_2 was set to $(L-5)$ in each case, i.e. the last 5 IMFs were not thresholded (see Fig 6.3).

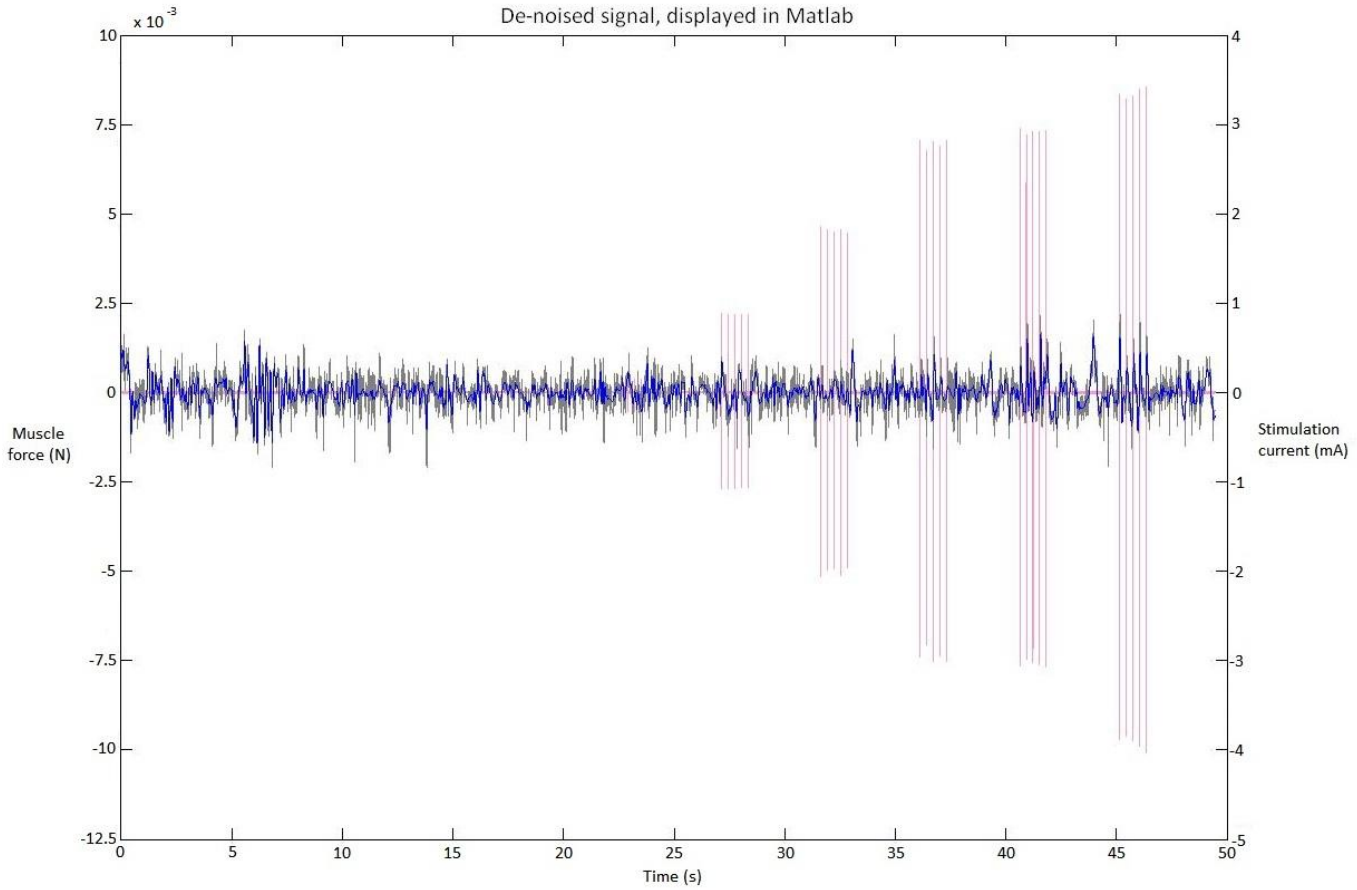

Figure 6.4: **The final de-noised signal. De-noised signal is plotted in blue, stimulation pulses are plotted in pink and original signal is plotted in grey for direct comparison.**

In each case 20 versions of the signal were created and de-noised (see Section 4.3.6.2). All 20 versions were averaged for the final result (see Fig. 6.4 and Fig. 6.5).

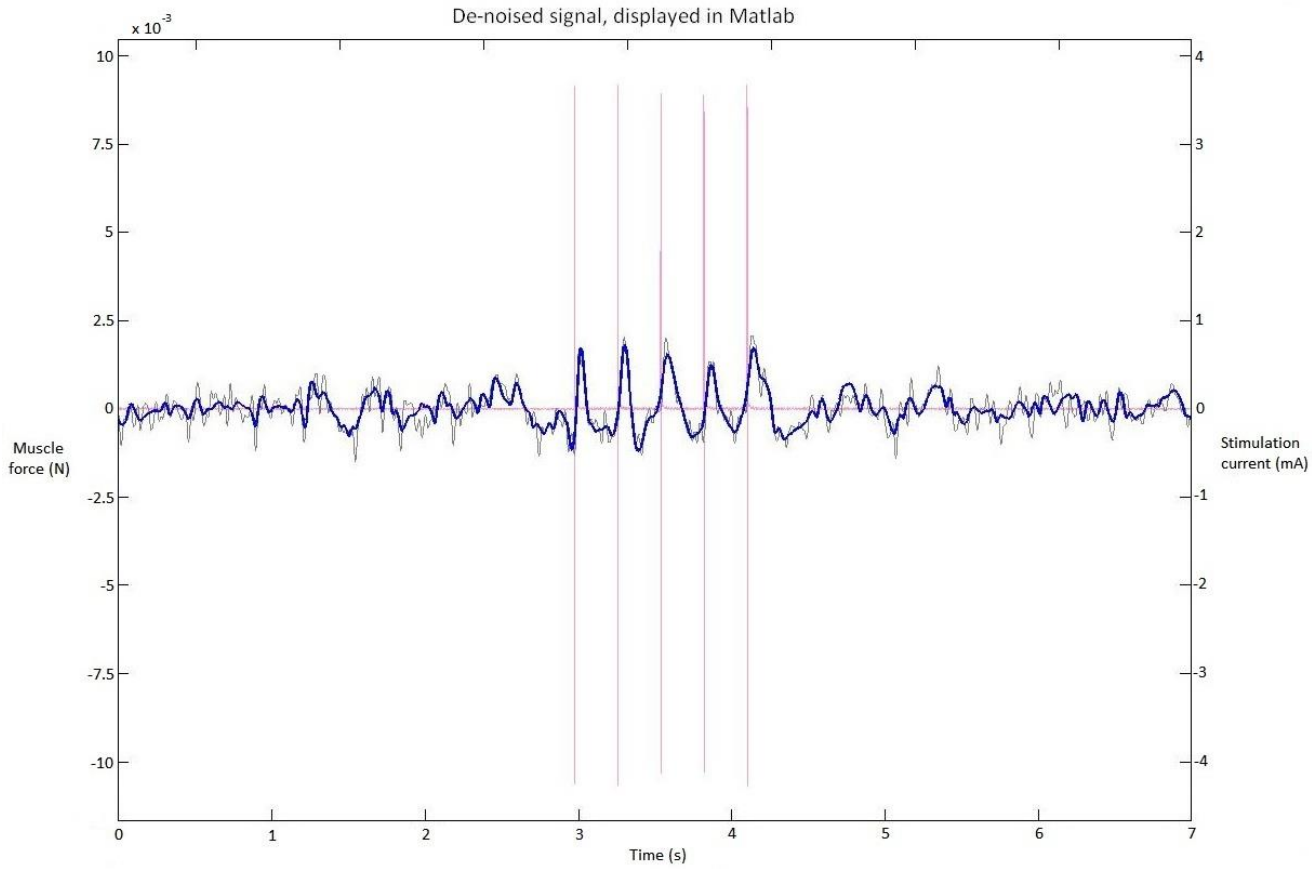

Figure 6.5: **The final de-noised signal zoomed in on 5 twitches. De-noised signal is plotted in blue, stimulation pulses are plotted in pink and original signal is plotted in grey for direct comparison.**

6.3 Signal-to-noise ratio estimation

Signal de-noising techniques are commonly evaluated by their effect on signal-to-noise ratio (for example (Kopsinis & McLaughlin 2009; Rosas-Orea et al. 2005)). Signal-to-noise ratio is defined by:

$$SNR = \frac{P_{signal}}{P_{noise}} \tag{22}$$

where P_s and P_n are the power in the signal and noise respectively. Power is defined as the average energy in the signal, and is given by:

$$P = \frac{1}{N}\sum_{n=0}^{N-1} x^2(n) \tag{23}$$

where n is the number of samples and x_i is the signal value at sample i.

Since the signal and noise are not well separated their power must be estimated. Noise power was assumed to be relatively constant throughout the signal. P_n was estimated by averaging power in the two adjacent noise-only subsections of each input pulse (see Fig 6.6). P_s was more difficult to estimate as squaring a sample value containing both signal and noise results in cross-terms that

artificially inflate the value. To reduce these cross-terms an alternative definition of signal-to-noise ratio was used:

$$SNR = \left(\frac{A_{Signal}}{A_{Noise}}\right)^2 \tag{24}$$

where A_s and A_n are the root mean square (RMS) amplitudes of the signal and noise respectively. RMS amplitude is given by:

$$A = \sqrt{\frac{1}{N}\sum_{n=0}^{N-1} x^2(n)} \tag{25}$$

Noise amplitude is estimated using:

$$A_{Noise} \cong \frac{(A_{Noise\ section\ 1} + A_{Noise\ section\ 2})}{2} \tag{26}$$

where $A_{Noise\ section\ 1}$ is the RMS value of samples 1000 to 4000 of a given section and $A_{Noise\ section\ 2}$ is the RMS value of samples 10000 to 13000 (see Fig. 6.7). Signal-to-noise ratio is then estimated using:

$$SNR \cong \left(\frac{A_{Signal\ and\ noise} - A_{Noise}}{A_{Noise}}\right)^2 \tag{27}$$

where $A_{Signal+noise}$ is the RMS value of samples 5500 to 8500. Each RMS value was calculated over 3000 samples to allow direct comparison. This method was used both before and after de-noising.

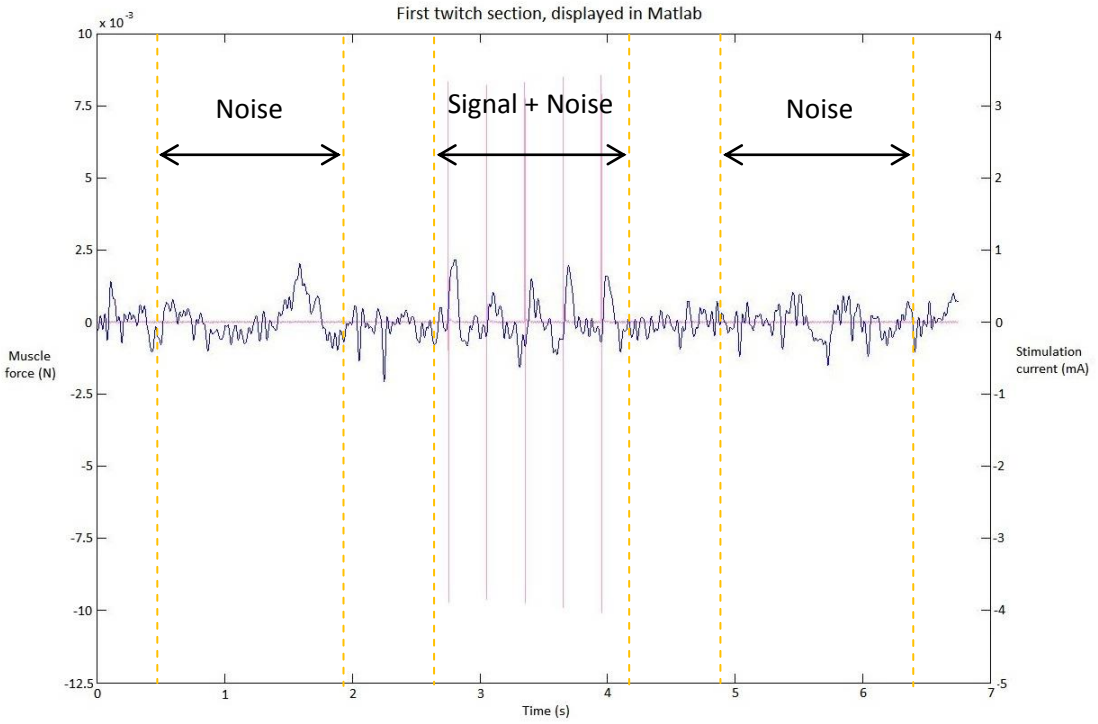

Figure 6.6: **Potential twitch section with noise subsections indicated. "Signal + Noise" demarcates the subsection considered to contain both signal and noise. "Noise" demarcates the subsections considered to contain only noise.**

6.4 Template matching

6.4.1 Template creation

The shape of each twitch in a section was considered individually (see Fig. 6.7). Each twitch was considered to be contained in the 600 samples (0.3 seconds) following the corresponding stimulation pulse.

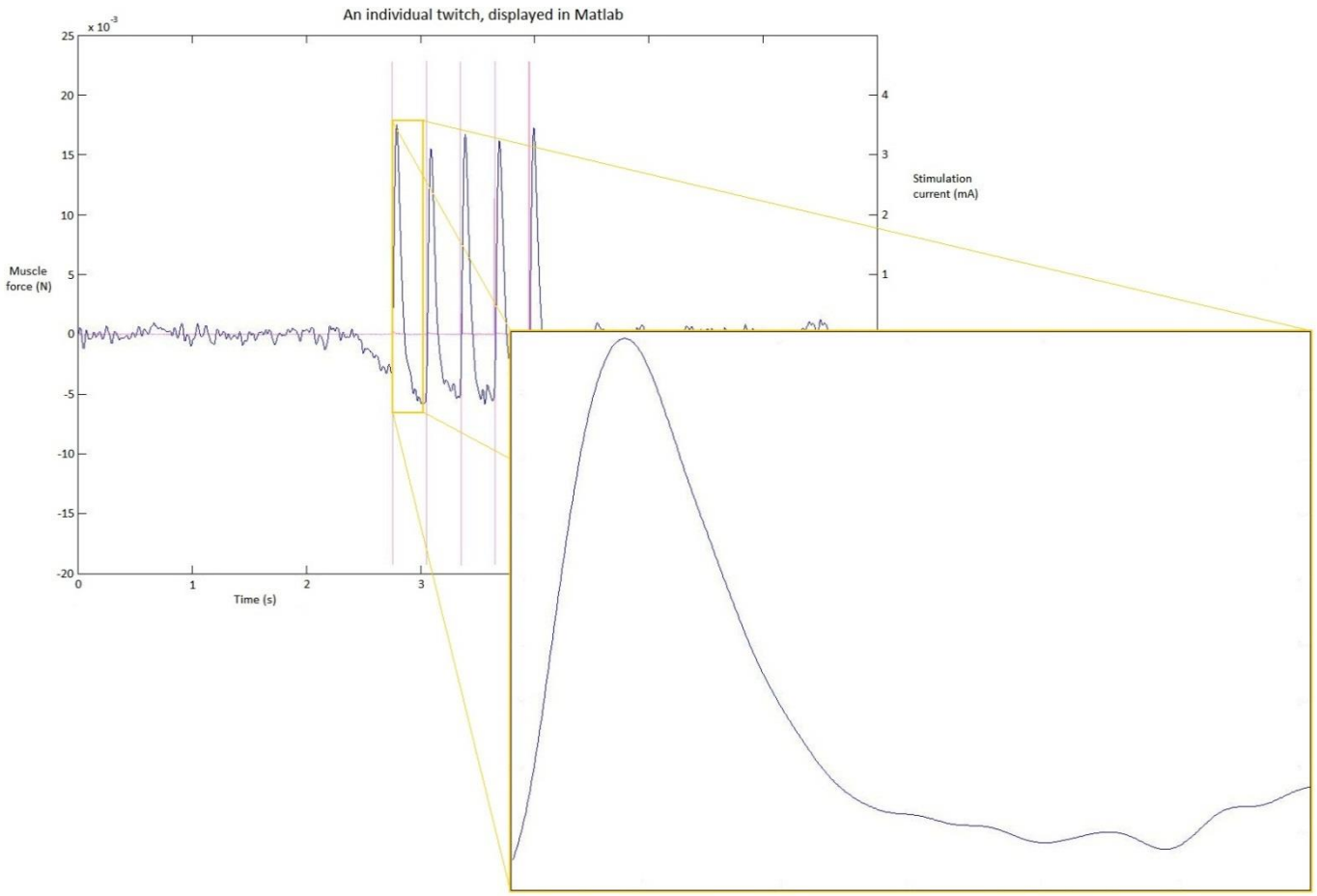

Figure 6.7: An example of one twitch.

The template was developed based on apparent twitches (see Section 5.5.2). 50 apparent twitches with approximately equal peak values were chosen and averaged (see Fig. 6.8). Twitches from both healthy and denervated muscles were used. The peak value used was chosen arbitrarily.

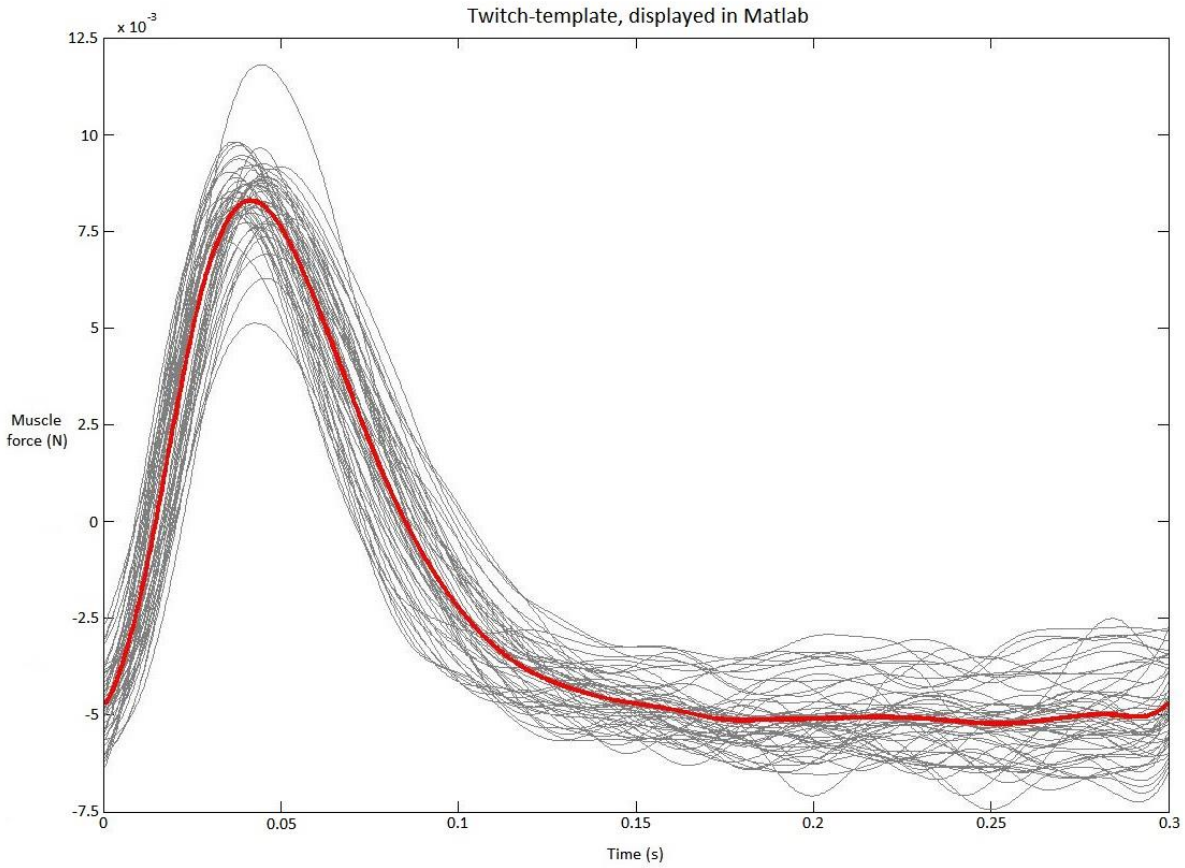

Figure 6.8: **Twitch template, derived by averaging apparent twitches. Apparent twitches are plotted in grey and the resulting template is plotted in red.**

6.4.2 Template fitting

A common metric of the match between a potential spike and a spike template is the cross correlation (Kim & McNames 2007). This metric is also known as the sliding dot product. It represents the similarity of two waveforms, given a time lag, and is commonly used to search a long signal for a shorter, known feature. The cross correlation is given by:

$$(x \star y)(n) = \sum_{m=-\infty}^{\infty} x^*(m)y(n+m) \tag{28}$$

where x^* is the complex conjugate of x, and n is the lag. Since the position of the stimulation pulse was known, the template was fitted by setting the lag to 0 (see Fig. 6.9). It was assumed that the twitch morphology was constant regardless of the peak twitch value.

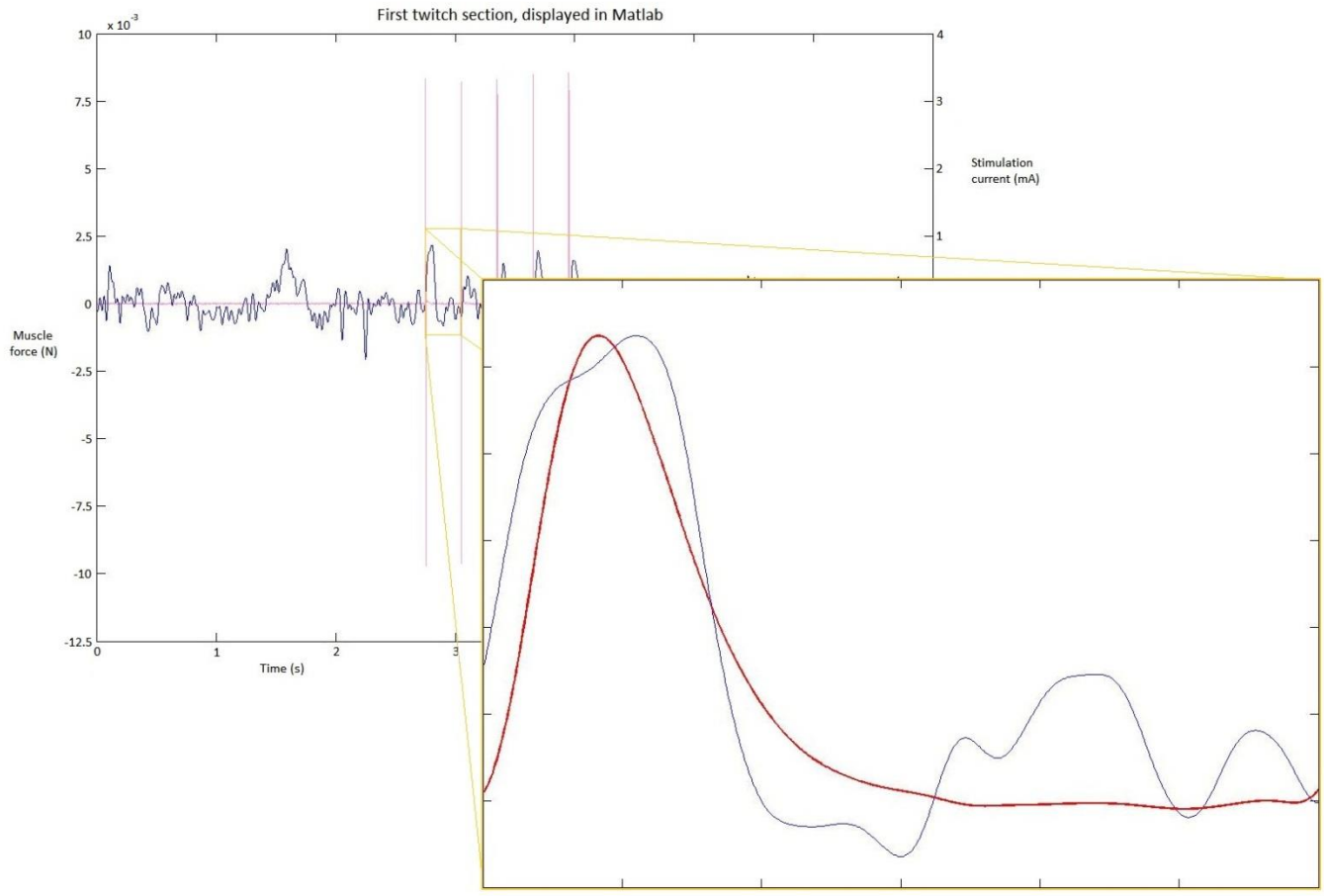

Figure 6.9: **Template, plotted in red, fitted to the first twitch in the first twitch section, plotted in blue. The template has been scaled for a direct comparison. In this case the correlation was 0.8988.**

6.5 Statistical analysis

6.5.1 Overview

The effects of EMD de-noising on the estimated signal-to-noise ratios, and twitch-template correlations were considered separately. In both cases the values before and after de-noising were compared using the Wilcoxon signed-rank test. Parametric tests (e.g. paired samples t-test or ANOVA) could not be used as the populations were not normally distributed. Normality was assessed using the Shapiro-Wilk test. All calculations were done using SPSS 20.0.0.

6.5.2 Groupings

In both cases the values were grouped by length of time denervated (if any), stimulation pulse width and whether EMD de-noising had been applied or not (see Fig. 6.10). In the case of the twitch-template correlation, values were additionally grouped by twitch number (see Fig. 6.11).

The analysis was simplified by removing groupings if no significant difference was found between members of those groups. Denervation groups were assessed using a Kruskal-Wallis test. Pulse width groups and individual twitch number groups were assessed using a Friedman test (as the same muscle was used throughout).

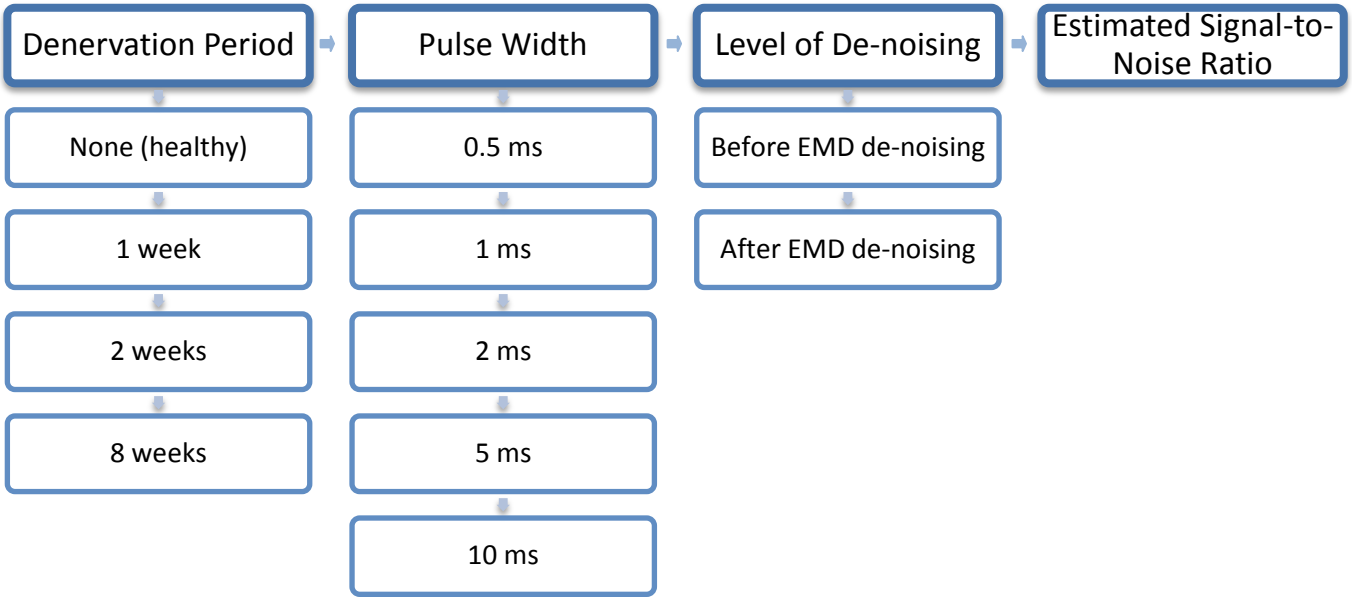

Figure 6.10: **Grouping of signal-to-noise ratio values. Independent variables are the denervation period, pulse width and level of de-noising. The dependant variable is the estimated signal-to-noise ratio.**

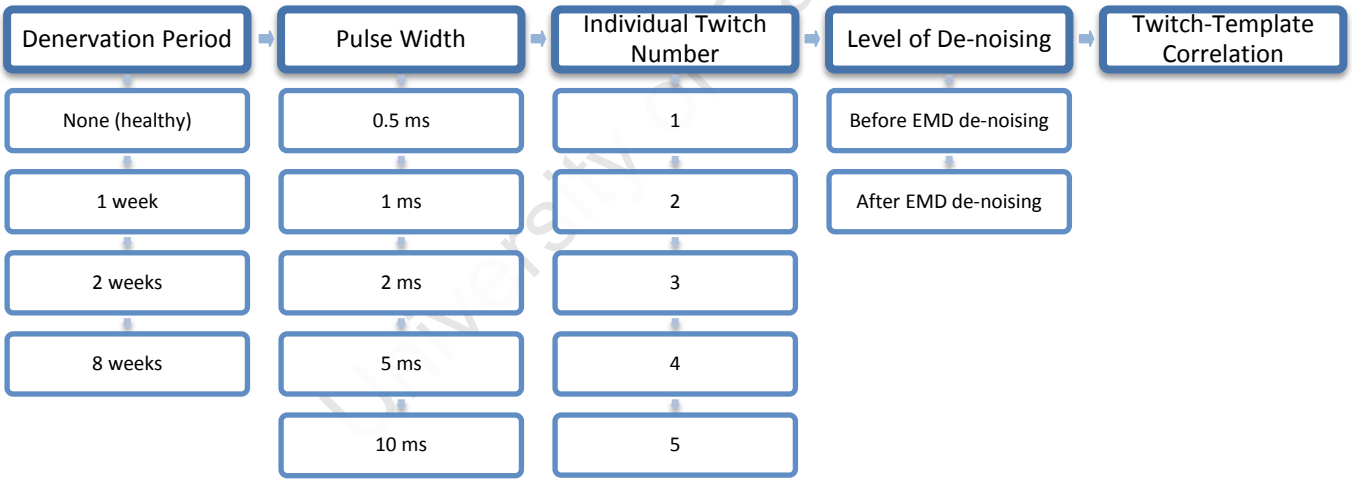

Figure 6.11: **Grouping of twitch-template correlation values. Independent variables are the denervation period, pulse width, individual twitch number and level of de-noising. The dependant variable is the twitch-template correlation.**

Summary of methodology

The soleus muscles of 35 Long Evans rats were used. Each rat was unilaterally denervated, with the right sciatic nerve being sectioned and ligated. Five rats were used as a pilot study and practice group for all the procedures. The remaining 30 were split into 3 groups of 10 each:

- One group was short term, with a denervation period of 1 week.
- One group was medium term, with a denervation period of 2 weeks.
- One group was long term, with a denervation period of 8 weeks.

After the denervation period, rats were euthanized by decapitation. In each case, both left and right soleus muscles were explanted.

Explanted muscles were housed in a Perspex tissue bath. The bath was filled with Ringer's solution. The solution completely submerged the muscle. Carbogen was bubbled through the solution. The contents of the bath were maintained at approximately 36.5 °C.

Muscles were secured by one end to the tissue bath, using a surgical suture. The opposite end was then secured to a force transducer. The force transducer was comprised of a strain gauge connected in a Wheatstone bridge configuration. The voltage output of the transducer was amplified and digitised using a Powerlab biological amplifier and LabView 7 software. The digitised signal could then be imported to Matlab for further analysis. An FIR digital filter, with a pass-band of 0.1 – 25 Hz, was applied to all force transducer output signals.

Stainless steel, Teflon-coated electrodes were used to stimulate the muscles. Two electrodes were used, and arranged in a bipolar configuration. Plastic spacers were used to separate the electrodes from each other by 2 mm and from the muscle by 1 mm. Electrodes were situated ¼ of the length of the muscles away from the tendons, to reduce the chance of activating the neuromuscular junctions. The electrode tips were submerged in Ringer's solution.

Stimulation pulses were generated using the Pulsar 6b pulse generator. Biphasic, constant-voltage pulses were used. Each muscle was stimulated using 5 pulse widths: 0.5, 1, 2, 5 and 10 ms. For each pulse width, a range of pulse amplitudes were used: 0 to 50 V, at intervals of 1 V. Five pulses were applied at each pulse amplitude. These are collectively referred to as a pulse group.

A 1 kΩ resistor was connected in series with the electrodes. The voltage across this resistor was amplified and digitised, similarly to the force transducer voltage. This digitised signal was also imported to Matlab, to aid further processing and analysis.

Twitches were identified by comparison to an automatic threshold, based on a noise-only section in the signal. If the signal portions corresponding to each of the 5 pulses of a particular pulse group were all above this threshold, they were considered to be twitches. These 5 twitches are collectively referred to as a twitch section.

Only the twitch section corresponding to the lowest pulse amplitude for a given pulse width was considered. This section is referred to as the first twitch section. The signal portion after the first twitch section was discarded. If no twitch section was found, the entire signal was discarded.

Resulting signals were de-noised, using an EMD-based de-noising algorithm. First the signal was decomposed into IMFs using the standard EMD algorithm. Each IMF was then thresholded separately, using a multiple of the universal threshold and the soft SCAD thresholding strategy. Thresholding was done using intervals based on IMF zero crossings, known as iterative interval thresholding. Thresholded IMFs were summed to create a de-noised version of the original signal. The 1st IMF was randomly altered, and the process was repeated for a total of 20 de-noised versions. These versions were averaged for the final de-noised signal.

The recognisability of the twitches was quantified in two ways. The signal-to-noise ratio of the twitch sections was estimated based on RMS value of signal portions. Twitches were also cross-correlated with a twitch-template. The template was created by averaging multiple known twitches. Recognisability was assessed both before and after de-noising.

The effect of the EMD-based de-noising on the recognisability of twitches was compared using the Wilcoxon Signed Rank test. A non-parametric test was used as the data was not sufficiently normal. Normality was assessed using the Shapiro-Wilk test.

Chapter 7: Results and conclusions

7.1 Statistical analysis

7.1.1 Grouping simplification

7.1.1.1 Signal-to-noise ratio

A significant difference was found between the signal-to-noise ratio values within the different denervation periods (see Table 7.1). Therefore, these groups were considered separately in subsequent analyses.

Table 7.1: Comparisons of signal-to-noise ratio values within different denervation periods. Significance values were calculated using a Kruskal-Wallis test.

	Chi-square	df	N	Asymp. Sig.	Mean rank of signal-to-noise ratios at specified denervation period			
					Healthy	Denervated: 1 week	Denervated: 2 weeks	Denervated: 8 weeks
Before de-noising	8.141	3	144	0.043	67.14	88.54	79.88	59.2
After de-noising	8.648	3	144	0.034	65.27	86.21	85	62.35

No significant difference was found between signal-to-noise ratio values within the different pulse width groups within denervation periods (see Table 7.2 and Table 7.3 for values before and after de-noising respectively). Therefore, these values were grouped together and the effects of the pulse width were not considered in subsequent analyses.

Table 7.2: Comparisons of signal-to-noise ratio values (before de-noising) within different pulse widths for each denervation period. Significance values were calculated using a Friedman test.

Denervation Period	Chi-square	df	N	Asymp. Sig.	Mean rank of signal-to-noise ratios at specified pulse width				
					0.5 ms	1 ms	2 ms	5 ms	10 ms
None (healthy)	4.195	4	70	0.38	30.11	40.06	38.44	28.83	39.29
1 Week	2.931	4	28	0.569	14.8	11.29	12.75	15.14	19.2
2 Weeks	3.53	4	26	0.473	25	13.8	10.86	15.14	12.5
8 Weeks	3.498	3	20	0.321	9	7	N/A	9.86	13.57

Table 7.3: **Comparisons of signal-to-noise ratio values (after de-noising) within different pulse widths for each denervation period. Significance values were calculated using a Friedman test.**

Denervation Period	Chi-square	df	N	Asymp. Sig.	Mean rank of signal-to-noise ratios at specified pulse width				
					0.5 ms	1 ms	2 ms	5 ms	10 ms
None (healthy)	3.778	4	70	0.437	30.33	36.35	38.44	29.89	41.76
1 Week	3.475	4	28	0.482	16.8	12	12.5	12.86	19.6
2 Weeks	1.22	4	26	0.875	17	14	12.86	15.29	11.17
8 Weeks	2.32	3	20	0.509	7.5	9.5	N/A	9.29	13.14

The final grouping of the values is shown in Fig. 7.1. Thus there are 2 independent variables (denervation period and level of de-noising). There is one dependent variable (estimated signal-to-noise ratio).

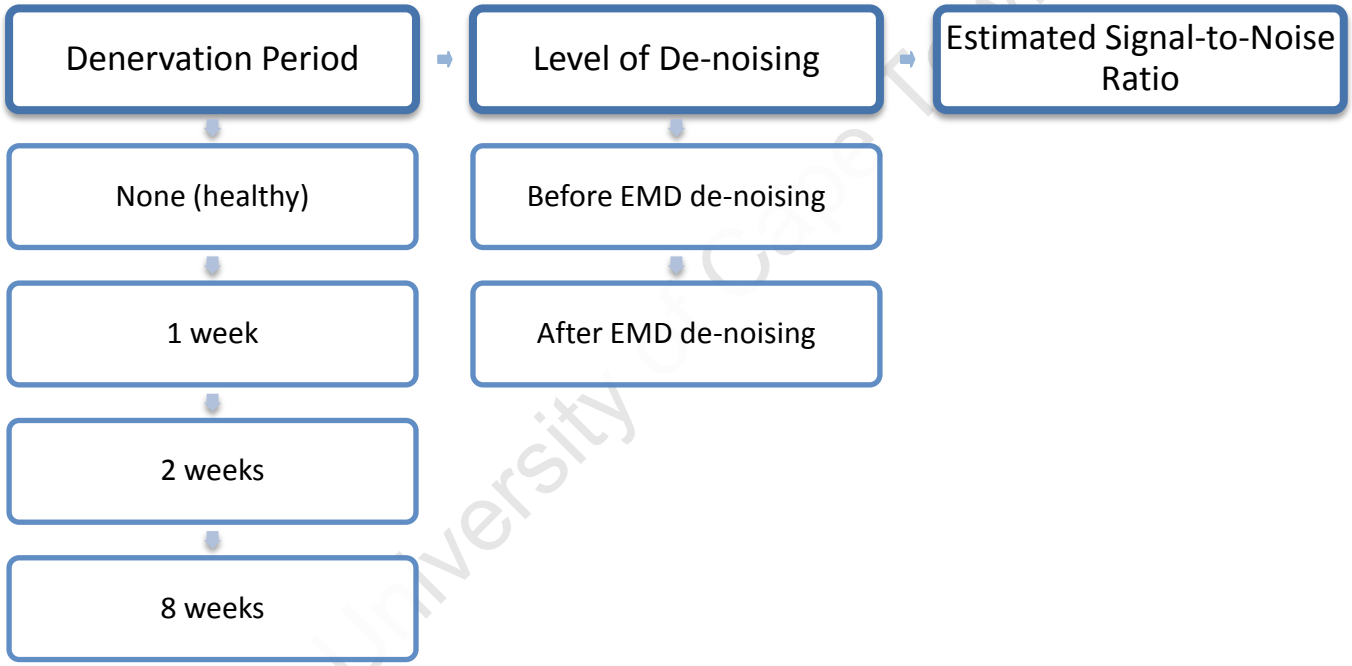

Figure 7.1: **Final grouping of signal-to-noise ratio values. Independent variables are the denervation period and level of de-noising. The dependant variable is the estimated signal-to-noise ratio.**

7.1.1.2 Twitch-template correlation

A significant difference was found between the twitch-template correlations (before de-noising) within the individual twitches (see Table 7.4). A possible explanation for this is that the muscles hadn't fully recovered between stimulation pulses. This is supported by the fact that the twitch 1 correlation (before de-noising) had the highest mean rank. Therefore, only twitch 1 was considered in subsequent analyses.

Table 7.4: Comparisons of twitch-template cross correlation values (before and after de-noising) for different twitches within a twitch section. Significance values were calculated using a Friedman test.

	Chi-square	df	N	Asymp. Sig.	Mean rank of twitch-template correlations at specified twitch				
					Twitch 1	Twitch 2	Twitch 3	Twitch 4	Twitch 5
Before de-noising	17.905	4	144	>0.001	3.27	3.15	2.63	3.17	2.78
After de-noising	8.428	4	144	0.077	3.13	3.15	2.69	3.1	2.93

A significant difference was also found between twitch-template correlation values within the different denervation periods (see Table 7.5). Therefore, these groups were considered separately in subsequent analyses.

Table 7.5: Comparisons of twitch-template cross correlation values within different denervation periods. Significance values were calculated using a Kruskal-Wallis test.

	Chi-square	df	N	Asymp. Sig.	Mean rank of twitch-template correlations at specified denervation period			
					Healthy	Denervated: 1 week	Denervated: 2 weeks	Denervated: 8 weeks
Before de-noising	17.529	3	144	>0.001	64.84	99.36	77.12	55.7
After de-noising	15.85	3	144	>0.001	63.44	98.41	77.42	61.53

No significant difference was found between twitch-template correlation values within the different pulse width groups within denervation periods (see Table 7.6 and Table 7.7 for values before and after de-noising respectively). Therefore, these values were grouped together and the effects of the pulse width were not considered in subsequent analyses.

Table 7.6: Comparisons of twitch-template cross correlation values (before de-noising) within different pulse widths for each denervation period. Significance values were calculated using a Friedman test.

Denervation Period	Chi-square	df	Asymp. Sig.	Mean rank of twitch-template correlations at specified pulse width				
				0.5 ms	1 ms	2 ms	5 ms	10 ms
None (healthy)	2.142	4	0.71	29	35.18	31.33	39.61	37.12
1 Week	5.956	4	0.202	11.2	10.64	12.63	17.86	20
2 Weeks	2.857	4	0.582	25	14.2	11.43	13.86	13
8 Weeks	1.165	3	0.761	9.5	8	N/A	11.86	10.86

Table 7.7: **Comparisons of twitch-template cross correlation values (after de-noising) within different pulse widths for each denervation period. Significance values were calculated using a Friedman test.**

Denervation Period	Chi-square	df	Asymp. Sig.	Mean Rank of twitch template correlations at specified pulse width				
				0.5 ms	1 ms	2 ms	5 ms	10 ms
None (healthy)	4.108	4	0.392	29.78	34.59	26.56	40.89	38.47
1 Week	3.94	4	0.414	11	12.86	14.5	14.29	20.6
2 Weeks	4.204	4	0.379	23	17.8	13.14	11.29	11.33
8 Weeks	0.777	3	0.855	9.5	8.75	N/A	11.86	10.43

The final grouping of the values is shown in Fig. 7.2. Thus there are 2 independent variables (denervation period and level of de-noising). There is one dependent variable (twitch-template correlation).

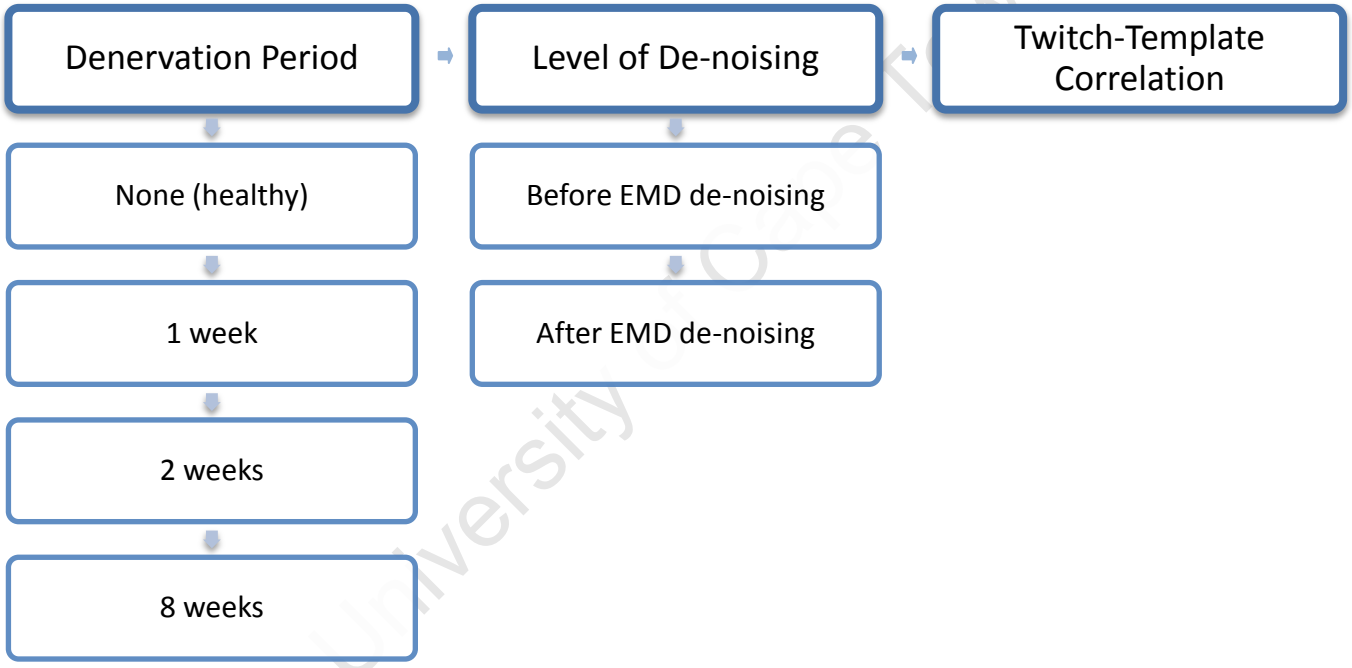

Figure 7.2: **Final grouping of twitch-template correlation values. Independent variables are the denervation period and level of de-noising. The dependant variable is the twitch-template correlation.**

7.1.2 Effects of EMD de-noising

7.1.2.1 Signal-to-noise ratio

For healthy muscles, a Wilcoxon Signed Ranks test (see Section 6.5.1) showed a significant difference between signal-to-noise ratio values, within the levels of de-noising ($Z = -6.982$, $P < 0.001$).

Table 7.8: Wilcoxon Signed Rank test results: signal-to-noise ratios for healthy muscles.

Descriptive Statistics

Healthy muscles	N	Mean	Std. Deviation	Minimum	Maximum	Percentiles		
						25th	50th (Median)	75th
Before de-noising	70	.941029	1.7384338	.0015	13.2461	.171825	.392000	1.039850
After de-noising	70	2.465939	3.8282066	.0006	26.3192	.379875	1.054850	3.166800

Ranks

Healthy muscles		N	Mean Rank	Sum of Ranks
(Signal-to-noise ratio after de-noising) – (Signal-to-noise ratio before de-noising)	Negative Ranks	6	8.25	49.50
	Positive Ranks	64	38.05	2435.50
	Ties	0		
	Total	70		

For muscles denervated for 1 week, a Wilcoxon Signed Ranks test showed a significant difference in signal-to-noise ratio values, before and after EMD de-noising ($Z = -4.623$, $P < 0.001$).

Table 7.9: Wilcoxon Signed Rank test results: signal-to-noise ratios for denervated muscles (1 week).

Descriptive Statistics

Denervated muscles: 1 week	N	Mean	Std. Deviation	Minimum	Maximum	Percentiles		
						25th	50th (Median)	75th
before de-noising	28	1.535250	1.7261056	.0390	6.9240	.374125	.802400	2.145175
after de-noising	28	4.869525	6.2477236	.0528	25.0574	.877975	2.853550	6.241575

Ranks

Denervated muscles: 1 week		N	Mean Rank	Sum of Ranks
(Signal-to-noise ratio after de-noising) – (Signal-to-noise ratio before de-noising)	Negative Ranks	0	.00	.00
	Positive Ranks	28	14.50	406.00
	Ties	0		
	Total	28		

For muscles denervated for 2 weeks, a Wilcoxon Signed Ranks test showed a significant difference in signal-to-noise ratio values, before and after EMD de-noising (Z = -4.457, P < 0.001).

Table 7.10: Wilcoxon Signed Rank test results: signal-to-noise ratios for denervated muscles (2 weeks).

Descriptive Statistics

Denervated muscles: 2 weeks	N	Mean	Std. Deviation	Minimum	Maximum	Percentiles		
						25th	50th (Median)	75th
Before de-noising	26	1.017496	.9487195	.0488	3.4697	.255775	.496750	1.623975
After de-noising	26	4.200300	4.9486154	.1317	22.6391	.853125	2.970650	6.089225

Ranks

Denervated muscles: 2 weeks		N	Mean Rank	Sum of Ranks
(Signal-to-noise ratio after de-noising) – (Signal-to-noise ratio before de-noising)	Negative Ranks	0	.00	.00
	Positive Ranks	26	13.50	351.00
	Ties	0		
	Total	26		

For muscles denervated for 8 weeks, a Wilcoxon Signed Ranks test showed a significant difference in signal-to-noise ratio values, before and after EMD de-noising (Z = -3.808, P < 0.001).

Table 7.11: Wilcoxon Signed Rank test results: signal-to-noise ratios for denervated muscles (8 weeks).

Descriptive Statistics

Denervated muscles: 8 weeks	N	Mean	Std. Deviation	Minimum	Maximum	Percentiles		
						25th	50th (Median)	75th
Before de-noising	20	.543285	.5480563	.0040	1.9775	.169775	.272150	.776425
After de-noising	20	1.709310	1.7283816	.0053	6.5840	.257200	1.234950	2.739025

Ranks

Denervated muscles: 8 weeks		N	Mean Rank	Sum of Ranks
(Signal-to-noise ratio after de-noising) – (Signal-to-noise ratio before de-noising)	Negative Ranks	1	3.00	3.00
	Positive Ranks	19	10.89	207.00
	Ties	0		
	Total	20		

7.1.2.2 Twitch-template correlation

For healthy muscles, a Wilcoxon Signed Ranks test showed no significant difference in twitch-template correlation values, before and after EMD de-noising (Z = -0.524, P = 0.6).

Table 7.12: Wilcoxon Signed Rank test results: twitch-template cross correlations for healthy muscles.

Descriptive Statistics

Healthy muscles	N	Mean	Std. Deviation	Minimum	Maximum	Percentiles		
						25th	50th (Median)	75th
Before de-noising	70	0.7785	0.138	0.3475	0.9694	0.6748	0.8167	0.8832
After de-noising	70	0.7691	0.1674	0.2696	0.9707	0.6624	0.8203	0.8891

Ranks

Healthy muscles		N	Mean Rank	Sum of Ranks
(Correlation with template after de-noising) – (Correlation with template before de-noising)	Negative Ranks	39	34.15	1332.00
	Positive Ranks	31	37.19	1153.00
	Ties	0		
	Total	70		

For muscles denervated for 1 week, a Wilcoxon Signed Ranks test showed no significant difference in twitch-template correlation values, before and after EMD de-noising (Z = -0.478, P = 0.633).

Table 7.13: Wilcoxon Signed Rank test results: twitch-template cross correlations for denervated muscles (1 week).

Descriptive Statistics

Denervated muscles: 1 week	N	Mean	Std. Deviation	Minimum	Maximum	Percentiles		
						25th	50th (Median)	75th
Before de-noising	28	0.8799	0.0839	0.5967	0.9752	0.8539	0.9009	0.9318
After de-noising	28	0.8865	0.0584	0.7067	0.9575	0.8692	0.8858	0.9377

Ranks

Denervated muscles: 1 week		N	Mean Rank	Sum of Ranks
(Correlation with template after de-noising) – (Correlation with template before de-noising)	Negative Ranks	12	15.17	182.00
	Positive Ranks	16	14.00	224.00
	Ties	0		
	Total	28		

For muscles denervated for 2 weeks, a Wilcoxon Signed Ranks test showed no significant difference in twitch-template correlation values, before and after EMD de-noising (Z = -0.521, P = 0.603).

Table 7.14: Wilcoxon Signed Rank test results: twitch-template cross correlations for denervated muscles (2 weeks).

Descriptive Statistics

Denervated muscles: 2 weeks	N	Mean	Std. Deviation	Minimum	Maximum	Percentiles		
						25th	50th (Median)	75th
Before de-noising	26	0.8177	0.1226	0.4493	0.9638	0.7538	0.8352	0.9076
After de-noising	26	0.8306	0.1152	0.3941	0.9473	0.7868	0.8494	0.9138

Ranks

Denervated muscles: 2 weeks		N	Mean Rank	Sum of Ranks
(Correlation with template after de-noising) – (Correlation with template before de-noising)	Negative Ranks	13	11.92	155.00
	Positive Ranks	13	15.08	196.00
	Ties	0		
	Total	26		

For muscles denervated for 8 weeks, a Wilcoxon Signed Ranks test showed no significant difference in twitch-template correlation values, before and after EMD de-noising (Z = -0.859, P = 0.391).

Table 7.15: Wilcoxon Signed Rank test results: twitch-template cross correlations for denervated muscles (8 weeks).

Descriptive Statistics

Denervated muscles: 8 weeks	N	Mean	Std. Deviation	Minimum	Maximum	Percentiles		
						25th	50th (Median)	75th
Before de-noising	20	0.696	0.2352	0.1392	0.966	0.5755	0.7583	0.8998
After de-noising	20	0.7135	0.2464	0.15	0.9461	0.6155	0.772	0.9067

Ranks

Denervated muscles: 8 weeks		N	Mean Rank	Sum of Ranks
(Correlation with template after de-noising) – (Correlation with template before de-noising)	Negative Ranks	8	10.25	82.00
	Positive Ranks	12	10.67	128.00
	Ties	0		
	Total	20		

7.2 Overview of results

7.2.1 Summary

- The EMD-based de-noising resulted in a significant increase (in all cases $P < 0.001$) in the estimated signal-to-noise ratios.
- The EMD-based de-noising resulted in no significant difference (in all cases $P > 0.05$) to the twitch-template correlation values.

7.2.2 Discussion

Rat soleus muscles were electrically stimulated, and the resulting twitches were digitised and recorded. Twitch recognisability was quantified by two measures: signal-to-noise ratio and cross correlation with a twitch-template. An EMD-based de-noising technique, called iterative interval thresholding was applied to the recorded twitches. The effect of this de-noising on the twitch recognisability was assessed.

A high number (about 48%) of potential muscle twitches had to be discarded. This was due to rats being prematurely euthanized (due to distress, see Section 5.2.3) or pulses being insufficient to cause any detectable response (likely due to damage to the muscle during explantation). Less viable muscle stimulations came from the 8 week group, likely since this was when the experimental technique was still being refined.

The increase in the signal-to-noise ratios of the twitches supports the results of Kopsinis & McLaughlin (2009) and many others (see Section 4.3.3.2), who found similar increases. This indicates that proportionally more noise was removed than signal, increasing the relative power of any features within that signal. This suggests that automatic threshold-based classifiers would benefit from EMD-based de-noising. This is particularly true of thresholds based on deviations from the signal mean, such as equation (9).

While an increase in signal-to-noise ratio indicates an improvement in recognisability, twitches aren't necessarily easier to classify by any method. This is illustrated by the lack of change in the twitch-template correlation values. While the noise was reduced, the shape of the twitch was slightly distorted (see Fig. 6.5). This suggests that the increase in correlation due to the former was cancelled by the decrease due to the latter. Nevertheless, the shape was not distorted enough to significantly reduce the recognisability of the twitches (by these metrics).

The results suggest that more research on the effects of various de-noising strategies on twitch recognisability may be beneficial. Some examples include wavelet-based thresholding, or signal averaging (Mouraux & Iannetti 2008). A further avenue of investigation might be into alternative methods of twitch classification. Fields such as spike sorting have a well-developed literature and set of techniques (Lewicki 1998) that could be adapted to this area.

Template matching could also be improved by creating more specific templates. For example, a different template could be created for each denervation group. This could account for changes in twitch shape due to experimental factors.

Chronaxie and rheobase determination rely on accurate detection of initial muscle responses, and will therefore directly benefit from any improvements thereof. While results suggest potential

improvements to algorithmic response detection, visual detection may still be preferable for practical reasons. Algorithmic detectors require additional apparatus, experimental design and technical expertise. In the case of EMD de-noising, the algorithm also requires significant processing time to run. Algorithmic detectors, however, have the potential to reduce subjectivity and consistency of results and should ideally be used if the practicalities can be overcome.

A full table of results is included in Appendix D.

7.3 Conclusions

The objectives of this study were to assess whether EMD-based de-noising could reduce variability in detection of the response of skeletal muscle to electrical stimulation. Reduced variability in response detection could lead to improved chronaxie and rheobase determination. This could lead to improved electrical stimulation-based rehabilitation protocols and devices.

The EMD-based method, known as iterative interval thresholding, resulted in an increase in signal-to-noise ratio, with little obvious distortion of the desired signal shape. This suggests that the method would be beneficial to classification of muscle response, particularly if a noise-based threshold were used.

This conclusion also suggests potential further avenues of research, including alternative de-noising methods (such as wavelet analysis) as well as alternative classification methods (such as methods borrowed from spike sorting).

References

Adami, N. et al., 2007. Permanent denervation of rat tibialis anterior after bilateral sciatectomy: determination of chronaxie by surface electrode stimulation during progression of atrophy up to one year. *Basic And Applied Myology*, 17(6), pp.237–243.

Agarwal, V. & Tsoukalas, L.H., 2007. Denoising electrical signal via empirical mode decomposition. In *2007 iREP Symposium - Bulk Power System Dynamics and Control - VII. Revitalizing Operational Reliability*. Charleston, SC: IEEE, pp. 1–6.

Al-Amood, W.S. & Lewis, D.M., 1989. A comparison of the effects of denervation on the mechanical properties of rat and guinea-pig skeletal muscle. *Journal of Physiology*, 414(1 July), pp.1–16.

Antoniadis, A. & Fan, J., 2001. Regularization of wavelet approximations. *Journal of the American Statistical Association*, 96(455), pp.939–967.

Ashley, Z. et al., 2005. Determination of the chronaxie and rheobase of denervated limb muscles in conscious rabbits. *Artificial organs*, 29(3), pp.212–5.

Astaf'eva, N.M., 1996. Wavelet analysis: basic theory and some applications. *Physics-Uspekhi*, 39(11), pp.1085–1108.

Babb, T.L. & Kupfer, W., 1984. Phagocytic and metabolic reactions to chronically implanted metal brain electrodes. *Experimental Neurology*, 86(2), pp.171–182.

Baechle, T.R. & Earle, R.W., 2008. *Essentials of Strength Training and Conditioning* 3rd ed. T. R. Baechle & R. W. Earle, eds., Human Kinetics Publishers.

Bard, A.J. & Faulkner, L.R., 1980. *Electrochemical Methods: Fundamentals and Applications* 2nd ed., Wiley, 2001.

Bekoff, A. & Betz, W.J., 1977. Physiological properties of dissociated muscle fibres obtained from innervated and denervated adult rat muscle. *Journal of Physiology*, 271(1 September), pp.25–40.

Bi, N. et al., 2007. Robust image watermarking based on multiband wavelets and empirical mode decomposition. *IEEE Transactions on Image Processing*, 16(8), pp.1956–1966.

Du Bois-Reymond, E.H., 1849. *Untersuchungen über thierische elektricität*, G. Reimer.

Carlson, B.M., Billington, L. & Faulkner, J., 1996. Studies on the regenerative recovery of long-term denervated muscle in rats. *Restorative neurology and neuroscience*, 10(2), pp.77–84.

Chamberlain, S. & Lewis, D.M., 1989. Contractile characteristics and innervation ratio of rat soleus motor units. *Journal of Physiology*, 412(1 May), pp.1–21.

Chouard, C.H., Pialoux, P. & Mercadier, M., 1995. La biocompatbilité des implants cochléaires. *Bulletin de l'Académie nationale de médecine*, 179(3), pp.549–555.

Claasen, T.A.C.M. & Mecklenbräuker, W.F.G., 1980a. The Wigner distribution - a tool for time-frequency signal analysis. I. Continuous time signals. *Philips Journal of Research*, 35, pp.276–350.

Claasen, T.A.C.M. & Mecklenbräuker, W.F.G., 1980b. The Wigner distribution - a tool for time-frequency signal analysis. II. Discrete time signals. *Philips Journal of Research*, 35, pp.276–300.

Claasen, T.A.C.M. & Mecklenbräuker, W.F.G., 1980c. The Wigner distribution - a tool for time-frequency signal analysis. III. Relations with other time-frequency signal transformations. *Philips Journal of Research*, 35, pp.372–389.

Conrad, A.G., Teare, B.R. & Haggard, H.W., 1936. Electrical studies of living tissue. *Transactions of the American Institute of Electrical Engineers*, 55(7), pp.768–772.

Daubechies, I., 1992. *Ten Lectures on Wavelets*, SIAM.

Davies, A.M., 1987. The growth rate of sensory nerve fibres in the mammalian embryo. *Development (Cambridge, England)*, 100(2), pp.307–11.

Dennis, R.G. & Kosnik, P E, 2002. Mesenchymal Cell Culture: Instrumentation and Methods for Evaluating Engineered Muscle. In A. Atala & R. P. Lanza, eds. *Methods of Tissue Engineering*. Gulf Professional Publishing, pp. 307–316.

Dennis, R.G. & Dow, D.E., 2007. Excitability of skeletal muscle during development, denervation, and tissue culture. *Tissue engineering*, 13(10), pp.2395–404.

Donoho, D.L., 1995. De-noising by soft-thresholding. *IEEE Transactions on Information Theory*, 41(3), pp.613–627.

Donoho, D.L. & Johnstone, J.M., 1994. Ideal spatial adaptation by wavelet shrinkage. *Biometrika*, 81(3), pp.425–455.

Doupe, J., 1943. Studies in denervation: I.-The contractility and excitability of denervated muscle. *Journal of neurology and psychiatry*, 6(3-4), pp.141–53.

Durand, D.M., 2006. Electrical stimulation of excitable systems. In J. D. Bronzino, ed. *Biomedical Engineering Fundamentals*. CRC/Taylor & Francis, 2006, pp. 520–535.

Eberstein, A. & Eberstein, S., 1996. Electrical stimulation of denervated muscle: is it worthwhile? *Medicine & Science in Sports & Exercise*, 28(12), pp.1463–1469.

ehumanbiofield, 2012. Neurons MC. Available at: http://ehumanbiofield.wikispaces.com/Neurons+MC [Accessed February 16, 2012].

Engel, A.G., 2008. The neuromuscular junction. *Handbook of clinical neurology*, 91, pp.103–48.

English, A.W., Wolf, S.L. & Segal, R.L., 1993. Compartmentalization of muscles and their motor nuclei: the partitioning hypothesis. *Journal of the American Physical Therapy Association*, 73(12), pp.857–867.

Di Fabio, R.P., 1987. Reliability of computerized surface electromyography for determining the onset of muscle activity. *Physical Therapy*, 67(1), pp.43–48.

Fan, J. & Li, R., 2001. Variable selection via nonconcave penalized likelihood and its oracle properties. *Journal of the American Statistical Association*, 96(456), pp.1348–1360.

Fick, A., 1863. *Beiträge zur vergleichenden Physiologie der irritabelen Substanzen*, F. Vieweg.

Finol, H.J., Lewis, D.M. & Owens, R., 1981. The effects of denervation on contractile properties of rat skeletal muscle. *Journal of Physiology*, 319, pp.81–92.

Fisher, G., Sayre, G.P. & Bickford, R.C., 1961. Histological changes in the cat's brain after introduction of metallic and plastic-coated wire. In D. E. Sheer, ed. *Electrical Stimulation of the Brain*. Austin: University of Texas Press, pp. 55–59.

Flanagan, J.L., 1972. *Speech analysis; synthesis and perception* 2nd ed., Springer-Verlang.

Flandrin, P., Gonçalves, P. & Rilling, G., 2004. Detrending and denoising with empirical mode decompositions. In *Proceedings of the 12th European Signal Processing Conference (EUSIPCO'04)*. pp. 1581–1584.

Follett, K.A. & Mann, M.D., 1986. Effective stimulation distance for current from macroelectrodes. *Experimental Neurology*, 92(1), pp.75–91.

Geddes, L.A., 2004. Accuracy limitations of chronaxie values. *IEEE transactions on bio-medical engineering*, 51(1), pp.176–81.

Geddes, L.A., 1999. Chronaxie. *Australasian Physical and Engineering Sciences in Medicine*, 22(1), pp.13–17.

Geddes, L.A., 1994. The first stimulators-reviewing the history of electrical stimulation and the devices crucial to its development. *IEEE Engineering in Medicine and Biology Magazine*, 13(4), pp.532–542.

Geddes, L.A. & Bourland, J.D., 1985. The strength-duration curve. *IEEE Transactions on Biomedical Engineering*, BME-32(6), pp.458–459.

Gillespie, J.H., 1932. Facts and theories about muscular activity. *The Ulster medical journal*, 1(3), pp.191–6.

Gotch, F. & Macdonald, J.S., 1896. Temperature and excitability. *Journal of Physiology*, 20(4-5), pp.247–297.

Graps, A., 1995. An introduction to wavelets. *IEEE Computational Science and Engineering*, 2(2), pp.50–61.

Gutmann, E. & Zelena, J., 1962. Morphological changes in the denervated muscle. In *The Denervated Muscle*. Prague: Czechoslovak Academy of Sciences, pp. 57–102.

Haykin, S.S., 1995. *Advances in Spectrum Analysis and Array Processing* S. S. Haykin, ed., Prentice Hall.

Hodgkin, A.L. & Huxley, A.F., 1952. A quantitative description of membrane current and its application to conduction and excitation in nerve. *Journal of Physiology*, 117(4), pp.500–544.

Holsheimer, J. et al., 2000. Chronaxie calculated from current-duration and voltage-duration data. *Journal of Neuroscience Methods*, 97(1), pp.45–50.

Hoorweg, J.L., 1892. Ueber die elektrische Nervenerregung. *Pflüger, Archiv für die Gesammte Physiologie des Menschen und der Thiere*, 52(3-4), pp.87–108.

Huang, N.E. et al., 2003. Applications of Hilbert-Huang transform to non-stationary financial time series analysis. *Applied Stochastic Models in Business and Industry*, 19(3), pp.245–268.

Huang, N.E., 2011. Instantaneous frequencies and trends for nonstationary nonlinear data. In *IMA Hot Topics Workshop*.

Huang, N.E. et al., 1998. The empirical mode decomposition and the Hilbert spectrum for nonlinear and non-stationary time series analysis. *Proceedings of the Royal Society A: Mathematical, Physical and Engineering Sciences*, 454(1971), pp.903–995.

Huang, N.E., Shen, Z. & Long, S R, 1999. A new view of nonlinear water waves: The Hilbert Spectrum 1. *Annual Review of Fluid Mechanics*, 31(1), pp.417–457.

Von Humboldt, A. & Holl, F., 2009. *Mein vielbewegtes Leben : der Forscher über sich und seine Werke*, Frankfurt am Main : Eichborn Berlin.

Irnich, W., 2002. Georges Weiss' fundamental law of electrostimulation is 100 years old. *Pacing and Clinical Electrophysiology : PACE*, 25(2), pp.245–248.

Irnich, W., 2010. The terms " chronaxie " and " rheobase " are 100 years old. *October*, 33(April), pp.491–496.

Jung, R. et al., 2009. Chronic neuromuscular electrical stimulation of paralysed hindlimbs in a rodent model. *Journal of Neuroscience Methods*, 183(2), pp.241–254.

Kaleem, M.F. et al., 2011. Using a variation of Empirical Mode Decomposition to remove noise from signals. In *21st International Conference on Noise and Fluctuations*. IEEE, pp. 123–126.

Karagiannis, A. & Constantinou, P., 2008. Comparative study of empirical mode decomposition applied in experimental biosignals. In *2008 8th IEEE International Conference on BioInformatics and BioEngineering*. IEEE, pp. 1–6.

Karagiannis, A. & Constantinou, P., 2009. Noise components identification in biomedical signals based on empirical mode decomposition. In *2009 9th International Conference on Information Technology and Applications in Biomedicine*. IEEE, pp. 1–4. Available at: http://ieeexplore.ieee.org/lpdocs/epic03/wrapper.htm?arnumber=5394300 [Accessed February 8, 2013].

Kent, M., 2006. *Oxford Dictionary of Sports Science and Medicine* 3rd ed., Oxford University Press.

Kim, S. & McNames, J., 2007. Automatic spike detection based on adaptive template matching for extracellular neural recordings. *Journal of neuroscience methods*, 165(2), pp.165–74.

Kipnis, N., 1987. Luigi Galvani and the debate on animal electricity, 1791–1800. *Annals of Science*, 44(2), pp.107–142.

Kopsinis, Y. & McLaughlin, S., 2009. Development of EMD-based denoising methods inspired by wavelet thresholding. *IEEE Transactions on Signal Processing*, 57(4), pp.1351–1362.

Kopsinis, Y. & Mclaughlin, S., 2008a. Empirical mode decomposition based denoising techniques. In *Proceedings of the 1st IAPR Workshop on Cognitive Informatics Processes*. pp. 42–47.

Kopsinis, Y. & Mclaughlin, S., 2008b. Empirical mode decompostion based soft-thresholding. In *Proceedings of the 16th European Signal Processing Conference, EUSIPCO*.

Kopsinis, Y. & McLaughlin, S., 2009. EMPIRICAL MODE DECOMPOSITION BASED DENOISING TECHNIQUES. *Technology*, (2), pp.42–47.

Kotsias, B.A. & Muchnik, S., 1987. Mechanical and electrical properties of denervated rat skeletal muscles. *Experimental Neurology*, 97(3), pp.516–528.

Lapicque, L., 1909. Définition expérimentale de l'excitabilité. *Comptes Rendus Soc. Biol.*, 77, pp.280–283.

Lapicque, L., 1931a. Has the muscular substance a longer chronaxie than the nervous substance? *Journal of Physiology*, 73(2), pp.189–214.

Lapicque, L., 1931b. On electric stimulation of muscle through ringer's solution. *Journal of Physiology*, 73(3), pp.219–246.

Lewicki, M.S., 1998. A review of methods for spike sorting: the detection and classification of neural action potentials. *Network (Bristol, England)*, 9(4), pp.R53–78.

Lewis, D.M., 1972. The effect of denervation on the mechanical and electrical responses of fast and slow mammalian muscle. *Journal of Physiology*, 222, pp.51–75.

Li, Y. et al., 2009. Sleep stage classification based on EEG Hilbert-Huang transform. In *2009 4th IEEE Conference on Industrial Electronics and Applications*. IEEE, pp. 3676–3681.

Lilly, J.C. et al., 1955. Brief, noninjurious electric waveform for stimulation of the brain. *Science*, 121(3144), pp.468–469.

Lilly, J.C., Austin, G.M. & Chambers, W.W., 1952. Threshold movements produced by excitation of cerebral cortex and efferent fibers with some parametric regions of rectangular current pulses (cats and monkeys). *Journal of Neurophysiology*, 15(4), pp.319–341.

Liu, S.C., 1970. Evolutionary power spectral density of strong-motion earthquakes. *Bulletin of the Seismological Society of America*, 60(3), pp.891–900.

Lucas, K., 1907a. On the rate of variation of the exciting current as a factor in electric excitation. *Journal of Physiology*, 36(4-5), pp.253–274.

Lucas, K., 1907b. The analysis of complex excitable tissues by their response to electric currents of short duration. *Journal of Physiology*, 35(4), pp.310–331.

Lucas, K., 1907c. The excitable substances of amphibian muscle. *Journal of Physiology*, 36(2-3), pp.113–135.

Lucas, K. & Mines, G.R., 1907. Temperature and excitability. *Journal of Physiology*, 36(4-5), pp.334–346.

Majji, A.B. et al., 1999. Long-term histological and electrophysiological results of an inactive epiretinal electrode array implantation in dogs. *Investigative Opthalmology and Visual Science*, 40(9), pp.2073–2081.

Marieb, E.N., 2001. *Human Anatomy & Physiology 5th edition*, Benjamin Cummings.

Mauro, A., 1969. The role of the voltaic pile in the Galvani-Volta controversy concerning animal vs . metallic electricity. *Journal of the History of Medicine and Allied Sciences*, XXIV(2), pp.140–150.

McNeal, D.R., 1976. Analysis of a model for excitation of myelinated nerve. *IEEE Transactions on Biomedical Engineering*, BME-23(4), pp.329–337.

Merrill, D.R., Bikson, M. & Jefferys, J.G.R., 2005. Electrical stimulation of excitable tissue: design of efficacious and safe protocols. *Journal of Neuroscience Methods*, 141(2), pp.171–98.

Midrio, M., 2006. The denervated muscle: facts and hypotheses. A historical review. *European Journal of Applied Physiology*, 98(1), pp.1–21.

Miller, D.J., 2004. Sydney Ringer; physiological saline, calcium and the contraction of the heart. *Journal of Physiology*, 555(Pt 3), pp.585–7.

Molla, M.K.I. & Hirose, K., 2007. Single-mixture audio source separation by subspace decomposition of Hilbert Spectrum. *IEEE Transactions on Audio, Speech and Language Processing*, 15(3), pp.893–900.

Monahan, A.H., 2001. Nonlinear principal component analysis: Tropical Indo–Pacific sea surface temperature and sea level pressure. *Journal of Climate*, 14(2), pp.219–233.

Mortimer, J., 1981. Motor prostheses. In *Handbook of Physiology*. pp. 155–187.

Mortimer, J.T., Shealy, C.N. & Wheeler, C., 1970. Experimental nondestructive electrical stimulation of the brain and spinal cord. *Journal of neurosurgery*, 32(5), pp.553–9.

Mouraux, A. & Iannetti, G.D., 2008. Across-trial averaging of event-related EEG responses and beyond. *Magnetic resonance imaging*, 26(7), pp.1041–54. Available at: http://www.ncbi.nlm.nih.gov/pubmed/18479877 [Accessed February 9, 2013].

Nicholls, J.G., 1956. The electrical properties of denervated skeletal muscle. *Journal of Physiology*, 131(1), pp.1–12.

Ogallo, L.J., 1989. The spatial and temporal patterns of the East African seasonal rainfall derived from principal component analysis. *International Journal of Climatology*, 9(2), pp.145–167.

Olson, L., 2002. Clearing a path for nerve growth. *Nature-London*, 416(11 April), pp.589–590.

Peckham, P.H. & Knutson, J.S., 2005. Functional electrical stimulation for neuromuscular applications. *Annual review of biomedical engineering*, 7, pp.327–60.

Pellegrino, C., 1963. An electron microscope study of denervation atrophy in red and wite skeletal muscle fibers. *The Journal of Cell Biology*, 17(2), pp.327–349.

Powers, R.E., Swick, H.M. & McQuillen, M.P., 1978. Human nerve excitability. *Journal of Neurology, Neurosurgery and Psychiatry*, 41(7), pp.642–8.

Priestley, M.B., 1965. Evolutionary spectra and non-stationary processes. *Journal of the Royal Statistical Society. Series B*, 27(2), pp.204–237.

Pudenz, R.H., Bullara, L.A., Dru, D., et al., 1975. Electrical stimulation of the brain. II. Effects on the blood-brain barrier. *Surgical neurology*, 4(2), pp.265–70.

Pudenz, R.H., Bullara, L.A., Jacques, S., et al., 1975. Electrical stimulation of the brain. III. The neural damage model. *Surgical neurology*, 4(4), pp.389–400.

Qin, B. & Shi, P., 2002. Empirical mode multi-scale image decomposition. *Journal of Engineering Graphics*, 1(4), pp.73–78.

Ranck, J.B., 1975. Which elements are excited in electrical stimulation of mammalian central nervous system: A review. *Brain Research*, 98(3), pp.417–440.

Reinsch, C.H., 1967. Smoothing by spline functions. *Numerische Mathematik*, 10(3), pp.177–183.

Rilling, G., Flandrin, P. & Gonçalves, P., 2003. On empirical mode decomposition and its algorithms. In *Proceedings of IEEE-EURASIP Workshop on Nonlinear Signal and Image Processing*. pp. 8–11.

Ringer, S., 1883. A further contribution regarding the influence of the different constituents of the blood on the contraction of the heart. *Journal of Physiology*, 4(1), pp.29–42.

Ritchie, A.E., 1944. The electrical diagnosis of peripheral nerve injury. *Brain - A Journal of Neurology*, 67(4), pp.314–330.

Rosas-Orea, M.C.E. et al., 2005. A comparative simulation study of wavelet based denoising algorithms. In *15th International Conference on Electronics, Communications and Computers (CONIELECOMP'05)*. IEEE, pp. 125–130.

Rushton, W.A.H., 1930. Excitable substances in the nerve-muscle complex. *Journal of Physiology*, 70(4), pp.317–337.

Rushton, W.A.H., 1932a. Identification of Lucas's α excitability. *Journal of Physiology*, 75(4), pp.445–470.

Rushton, W.A.H., 1932b. Identification of the gamma excitability in muscle. *Journal of Physiology*, 75(2), pp.161–189.

Rushton, W.A.H., 1927. The effect upon the threshold for nervous excitation of the length of nerve exposed, and the angle between current and nerve. *Journal of Physiology*, 63(4), pp.357–377.

Salmons, S. et al., 2005. Functional electrical stimulation of denervated muscles: basic issues. *Artificial organs*, 29(3), pp.199–202.

Seddon, H.J., 1942. A classification of nerve injuries. *British medical journal*, 2(4260), pp.237–9.

Sherwood, L., 2001. *Human Physiology: From Cells to Systems* 7th ed., Cengage Learning.

De Smedt, J.E., 1950. Étude Expérimentale de la Déigénérescence Wallérienne et de la Rétnnervation du Muscle Squelettique. I. — Évolution de la Constante de Temps D'Excitation. *Archives Of Physiology And Biochemistry*, 58(1), pp.23–68.

Stensaas, S.S. & Stensaas, L.J., 1978. Histopathological evaluation of materials implanted in the cerebral cortex. *Acta Neuropathologica*, 41(2), pp.145–155.

Sulakhe, P. V, Drummond, G.I. & Ng, D.C., 1973. Calcium binding by skeletal muscle sarcolemma. *The Journal of Biological Chemistry*, 248(25 June), pp.4150–4157.

Thesleff, S., 1974. Physiological effects of denervation of muscle. *Annals of the New York Academy of Sciences*, 228(1), pp.89–104.

Titchmarsh, E.C., 1948. *Introduction to the Theory of Fourier Integrals* 2nd ed., Clarendon Press.

Tomasi, W., 2001. *Electronic Communication Systems: Fundamentals through Advanced* 4th ed., Prentice Hall.

Turner, S., Gibson, C.M. & Donnelly, M.A., 2009. Paralysis Facts & Figures. Available at: http://www.christopherreeve.org/site/c.mtKZKgMWKwG/b.5184189/k.5587/Paralysis_Facts__Figures.htm [Accessed September 15, 2010].

Vitro, I. et al., 2007. Excitability and isometric contractile properties of mammalian skeletal muscle constructs engineered in vitro. *In Vitro*, (May 2000), pp.327–335.

Watts, C.F., 1924. The effect of curari and denervation upon the electrical excitability of striated muscle. *Journal of Physiology*, 59(2-3), pp.143–152.

Weiss, G., 1901. Sur la possibilité de rendre comparables entre less appareils servant à l'excitation électrique. *Arch ital Biol*, 35, pp.413–446.

Weng, B., Blanco-Velasco, M. & Barner, K.E., 2006. ECG denoising based on the empirical mode decomposition. In *Annual International Conference of the IEEE Engineering in Medicine and Biology Society*. pp. 1–4.

Wheeler, B.C. & Heetderks, W.J., 1982. A comparison of techniques for classification of multiple neural signals. *IEEE transactions on bio-medical engineering*, 29(12), pp.752–9.

Wold, S., Esbensen, K. & Geladi, P., 1987. Principal component analysis. *Chemometrics and Intelligent Laboratory Systems*, 2(1-3), pp.37–52.

Wood, F. et al., 2004. On the variability of manual spike sorting. *IEEE transactions on bio-medical engineering*, 51(6), pp.912–8.

Zhang, H., 2006. Research on properties of empirical mode decomposition method. In *2006 6th World Congress on Intelligent Control and Automation*. IEEE, pp. 10001–10004.

Zhong, C. & Yan, M., 2002. Gearbox vibration recognition using empirical mode decomposition method. *Journal of the South China University of China*, 30(19), pp.245–268.

Appendix A: Ethics approval

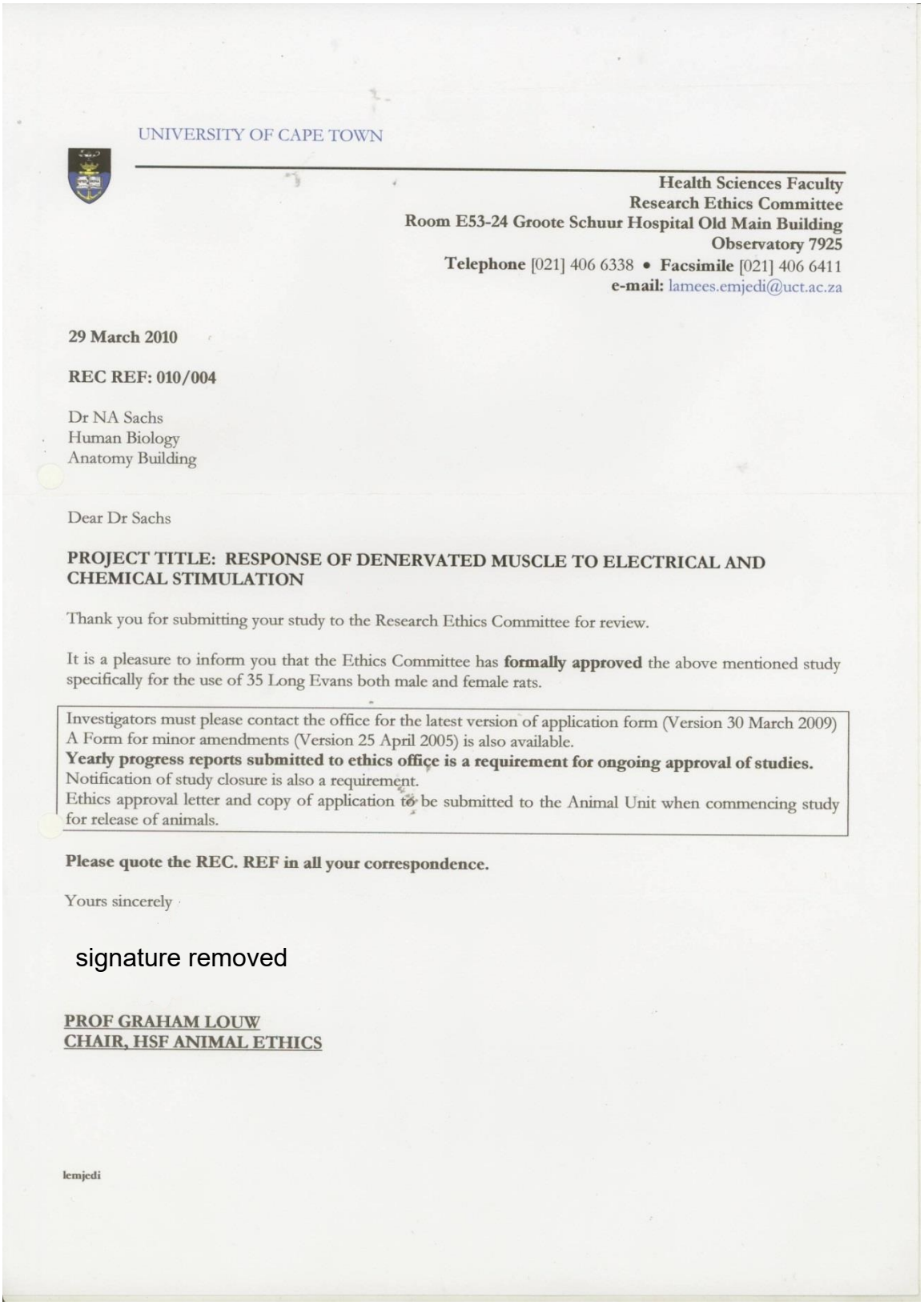

UNIVERSITY OF CAPE TOWN

Health Sciences Faculty
Research Ethics Committee
Room E53-24 Groote Schuur Hospital Old Main Building
Observatory 7925
Telephone [021] 406 6338 • **Facsimile** [021] 406 6411
e-mail: lamees.emjedi@uct.ac.za

29 March 2010

REC REF: 010/004

Dr NA Sachs
Human Biology
Anatomy Building

Dear Dr Sachs

PROJECT TITLE: RESPONSE OF DENERVATED MUSCLE TO ELECTRICAL AND CHEMICAL STIMULATION

Thank you for submitting your study to the Research Ethics Committee for review.

It is a pleasure to inform you that the Ethics Committee has **formally approved** the above mentioned study specifically for the use of 35 Long Evans both male and female rats.

Investigators must please contact the office for the latest version of application form (Version 30 March 2009)
A Form for minor amendments (Version 25 April 2005) is also available.
Yearly progress reports submitted to ethics office is a requirement for ongoing approval of studies.
Notification of study closure is also a requirement.
Ethics approval letter and copy of application to be submitted to the Animal Unit when commencing study for release of animals.

Please quote the REC. REF in all your correspondence.

Yours sincerely

signature removed

PROF GRAHAM LOUW
CHAIR, HSF ANIMAL ETHICS

lemjedi

Figure A.1: Approval letter from Research Ethics Committee

Appendix B: Matlab code

B.1 Overall process

B.1.1 Flowchart

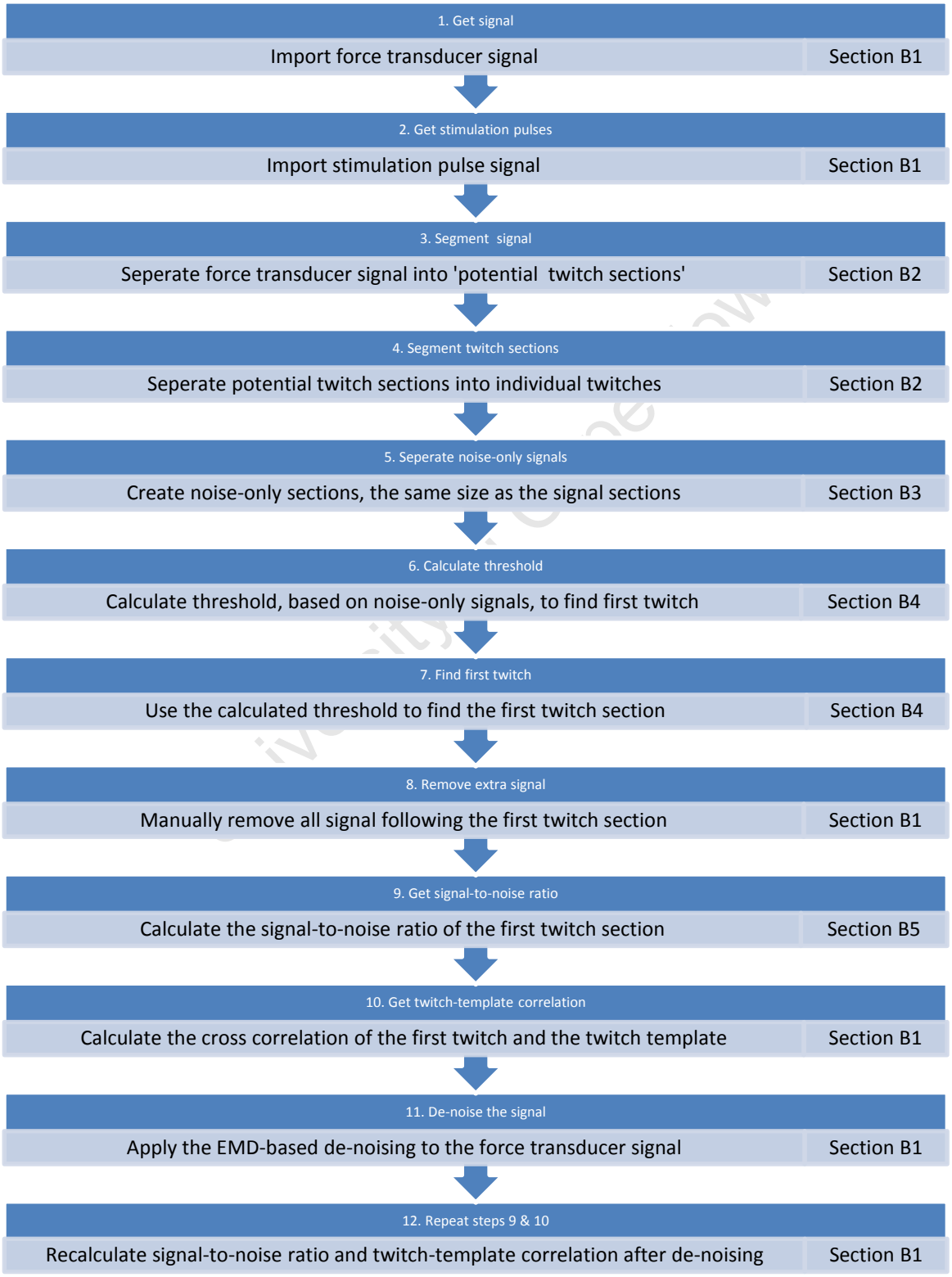

B.1.2 Code

```
%%import and break signal into useful sections

%given data_block1
%get main input and signal
input = downsample(data_block1(3,:),10);
signal = downsample(data_block1(1,:),10);

%break signal into fixed section based on input pulses (5 equal pulses)
section_sig = sect_auto(signal,input);
section_inp = sect_auto(input,input);


%break each section into twitches (used for comparison to model
twitch_block = make_t_block(section_sig);

%% Noise reference sections

%create noise-only sections (for twitch assessment references)
%first isolate noise from main signal (based on location of input pulses)
noise_compact = detwitch(signal,data_block1);

%100 sections of each are created to ensure a good representation
%ref for full sections
section_noise_big = sect_noise(noise_compact,100,13501);
%ref for individual twitch sections
section_noise_twitch = sect_noise(noise_compact,100,600);

% Find index such that the first twitch (as per the basic threshold) is
included
ft = find_twitch(twitch_block,noise_compact);

%Recalculate 'signal' and 'input', as well as the sections and twitch
block.
%Any signal beyond the first twitch is removed. This is done manually.

%SNR Values
SNR = signal2noise(section_sig(ft,:));

%import twitch model (manually; variable is called "template")
%calculate cross correlation using built-in Matlab function
t(1,:) = twitch_block(ft,1,:);
temp = xcorr(template,t,'coeff');
r = temp(600);

%de-noise signal
%The "EMDdenoise.m" code is available from:
%http://www.see.ed.ac.uk/~ykopsini/software.html
denoise = EMDdenoise(signal,'IIT',20,'circ',8,'softSCAD',0.4,2,5);
```

B.2 Signal separation

B.2.1 Flowchart

Note, this is applied to both the force transducer and the input stimulation pulse signals.

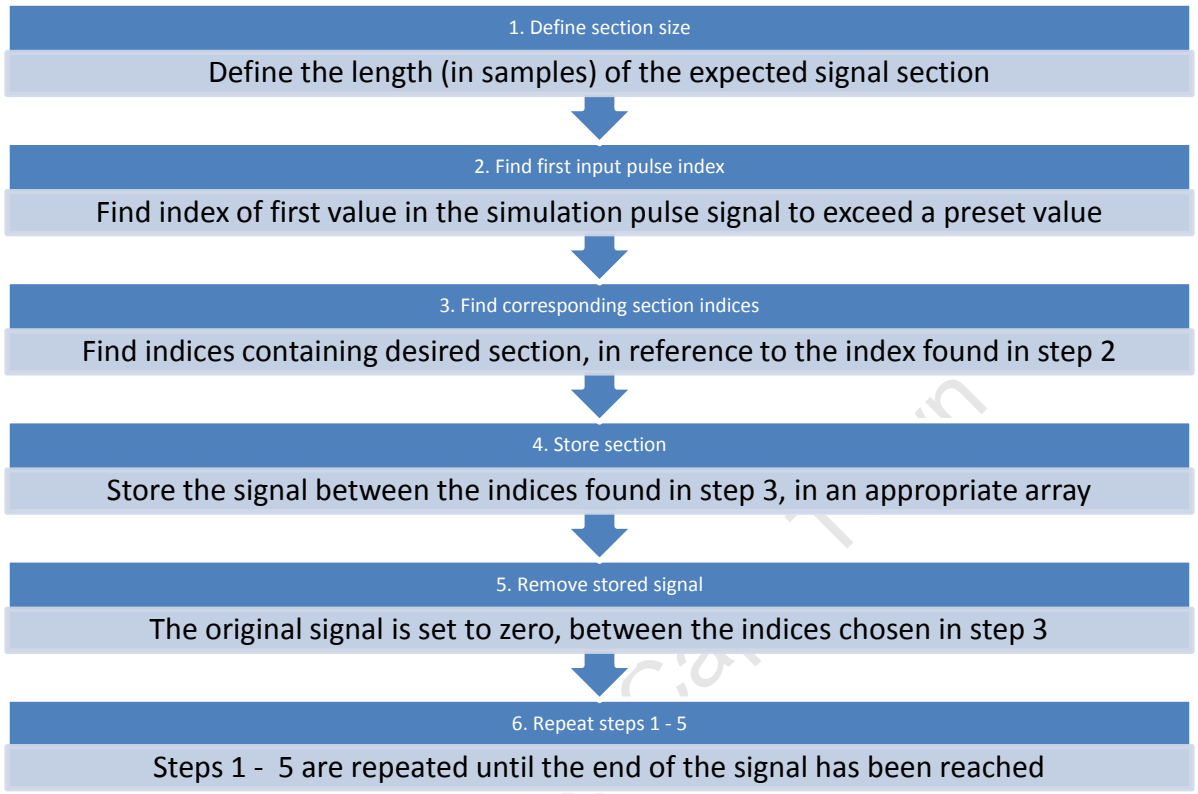

The force transducer signal sections are then further separated into an array of twitch signals.

B.2.2 Code

```
function section_sig = sect_auto(signal_,input_)

input = input_;
signal = signal_;

section_sig = 0;


%pre-define size of expected twitch sections
x1 = 5500;
x2 = 8000;

%signal sectioning

n = 1;

%first twitch section is done separately
while n < length(input)
    %find input-stimulation pulse
    if input(n) > 0.01
        %find appropriate indices of sections, based on first pulse
        for j = (n - x1):(n + x2)
```

```
            %store section in appropriate array
            section_sig(1,j - (n - x1) + 1) = signal(j);
            %clear stored signal (to avoid repeats)
            input(j) = 0;
        end
        n = length(input);
    end
    n = n + 1;
end

n = 1;
%process is repeated with minor modifications for the rest of the sections
while n < length(input)
    if input(n) > 0.01
        section_no = size(section_sig,1) + 1;

        %this included to avoid twitch section being longer than
        %remaining signal
        if (n + x2) > length(input)
            x2 = length(input) - n;
        end

        for j = (n - x1):(n + x2)
            section_sig(section_no,j - (n - x1) + 1) = signal(j);
            input(j) = 0;
        end
    end
    n = n + 1;
end


function twitch_block = make_t_block(section_sig)
%Breaks the signal sections down further into twitches, stores in an array,
%the first index is the section number, the second index is the twitch
%number

twitch_block = zeros(size(section_sig,1),5,600);

for i = 1:size(section_sig,1)
    for j = 1:600
        twitch_block(i,1,j) = section_sig(i,j + 5499);
        twitch_block(i,2,j) = section_sig(i,j + 6099);
        twitch_block(i,3,j) = section_sig(i,j + 6699);
        twitch_block(i,4,j) = section_sig(i,j + 7299);
        twitch_block(i,5,j) = section_sig(i,j + 7899);
    end
end
```

B.3 Noise-only signal

B.3.1 Flowchart

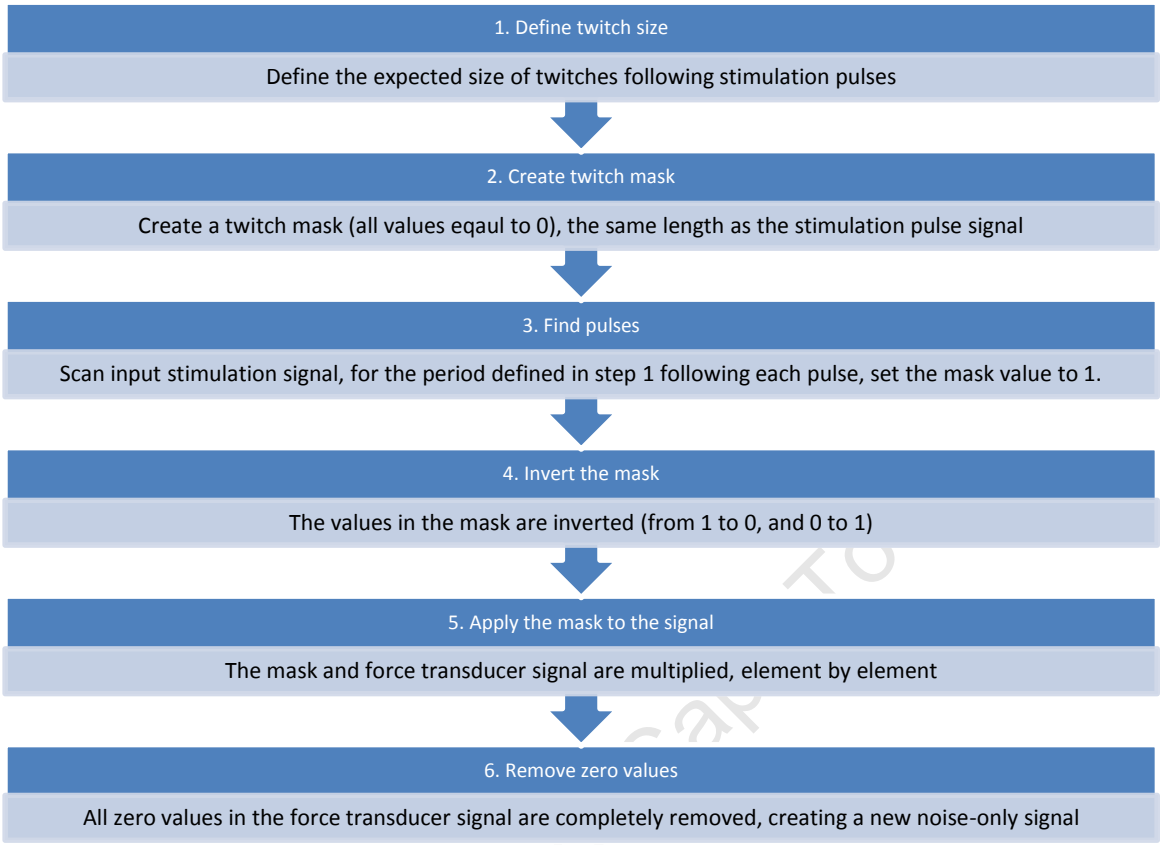

Sequential sections are randomly selected from the noise-only signal for comparison to signal sections.

B.3.2 Code

```
function noise_compact = detwitch(signal,data_block1)

input = downsample(data_block1(3,:),10);

stim = 1:(length(signal)-300);
high = 0;
count = 0;
i = 300;
```

```
%Scan the input pulse waveform and find the sections for which it is
%pulsing. An array stim is created, with a value of 1 during pulse
%sections, and 0 during non-pulse sections
while i < length(input)
    if input(i) > 0.01
        high = 1;
        count = 0;
    end
    if high == 1
        count = count + 1;
    end
    if count > 1000
        high = 0;
        count = 0;
        i = i - 300;
    end

    i = i + 1;
    stim(i - 300) = high;
end

endi = length(stim);
for i = 1:300
    stim(endi + i) = 0;
end

%Invert stim and multiply the original signal by it, effectively setting
%to zero all values within pulse sections
noise = 1:length(signal);
for i = 1:length(signal)
    noise(i) = signal(i) * (1 - stim(i));
end

%Remove zero spaces in noise signal
noise_compact = noise(1);
for i = 2:length(noise)
    if noise(i) ~= 0
        noise_compact(length(noise_compact) + 1) = noise(i);
    end
end


function [section_noise] = sect_noise(noise,n,l)
%Creates sections within the noise-only signal, useful for comparison to
%signal sections of the same size

section_noise = zeros(n,l); %preallocate the size of the array

for j = 1:n

    start = ceil(rand(1) * (length(noise) - l));
    for i = start:(start + l -1)
        section_noise(j,i - start + 1) = noise(i);
    end

end
```

B.4 First twitch location

B.4.1 Flowchart

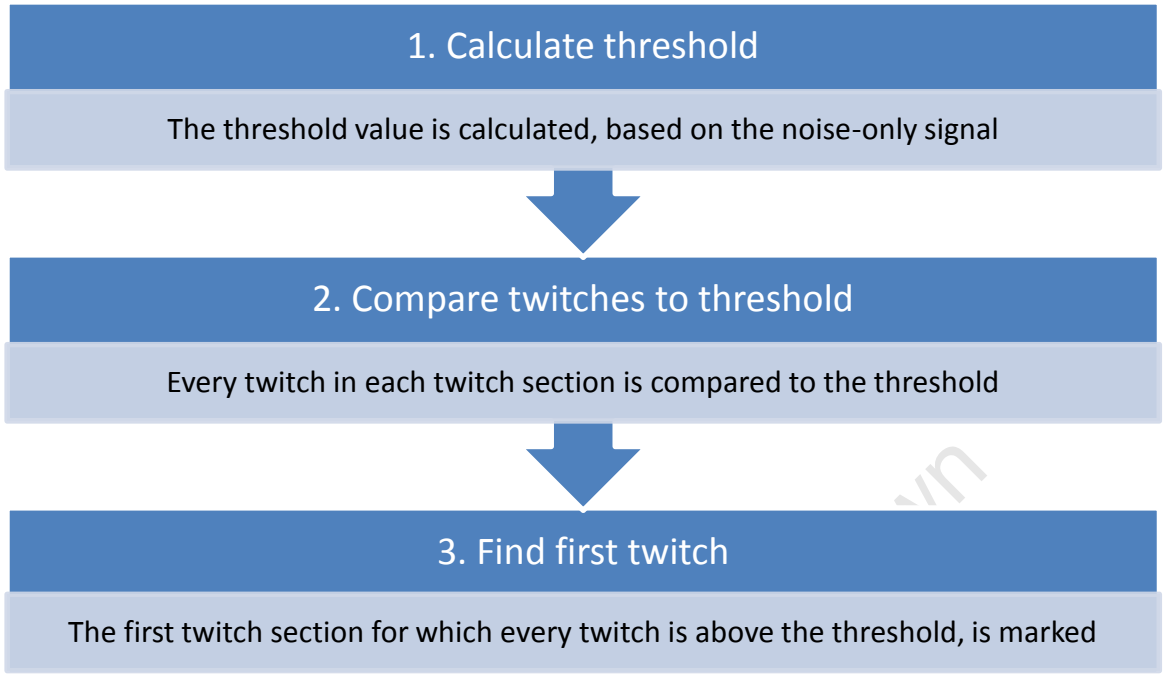

B.4.2 Code

```
function First_twitch = find_twitch(twitch_block,noise_compact)

%calculate a threshold (2 times the standard deviation of the noise-only
%signal)
threshold_trad = mean(noise_compact) + 2 * std(noise_compact);

%Find section for which the signal is above the threshold in all five
%expected twitch 'zones'
i = 1;
while (i < size(twitch_block,1)) && ~((max(twitch_block(i,1,:)) >
threshold_trad) && (max(twitch_block(i,2,:)) > threshold_trad) &&
(max(twitch_block(i,3,:)) > threshold_trad) && (max(twitch_block(i,4,:)) >
threshold_trad) && (max(twitch_block(i,5,:)) > threshold_trad))
    i = i + 1;
end

First_twitch_trad = i;

%If no twitch is found, the value is set to 0
if (i == size(twitch_block,1)) && ~((max(twitch_block(i,1,:)) >
threshold_trad) && (max(twitch_block(i,2,:)) > threshold_trad) &&
(max(twitch_block(i,3,:)) > threshold_trad) && (max(twitch_block(i,4,:)) >
threshold_trad) && (max(twitch_block(i,5,:)) > threshold_trad))
    First_twitch_trad = 0;
end

end
```

B.5 Signal-to-noise ratio

B.5.1 Flowchart

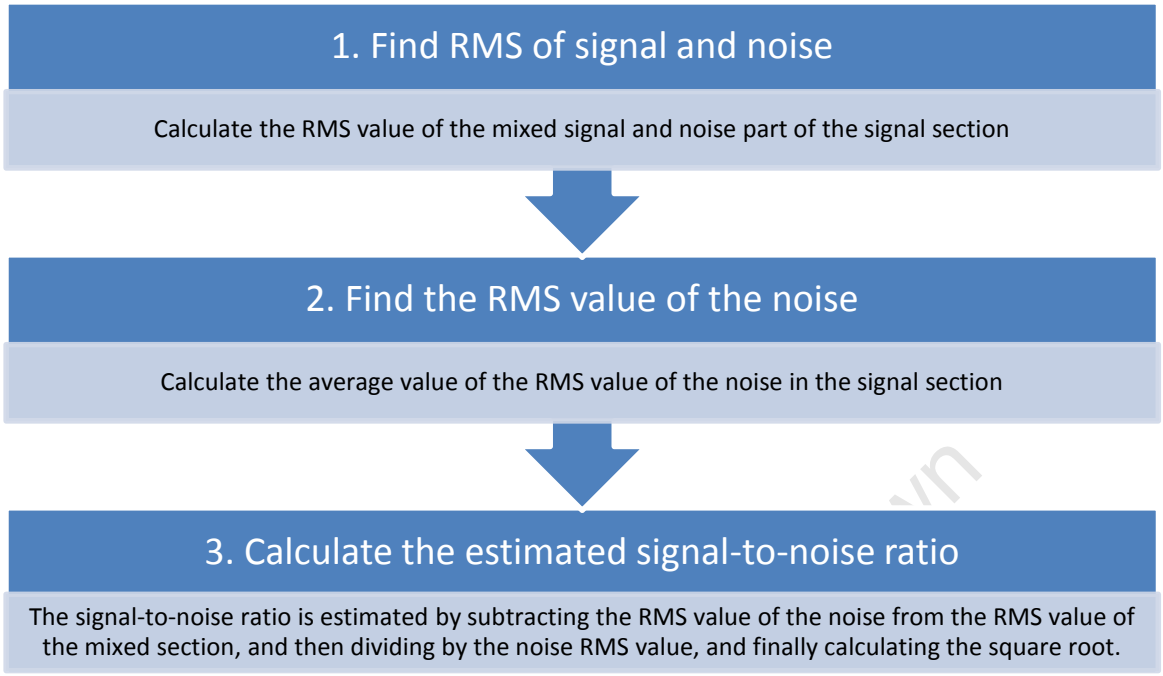

B.5.2 Code

```
function SNR = signal2noise(sig_sec)

%RMS of signal + noise section
RMS_sig = 0;
for i = 5500:8500
    RMS_sig = RMS_sig + sig_sec(i)^2;
end
RMS_sig = sqrt(RMS_sig/3000);

%RMS of Adjacent Noise
%Noise_left
RMS_n1 = 0;
for i = 1000:4000
    RMS_n1 = RMS_n1 + sig_sec(i)^2;
end
RMS_n1 = sqrt(RMS_n1/3000);

%Noise_right
RMS_n2 = 0;
for i = 10000:13000
    RMS_n2 = RMS_n2 + sig_sec(i)^2;
end
RMS_n2 = sqrt(RMS_n2/3000);

%Average of the two
RMS_nav = (RMS_n1 + RMS_n2)/2;


SNR = ((RMS_sig - RMS_nav)/RMS_nav)^2;  % using adjacent noise
```

Appendix C: Statistical tests

C.1 Shapiro-Wilks test

The Shapiro-Wilks test determines the normality of a sample set. Formally, it tests the null hypothesis that a given sample $x_1, \ldots, x_n$ comes from a normally distributed population.

The test statistic is given by:

$$\frac{(\sum \quad)}{\sum \quad \bar{x})}$$

where $x_{(i)}$ is the i^{th}-smallest number in the sample, known as the order statistic, and $\bar{x}$ is the sample mean.

The constant a_i is given by:

where

and are the expected values of the order statistics of independent and identically distributed random variables, sampled from the standard normal distribution. is the covariance matrix of those order statistics.

The value gives the significance of . If the resulting value is less than a certain α level, then the null hypothesis is rejected. A typical α level is 0.05.

C.2 Kruskal-Wallis one-way analysis of variance

The Kruskal-Wallis one-way analysis of variance by ranks tests for significant differences between groups within a sample set. Formally, it tests the null hypothesis that samples originate from the same distribution. It is a non-parametric equivalent of the one-way analysis of variance (ANOVA).

To perform the test, the data from all groups are ranked together (i.e. ranked from 1 to N, lowest to highest). If two values are tied they are assigned the average of the ranks they would have received had they not been tied.

The test statistic K is given by:

$$\frac{\sum \quad \bar{r} \quad \bar{r})}{\sum_{i=1}^{g} \sum_{j=1}^{n_i} (r \quad \bar{r})}$$

where n_i is the number of observations in group i, is the rank (among all observations) of observation i from group j, $\bar{r}_i$ is the average of all ranks in group i and $\bar{r}$ is the average of all r_{ij}.

If the significance p is below a certain α level, then the null hypothesis is rejected and there is evidence of a difference between at least two of the sample groups. The significance level is approximated by:

$$\Pr(x \qquad K)$$

C.3 Wilcoxon signed-rank test

The Wilcoxon signed-rank test is used to compare matched samples. Formally, it tests the null hypothesis that the median difference between matched pairs in a sample set is zero. It is a non-parametric equivalent of the paired Student's t-test.

To perform the test, first the difference between sample pairs is calculated:

$$|x \qquad |$$

where and are the paired measurements of sample . If any sample pair difference is equal (or close enough) to 0, that sample is discarded. The sample pair differences are ranked (from 1 to N, lowest to highest). If two values are tied they are assigned the average of the ranks they would have received had they not been tied.

The test statistic is given by:

$$\left|\sum[s \;\; n(x \qquad).R_i]\right|$$

where is the number of (reduced) samples and is the rank of the sample pair difference .

Appendix D: Results tables

D.1 Signal-to-noise ratio values

Table D.1: Estimated signal-to-noise ratio values of healthy muscles.

Pulse width (ms)	Estimated signal-to-noise ratio before de-noising	Estimated signal-to-noise ratio after de-noising
5	0.0211	0.0058
10	0.0665	0.1079
1	0.9431	2.5748
2	0.1724	0.6277
5	0.0706	0.1138
10	1.6902	4.8283
0.5	0.2581	0.7032
1	0.7155	2.499
2	0.3008	1.184
5	0.8021	5.5378
0.5	0.2871	0.7863
2	0.4063	1.2936
5	0.1245	0.8747
10	0.3908	2.815
0.5	0.3928	1.0594
1	3.0212	6.6821
10	0.0624	0.0538
1	0.8582	1.5456
5	0.29	1.0285
10	0.2329	1.2071
0.5	0.4078	0.869
1	0.1673	0.2726
1	0.1079	0.0432
2	0.0092	0.0233
5	0.2026	0.1382
10	0.2539	0.7741
0.5	0.1701	0.3889
1	1.0085	2.3174
5	0.8274	2.2617
10	2.3551	4.7521
1	13.2461	26.3192
2	0.9074	3.9737
5	0.0188	0.412
10	0.0811	0.1485
2	1.4192	3.4161
5	0.0641	0.0711
10	0.7846	2.3079
0.5	0.2001	0.4733
1	0.9566	1.8312
2	1.3043	3.7526

Table D.2: Estimated signal-to-noise ratio values for healthy muscles continued.

Pulse width (ms)	Estimated signal-to-noise ratio before de-noising	Estimated signal-to-noise ratio after de-noising
5	2.5103	6.8462
1	0.1651	0.4715
2	0.4633	1.0503
5	0.194	0.6611
1	0.3926	0.3513
0.5	2.193	5.577
1	3.154	5.8427
5	0.2018	0.3159
10	2.4531	2.9361
1	0.0599	0.0729
2	1.1339	1.7063
5	1.6457	4.5892
10	0.3566	1.7751
1	0.7137	5.3039
5	0.2258	0.9034
10	1.6199	6.5987
1	0.2123	0.3528
5	0.0067	0.0006
10	0.0015	0.0047
0.5	0.2445	1.239
1	0.3593	0.7248
5	0.5284	0.7036
10	1.5162	3.0837
0.5	0.107	0.1131
1	0.4095	0.496
5	0.3914	0.6654
10	0.5186	3.0549
10	2.0614	14.1026
5	2.1093	6.2728
10	4.3245	6.7256

Table D.3: Estimated signal-to-noise ratio values of muscles denervated for 1 week.

Pulse width (ms)	Estimated signal-to-noise ratio before de-noising	Estimated signal-to-noise ratio after de-noising
5	0.2301	0.687
10	5.334	25.0574
0.5	3.6928	11.4066
1	0.8489	4.983
2	0.794	2.721
5	1.486	2.6351
0.5	0.368	1.5649
1	0.73	1.04
2	0.1644	0.1819
5	0.7267	0.9448
0.5	0.5014	0.8557
1	0.1273	0.2944
5	1.7716	4.2345
10	2.487	6.6611
0.5	2.2697	7.86
1	0.5592	1.6906
5	4.0713	8.8031
10	1.7185	4.5573
0.5	0.5791	3.6972
1	0.3925	1.3826
1	0.039	0.0528
2	0.8108	3.0211
5	1.1188	2.9861
10	3.5383	13.3283
1	6.924	21.5956
2	1.4189	3.4284
5	0.2351	0.5912
10	0.0496	0.085

Table D.4: Estimated signal-to-noise ratio values of muscles denervated for 2 weeks.

Pulse width (ms)	Estimated signal-to-noise ratio before de-noising	Estimated signal-to-noise ratio after de-noising
1	0.0618	0.177
2	1.3116	9.7879
5	0.41	2.9964
10	0.2506	0.4547
1	1.7596	6.0162
2	0.0488	0.1317
5	0.5189	2.9449
10	0.3234	0.8891
2	1.5313	10.7498
5	1.7145	22.6391
10	0.4262	1.0993
1	1.473	7.0668
2	0.4746	1.4739
5	0.269	1.0084
10	2.4646	8.9282
2	0.1051	0.2644
5	0.2575	0.7452
10	0.0569	0.1598
1	0.8906	3.1621
2	1.5288	3.617
5	3.4697	5.6744
10	2.3493	5.8098
0.5	2.5374	5.1712
1	0.4548	1.0218
2	0.1731	0.9104
5	1.5938	6.3083

Table D.5: Estimated signal-to-noise ratio values of muscles denervated for 8 weeks.

Pulse width (ms)	Estimated signal-to-noise ratio before de-noising	Estimated signal-to-noise ratio after de-noising
5	0.083	0.2081
10	0.742	3.6273
0.5	0.004	0.0053
1	0.0512	0.2362
5	0.2405	0.5619
10	0.2587	1.4828
5	0.4074	1.396
10	0.7879	1.0739
0.5	1.0585	2.0708
1	0.1621	0.3202
5	0.2475	0.1666
10	1.6399	2.7426
1	0.628	2.7283
5	1.9775	6.584
10	0.2856	0.6486
5	0.7268	3.8684
10	0.1928	1.0305
1	0.2134	1.4306
5	0.0445	0.1209
10	1.1144	3.8832

D.2 Twitch-template correlation values

Table D.6: Twitch-template cross correlation values of healthy muscles.

Pulse width (ms)	Twitch-template cross correlation before de-noising	Twitch-template cross correlation after de-noising
5	0.8843	0.9427
10	0.7368	0.7378
1	0.862	0.8211
2	0.7985	0.7976
5	0.8654	0.9426
10	0.8147	0.8742
0.5	0.7333	0.793
1	0.9162	0.8998
2	0.4359	0.2696
5	0.8187	0.8977
0.5	0.8488	0.895
2	0.6604	0.6412
5	0.6489	0.7536
10	0.6448	0.6457
0.5	0.6885	0.6631
1	0.9103	0.908
10	0.8458	0.8092
1	0.78	0.865
5	0.8186	0.8564
10	0.8005	0.7753
0.5	0.8461	0.8076
1	0.7215	0.4221
1	0.7412	0.6202
2	0.7891	0.7649
5	0.6661	0.6279
10	0.8217	0.8841
0.5	0.577	0.4276
1	0.7731	0.8153
5	0.9625	0.9707
10	0.8612	0.8869
1	0.878	0.8682
2	0.6722	0.6243
5	0.9413	0.9009
10	0.6017	0.7279
2	0.8855	0.8827
5	0.4683	0.4244
10	0.8534	0.8766
0.5	0.8536	0.8637
1	0.7907	0.938
2	0.819	0.7544
5	0.9432	0.9119
1	0.627	0.8196
2	0.8519	0.7385
5	0.4567	0.3748
1	0.6756	0.5229

Table D.7: Twitch-template cross correlation values of healthy muscles continued.

Pulse width (ms)	Twitch-template cross correlation before de-noising	Twitch-template cross correlation after de-noising
0.5	0.927	0.9457
1	0.8747	0.7835
5	0.7692	0.776
10	0.9078	0.854
1	0.6643	0.3796
2	0.8642	0.9232
5	0.908	0.877
10	0.5947	0.6386
1	0.3475	0.3926
5	0.774	0.8125
10	0.9441	0.9318
1	0.7318	0.8399
5	0.7293	0.821
10	0.553	0.6602
0.5	0.5923	0.5819
1	0.9075	0.8871
5	0.8828	0.8004
10	0.7908	0.8253
0.5	0.6521	0.4958
1	0.9457	0.9096
5	0.896	0.8563
10	0.8509	0.8811
10	0.9206	0.9117
5	0.9055	0.8968
10	0.9694	0.911

Table D.8: Twitch-template cross correlation values of muscles denervated for 1 week.

Pulse width (ms)	Twitch-template cross correlation before de-noising	Twitch-template cross correlation after de-noising
5	0.9511	0.9167
10	0.9636	0.9379
0.5	0.9579	0.9381
1	0.7512	0.8242
2	0.9318	0.945
5	0.9752	0.9575
0.5	0.7219	0.7512
1	0.9075	0.9221
2	0.8863	0.869
5	0.9075	0.9238
0.5	0.5967	0.7067
1	0.8184	0.8505
5	0.9318	0.8918
10	0.8943	0.8798
0.5	0.9535	0.9377
1	0.918	0.9386
5	0.921	0.8699
10	0.9657	0.9375
0.5	0.7892	0.8646
1	0.8764	0.8954
1	0.84	0.8742
2	0.8671	0.876
5	0.8786	0.8233
10	0.9231	0.9503
1	0.9097	0.8748
2	0.8541	0.876
5	0.8538	0.871
10	0.8929	0.9194

Table D.9: Twitch-template cross correlation values of muscles denervated for 2 weeks.

Pulse width (ms)	Twitch-template cross correlation before de-noising	Twitch-template cross correlation after de-noising
1	0.8871	0.9137
2	0.92	0.9046
5	0.9257	0.8966
10	0.8409	0.8161
1	0.9484	0.9439
2	0.6297	0.8405
5	0.94	0.9253
10	0.8295	0.7721
2	0.8878	0.8582
5	0.7941	0.7805
10	0.886	0.9141
1	0.7497	0.8078
2	0.8215	0.8306
5	0.7916	0.7723
10	0.8766	0.883
2	0.8933	0.9017
5	0.6081	0.6294
10	0.7583	0.7889
1	0.7098	0.8054
2	0.4493	0.3941
5	0.9638	0.9145
10	0.8222	0.8074
0.5	0.9538	0.9191
1	0.9035	0.9473
2	0.7551	0.8638
5	0.7156	0.7656

Table D.10: Twitch-template cross correlation values of muscles denervated for 8 weeks.

Pulse width (ms)	Twitch-template cross correlation before de-noising	Twitch-template cross correlation after de-noising
5	0.6168	0.6027
10	0.6599	0.7197
0.5	0.1948	0.2138
1	0.497	0.3622
5	0.8895	0.8911
10	0.8648	0.861
5	0.9032	0.8963
10	0.7707	0.909
0.5	0.9123	0.9135
1	0.9409	0.9442
5	0.966	0.9461
10	0.9369	0.8998
1	0.4933	0.4284
5	0.6443	0.6539
10	0.1392	0.15
5	0.5695	0.6689
10	0.7458	0.7956
1	0.5936	0.732
5	0.7866	0.9332
10	0.7943	0.7484